An alternative way of drying; supercritical CO_2 extraction/drying for fast and effective removal of organic solvents from an active pharmaceutical ingredient

by Georgia Sanxaridou

A thesis in fulfilment of the requirements for the degree of

Doctor of Philosophy

Department of Chemical and Process Engineering

University of Strathclyde, Glasgow

August 2024

Declaration of authenticity and Author's rights

This thesis is the result of the author's original research. It has been composed by the author and has not been previously submitted for examination which has led to the award of a degree.'

Signed:  Date: 08/12/24

Pandemic impact statement

My PhD started in October 2016 with a minimum duration of studies of three and half years. In the first six months, I fulfilled the Doctoral Training Centre (DTC) training programme, which included assignments, workshops and team building exercises. From June 2017 until December 2019, I had completed most of the experimental work for chapters 4, 5 and 6. According to my first thesis outline, the last experimental chapter would have included the work conducted during my placement with Eli Lilly, in Indianapolis, USA. The placement was planned to start in January 2020; however, it was delayed and rescheduled for March 2020. At that time, I had already left my apartment in Glasgow and decided to voluntarily suspend my studies for the assumed duration of the project. Due to the Covid-19 pandemic, the placement was cancelled and I spent the entire duration of my suspension at home in Greece. During that period, I focused mostly on writing up using my lab notes and any useful material I had available with me. At the end of September 2020, I was able to return to Glasgow to carry out some remaining experiments in the last month of my studentship. Unfortunately, the experimental setup was not working, thus I tried to recover all the obtained data for completing my thesis. In November 2020, I travelled back to Greece and continued writing my dissertation. While in February 2021, I moved to Sweden and started my career as a development scientist at

EnginZyme AB based in Stockholm. At that point, I had to finalise writing chapters 6 and 7 including the conclusions; however, it was difficult for me to combine both work and thesis writing. In October 2022, I was given the opportunity to take a month of leave of absence and complete my thesis.

Signed by the supervisor:

Chris Price PhD FRSC CChem

Professor of Industrial Crystallization & Isolation
Department of Chemical & Process Engineering
University of Strathclyde

Signed by the researcher: Georgia Sanxaridou

Abstract

This research investigates supercritical carbon dioxide ($scCO_2$) technology as an alternative way of efficiently drying active pharmaceutical ingredients (APIs). Potential benefits of this green process technology include the minimisation of the solvent residues in the drug substance to a degree not achievable by conventional methods, milder process conditions and shorter drying times, which might lead to more energy-effective process. Another benefit for pharmaceutical materials processed in organic solvents is that using supercritical CO_2 offers a possible route to a sterile product.

This study conducts a comparative experimental analysis between supercritical CO_2 extraction/drying and conventional drying using an agitated filter dryer (AFD). The focus of this research is the removal of a challenging organic solvent, named dodecane, from paracetamol cakes. Apart from the drying performance, the study also evaluates the final product properties and energy consumption associated with each method. To conduct this experimental analysis, a Design of Experiments (DOE) methodology is employed to optimise both the conventional drying and supercritical CO_2 treatment. In conventional drying, critical parameters such as temperature (50-70 °C), N_2 flow rate (0.2-0.8 L/min), solid loading (60-150 g), and drying mode (static or agitated) are systematically studied, while maintaining a fixed pressure of 500 mbar. In the case of

supercritical CO_2 treatment, the study focuses on optimising temperature (50-70 °C), pressure (80-200 bar), CO_2 flow rate (10-30 g/min) and solid loading (60-150 g).

The findings revealed that, in the case of the AFD, the solid loading significantly influenced the drying performance. Dodecane residues were successfully reduced down to $8 \cdot 10^{-3}$ mg/g within a drying period of 3 hours using a 60 g cake sample. In contrast, 150 g cakes failed to meet the defined criteria (> 12.5 mg/g) even after an extended drying period of 5 hours. Supercritical CO_2 treatment consistently minimised the solvent concentrations ($2 \cdot 10^{-3}$ to $25 \cdot 10^{-3}$ mg/g) across various cake sizes, demonstrating faster (2 to 4 hours) and more complete drying than the conventional method. Particle size changes in particular agglomeration were observed in both drying techniques, but $scCO_2$ resulted in softer agglomerates with a higher brittleness index. The best combination of factors in the case of the AFD was 60 g cake, 70 °C, 0.8 L/min N_2 flow rate and intermittent agitation. For the $scCO_2$ extraction/drying, the optimal conditions were 150 g cake, 200 bar, 60 °C, and 20 g/min CO_2 flow rate. Finally, the energy analysis showed that $scCO_2$ technology was substantially more energy-efficient than AFD. At the optimal conditions, the normalised energy consumption for $scCO_2$ was around 21 $kWh/kg_{solids}/kg_{solvent}$, whereas AFD required a considerably higher energy input of 147 $kWh/kg_{solids}/kg_{solvent}$.

Acknowledgements

Foremost, I would like to thank both my supervisors Professor Chris Price and Professor John Robertson for their mentorship and valuable input during my PhD. I consider myself incredibly lucky to have worked with them and be part of their team.

I would like also to acknowledge all my colleagues from both Department of Chemical Engineering and CMAC who have helped me with their opinions, ideas and recommendations.

Special thanks to Anatune for providing me with the opportunity to have access to one of their SIFT-MS instruments.

I am grateful to EPSRC and the Doctoral Training Centre in Continuous Manufacturing and Crystallisation (Grant Ref: EP/K503289/1) and the Centre for Innovative Manufacturing in Continuous Manufacturing and Crystallisation (Grant Ref EP/I033459/1) for funding this work.

Lastly, many thanks to my family and friends for their endless patience and support during the four years of my PhD. I could not have undertaken this journey without their encouragement.

Table of Contents

List of figures

List of tables

1 Introduction

1.1 Context of research

Drying plays a crucial role in the downstream processes of API production. It often has a large impact on the subsequent stages of manufacturing including powder blending and tabletting while also playing a crucial role in determining the critical quality attributes of the API and the formulated medicine. This complex separation technology aims to remove volatile substances from wetted solids via heat and mass transfer mechanisms. Its primary goal is to reduce solvent residues to safe levels that are set according to patient safety and product stability requirements. Simultaneously, it is imperative to attain specific physical property characteristics in the isolated API, including the formation of free-flowing powder with the required particle size distribution, and facilitating preservation and storage [1].

Although, drying is recognised as a unit operation of high importance, it often remains as a bottleneck during API manufacturing. Most APIs are organic compounds that are heat sensitive and decompose when exposed to high temperatures. Additionally, these substances may lack a crystalline structure, exhibit very fine particle sizes, and require the elimination of toxic solvents. Achieving a low solvent content during drying, typically below one percent, is

often challenging for such products. The drying process is further complicated by the tendency of the material to form lumps during the process, leading to potential hardening issues [2]. Consequently, meeting the required low solvent content becomes difficult and prolonged drying cycles are required to achieve satisfactory results. Moreover, drying is an energy-intensive unit operation, with approximately 20% of the energy consumption in the pharmaceutical industry attributed to it [1]. Thus, there is a clear need to improve existing drying technologies or explore alternative drying methods to achieve a balance between product quality and drying time.

1.1.1 Current conventional drying techniques

The conventional methods of drying that are used in pharmaceutical manufacturing are classified according to the mechanisms by which the heat is transferred; convection (direct) and conduction (indirect) [3]. In convection, the material is exposed to an inert heated gas that flows through the bulk wet solid and helps to evaporate and remove residual solvent. Whereas, in conductive drying the solvent wet product material comes directly in contact with heated surfaces. A number of different dryer types currently used in the pharmaceutical industry are referred in **Table 1.1** and their basic principles are described extensively in many textbooks and handbooks [4]. Compared to convective type

of dryers, contact dryers offer better thermal efficiency, consume less energy and in combination with vacuum are favourable for heat sensitive materials [5].

Table 1.1. Conventional type of dryers used in pharmaceutical manufacturing.

Techniques	**Advantages**	**Disadvantages**
Agitated filter dryers	Easy to operate, high content uniformity due to agitation, high capacity of solids, high containment minimizing the risk of human exposure	Attrition due to agitation, heel removal is difficult
Vacuum tray dryer	Efficient for heat sensitive materials, wide input solvent level accommodated oxidation protection (possibly true for all dryers using nitrogen)	High operating costs due to cost of generating a vacuum in a GMP environment, low efficiency of the equipment, lack of agitation tends to favor lumping and uneven impurity distribution, manual discharge presents human exposure hazard
Lyophilizer	Good for volatile and thermally labile substances, oxidation protection	Long duration of drying, high energy consumption, high cost of the equipment
Fluid bed dryer	Continuous system, possible automation, uniform drying process	Not suitable for friable materials and large particles
Spray dryer	Preferred method for thermally sensitive products, continuous process, can be used to make amorphous material to enhance patient exposure to the drug substance	Thermal efficiency is relatively low, high energy demand, potentially high maintenance costs, may be difficult to control solid state form
Rotary dryer	Large capacity production, continuous operation	Low thermal efficiency, heat loss is large, use generally confined to bulk chemicals generally not used in pharmaceutical manufacturing.

However, the main challenge related to contact dryers is that it is difficult to design and engineer them [6]. Convective and conductive drying could be also combined for superior heat and mass transfer performances. This drying mode involves a hot gas flow through the solid bed, which at the same time is heated through the walls of the dryer.

1.1.2 Conventional drying: Agitated filter dryers (AFD)

Different types of equipment, such as fluidised bed dryers, filter dryers, and conical dryers can be used for APIs depending on the product specifications and safety requirements. However, the agitated filter dryer (AFD) is widely favoured in pharmaceutical companies, particularly for API production involving highly toxic substances [7]. The agitated filter dryer is widely used due to its capability to perform filtration, washing and drying in a single plant unit, reducing potential for human exposure during material handling and losses during transfer. Its key feature is the multipurpose agitator, which ensures high uniformity of content. Additionally, it offers flexibility with various drying modes including cold or hot air blowing, pressure, or vacuum drying, depending on specific requirements [7].

Despite the benefits of using agitated filter dryers in drug production, there are notable drawbacks. A significant disadvantage is the powder's susceptibility to agglomeration, a persistent issue in the pharmaceutical industry. This

phenomenon leads to the formation of hard, unbreakable lumps, and product degradation due to moisture content (residual solvent) within these lumps, causing common downstream challenges [7]. Another challenge associated with agitated drying is particle attrition, which can generate a significant amount of small particles. These fines typically exhibit poor flow properties [8] and can affect blending in drug product manufacturing, as well as the final tableting or encapsulation process [9].

1.1.3 An alternative drying technology: Supercritical CO_2 extraction/drying

The current study suggests the use of supercritical CO_2 extraction/drying to separate organic solvents from APIs. So far, there are a few reported applications of supercritical fluids on solvent removal from API solids. Kamihiri et al. [10] explored the removal of seven organic solvents from antibiotics using supercritical CO_2, while Bettini et al. [11] investigated the extraction of ethyl acetate from an alkylating anticancer drug under supercritical CO_2 conditions. Additionally, Falk and Randolf [12] conducted research on solvent extraction, focusing on the removal of DCM residues from gentamycin-loaded poly (l-lactide) microparticles.

While these studies show that $scCO_2$ extraction/drying is a feasible process for solvent removal from APIs, a more in-depth investigation is necessary to evaluate its efficacy compared to conventional drying methods. In this context, AFD is selected, because it is commonly employed in the pharmaceutical industry and extensively studied. If further investigation reveals that supercritical CO_2 technology offers superior separation performance compared to conventional methods, its development and adoption would be recommended. Several advantages of supercritical CO_2 technology make it a promising option for solvent removal from APIs, including:

1. Supercritical CO_2 is a dense gas with excellent physical properties (mentioned in section **2.2.1**) that facilitate the mass transfer resulting in high extraction rates.
2. The relatively low critical temperature of CO_2 allows for processing of heat-sensitive compounds, for example antibiotic manufacturing.
3. Supercritical CO_2 has sterilisation capabilities, making it suitable for pharmaceutical applications.
4. Furthermore, the $scCO_2$ extraction technology has been used successfully at commercial scale for over two decades including processes such as decaffeination of coffee beans and tea (see section **2.2.4**).

1.2 Aims and objectives of the thesis

This thesis aims to experimentally evaluate the efficacy of supercritical CO_2 extraction/drying in comparison to conventional drying of APIs. This assessment will encompass various aspects including drying performance, final product properties, and energy consumption. By undertaking this comprehensive analysis, the aim is to contribute to a deeper understanding of supercritical CO_2 extraction/drying as a potentially superior alternative to conventional drying techniques such as agitated drying.

To fulfil the goals of this project, the following research objectives were established:

- Designing and constructing a laboratory-scale agitated filter dryer capable of accommodating the $scCO_2$ extraction basket, thereby ensuring consistency in the properties of the wet cakes produced for both drying methods.
- Conducting a parametric study to optimise conventional drying using the laboratory-scale agitated filter dryer.
- Implementing an online analytical method to determine the endpoint of supercritical CO_2 extraction/drying, facilitating process optimisation.
- Investigating the impact of various parameters on supercritical CO_2 extraction/drying and optimising the process accordingly.

- Performing an energy consumption analysis for both supercritical CO_2 extraction/drying and conventional drying methods.
- Comparing the drying performance, final product properties, and energy consumption of both drying approaches to identify advantages and limitations.

1.3 Thesis outline

The thesis comprises eight main chapters that systematically investigate and compare the two studied drying technologies: agitated filter drying and supercritical CO_2 extraction/drying.

Chapter 2 establishes a theoretical foundation by exploring the fundamental aspects of drying, particularly using agitated filter dryers. The parameters influencing drying performance are comprehensively examined, and analytical processes and modelling approaches are reviewed. A substantial portion of the chapter is dedicated to supercritical fluids, emphasising on $scCO_2$ extraction principles as an alternative solvent removal method.

Chapter 3 adopts an experimental approach using MODDE software to optimise drying performance in a lab-scale agitated filter dryer. Various parameters, such as jacket temperature, drying mode, cake size, and nitrogen flow rate, are varied to identify optimal conditions for drying wet paracetamol

powder filter cakes. The results of this chapter are utilised to support the investigation of $scCO_2$ extraction/drying.

Chapter 4 focuses on employing supercritical CO_2 extraction for drying paracetamol particles post-washing. Selected Ion Flow Tube Mass Spectrometry is coupled with the process for real-time monitoring of organic solvent concentration changes. Preliminary experiments explore the impact of cake preheating on extraction kinetics, validating the use of SIFT-MS as an online analysis method.

Chapter 5 presents a parametric study to optimise the extraction/drying process for solvent removal introduced in **Chapter 4**. Variables such as pressure, temperature, CO_2 flow rate, and mass of substrate in the wet cake are evaluated. A mathematical model is applied to generalise experimental results, and MODDE software assesses the influence of operating variables on the process.

Chapter 6 conducts an energy consumption analysis for both drying technologies at studied operating conditions. For conductive drying under vacuum, energy consumption involves heat, nitrogen, and vacuum generation. In $scCO_2$ extraction/drying, energy consumption includes chiller, high-pressure pump, CO_2 heater, extraction vessel, and CO_2 compression. Optimal conditions

are used for energy calculations, and the impact of different parameters on energy consumption is investigated.

Chapter 7 evaluates the two drying technologies based on efficiency, final product properties, and energy consumption.

The main findings and recommendations for future work are summarised in **Chapter 8**, providing a comprehensive overview of the project.

2 Literature review

This current chapter provides a theoretical background of the various technologies used and studied in this thesis. The first sections are limited to conduct drying using agitated filter dryers. A summary of some drying fundamental aspects is briefly reviewed and a comprehensive description of the parameters affecting the drying performance is provided. Next, a review of relevant available analytical processes and recent modelling approaches are discussed. As the main core of this work is to study $scCO_2$ extraction/drying as a potential alternative way for solvent removal, a big part of this chapter is dedicated to supercritical fluids and their main principles.

2.1 Conventional drying

2.1.1 Agitated filter dryers (AFD)

Agitated filter dryers are classified as contact dryers and are widely used in pharmaceutical manufacturing as they allow filtration and drying to happen in one operation unit [13],[14]. Traditionally, those two processes were carried out in separate equipment and therefore, demanded considerable product handling during transportation. By combining those two unit operations into one, it eliminates the product loss/contamination including human exposure to potent drug substances [6]. Additionally, AFDs offer process flexibility and control to the manufacturer. Their compact design allows for minimal space requirement and they can be easily integrated in sterile environment, which is a frequent consideration in process plants. Moreover, these units are favoured in the pharmaceutical industry due to their ability to operate under reduced-pressure conditions [15]. This is particularly beneficial for drying thermally labile compounds, in which case a rigorous temperature control is implemented to avoid product degradation.

A typical AFD is designed as an enclosed cylindrical vessel, which contains a multipurpose agitator. The agitator operates through movement in both parallel and perpendicular axes. The cylindrical shell is usually made of stainless steel

material and integrated with a heated jacket, which controls the temperature of the vessel. A typical operating procedure for an AFD consists of three regimes; filtration, washing and drying. During filtration, the slurry is loaded into the filter vessel chamber and it is deliquored by removing the mother liquor either under pressure or under vacuum. The agitator is used at this stage for smoothing the cake's surface and sealing likely cracks before washing [3]. During the next regime, a solvent is spayed on the top of the cake allowing the packed bed to be washed uniformly. To this extent, the wash solvent displaces the mother liquor in a "piston-like" way and largely removes any dissolved impurity, which remains from the previous steps. After a defined number of washing steps and smoothing cycles, the cake is deliquored to reduce the solvent prior drying. A nitrogen blow through step tends to further reduce the cake moisture. When the third regime is initiated, the agitator slowly rotates to scrape and de-lump the cake while relatively gentle heating is supplied from the jacket.

2.1.2 Fundamentals of drying

By using conduct dryers, the heat is transferred into the wet product through conduction with the heated walls [14]. In the case where unstable compounds at elevated temperatures are dried, it is necessary to combine conduct drying with reduced pressure to lower the boiling point of the solvent. At the same time, the

vacuum carries away the evaporated solvent through a vent line whereas in the absence of it, the solvent is commonly removed by an inert carrier gas, usually nitrogen [16]. The solvent content is monitored over time throughout drying and is usually expressed as a percentage related to the weight of the dry media. The collected data can be plotted and presented in different ways. **Figure 2.1** shows typical drying curves for moisture content and drying rate versus time. Depending on the mechanism that dominates the rate of solvent removal, these plots are divided in three periods; the preheating, constant rate and falling rate [3]. In the preheating period A-B **Figure 2.1,** the unbound or free moisture, which saturates the surface of the particles, is evaporated. This period accounts for the time taken for the system to reach the temperature set point controlled by the jacket. After the warm up period, the drying rate reaches its maximum and remains constant up till the unbound moisture is evaporated, period B-C, **Figure 2.1.** The dominant drying mechanism at this stage is the heat transfer, after which the drying rate decreases as solids dry out. At the point C, where the constant period ends, the moisture content reaches a critical value, which refers to bound moisture. Bound moisture is the solvent physically or chemically adsorbed to the product and is eliminated during the falling rate period, C-E

Figure 2.1. While drying rate decreases at this stage, simultaneously the bed temperature increases to approach the temperature of the wall surface.

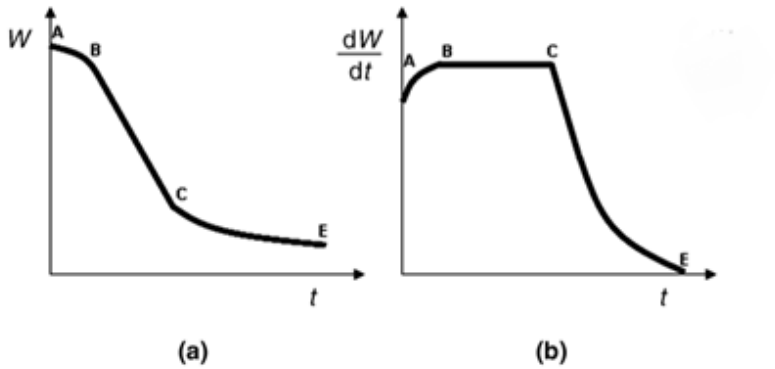

Figure 2.1. Drying curves for moisture and drying rate against time [16].

Regarding drying time, the initial period is usually neglected, as it lasts for a short time when compared to the other two following stages. During the constant rate period, the drying force is mainly driven by the temperature difference between the jacketed walls and the solvent to be removed. Assuming that the mass transfer rate, Φ_A, is independent on the moisture content and by integrating **Eq. (2.1)**, the drying time for the constant period can be estimated as follows, **Eq. (2.3)** [17].

$$X_A = \frac{m_A}{m_c} \quad \text{and } Y_A = \frac{m_A}{m_B}$$

$$\Phi_A = -\frac{1}{A} \cdot \frac{dm_A}{dt} = -\frac{m_c}{A} \cdot \frac{dX_A}{dt} \quad \textbf{Eq. (2.1)}$$

The moisture or solvent content in the cake per unit mass of solids is denoted as X_A, while Y_A is the water or solvent vapour pressure per unit mass of dry gas.

$$\tau = -\frac{m_c}{\Phi_A \cdot A}\int_{X_{A0}}^{X_{A\tau}} dX_A \qquad \textbf{Eq. (2.2)}$$

$$\tau_1 = -\frac{m_c \cdot (X_{A0} - X_{A\tau})}{\Phi_A \cdot A} = \frac{m_c \cdot (X_{A0} - X_{A\tau})}{K_U \cdot A \cdot (Y_{A_{wet}} - Y_A)} \qquad \textbf{Eq. (2.3)}$$

where K_U is mass transfer coefficient expressed by relative mass fractions ($kgAm^{-2}s^{-1}$), m_c is mass of dry filter cake (kg), A is surface area (m^2), τ_1 is drying time at constant rate period

In the falling rate period, the drying rate decreases exponentially as depicted in **Figure 2.1** and the heat transfer is no longer the dominant drying mechanism. Instead, mass transfer controls the solvent removal rate and the drying time during this period is obtained by integrating numerically the expression below [17].

$$\tau_2 = -\frac{m_c}{A}\int_{X_{A0}}^{X_{A\tau}} \frac{dX_A}{\Phi_A} \qquad \textbf{Eq. (2.4)}$$

where τ_2 is drying time in the falling rate period

2.1.3 Parameters affect drying performance

For maintaining the product quality, it is necessary to understand the parameters that influence drying and achieve the most favourable process conditions for an optimal result. There are several papers [6], [18], [19], [15], [20]

that deal with vacuum contact dryers. Some of them investigated experimentally the effect of key process parameters on drying kinetics and on final properties of the solid material. Those parameters involve pressure, jacket temperature, bed geometry, agitation and particle size [5].

2.1.3.1 Temperature and pressure

As it would be expected, an increase in temperature can speed up the drying process. High temperatures result in greater heat transfer between the heated wall and the bed, which therefore increase the evaporation rate inside the dryer. However, an acceptable temperature set point should be identified considering an upper limit to assure thermal stability of the product. In the case where low temperatures are required for drying APIs, the drying times can be minimised by varying the headspace pressure. Reducing the pressure results in a decrease in the boiling point of the solvent. When drying operates at temperatures above the solvents boiling point, the drying rate is improved significantly until the rate of solvent removal is limited by mass transfer phenomena [16]. Therefore, it is useful to understand the relationship between pressure and temperature. The pressure required for a particular solvent to be removed during a drying operation can be estimated by Antoine's equation. **Eq. (2.5**). This relationship

is used for most applications in pharmaceutical manufacturing and it provides a reasonable approximation.

$$\ln P^{sat} = A - \frac{B}{T+C} \quad \textbf{Eq. (2.5)}$$

where P^{sat} is the vapour pressure, T is temperature and A, B and C, constants which are determined empirically.

When vacuum is applied, it should also be noted that it is necessary to appropriately size the vacuum pump for the system [16]. Setting the pressure too low, the solvent vaporisation rate might be too high for the pump to remove the solvent, whereas higher pressure than the desired value may reduce the drying rate.

On the other hand, extreme drying conditions could influence the material physical properties. For example, increasing the drying temperature and/or reducing the pressure amplifies agglomeration of the solid material. In such cases, the drying time decreases as the drying rate is enhanced and when agitation occurs in the system, particles are exposed to shearing for shorter periods [21]. Therefore, the reduction in particle size due to attrition is less prominent. In addition, high temperatures increase the extent of agglomeration and the strength of the clusters by increasing API solubility in solvent. Fine crystals dissolve in the solvent phase and recrystallize during vaporisation of the liquid.

In this way, solid-liquid bridges are formed between particles, which tend to agglomerate in a larger lump.

Moreover, high temperatures increase the energy consumption. Opposed to this, low temperatures are not an efficient option either, because this results in very long drying times. A favourable combination of reduced pressure and temperature is advised with the second ranging between 40-60°C depending on the chemical stability of the drug substance being dried [3].

2.1.3.2 Bed geometry

Based on Kohout's [18] experimental investigation on the kinetics of vacuum contact drying of wet non-porous particles, the drying rate decreases with increasing bed depth. Additionally, Sahni [22] recently studied the trends for effect of fill level (25 %, 45 % and 75 %) on the drying performance in the filter-dryer as a function of bed temperature. The rate of solvent loss was greater for lower fill loads (25%) and decreased as the fill load increased under similar conditions. As the fill increases this provides more resistance to both heat and mass transfer through the bulk, resulting in longer drying times.

2.1.3.3 Agitation

Studies performed in agitated beds showed that the increased agitation speed reduce the drying time [6]. Stirring improves the heat and mass transfer rates by

inducing homogeneous mixing of particles in the dryer. The enhanced particle renewal rate increases the evaporation rate at the free surface, leading in shorter drying times. Furthermore, agitation is necessary for drying materials, which are sensitive to high temperatures, as it prevents the occurrence of hot spots in the bed, which would result from increased conduct time. On the other hand, agitation induces many processing issues. When it occurs continuously, there is substantial attrition due to the increased frequency of particle-particle and particle-impeller collisions [13]. Lekhal [21] showed that particle shearing usually dominates close to the impeller while in the low shear rate regions, agglomeration prevails resulting in broad particle size distribution. Birch and Marziano [23] reported that the formation of agglomerates is maximised if agitation is initiated at the beginning of the process, where the residual solvent content is above the critical level of solvent. Agglomeration is also prominent when wet particles undergo severe compression by the agitator at the initial drying stage. Compared to continuous stirring, intermittent stirring is proved a better drying method for preserving the product attributes due to minimum particle breakage and agglomeration phenomena.

2.1.3.4 Particle size

The particle size has a great impact on the drying rate and it cannot be neglected when studying the drying kinetics. As a rule of thumb, smaller particles have a greater surface area to volume ratio than larger particles; as a result, they dry much quicker for the same solvent loading. However, the increased wetted surface area is likely to result in an increased solvent loading per unit mass of solids. According to Papageorgiou et al. [24], micronised particles have higher potential to form agglomerates than the powder and granulated crystals. A possible explanation to this phenomenon is that drying micronised particles is hindered by recrystallization due to Gibbs Thomson effect [25]. The Gibbs Thomson equation, **Eq. (2.6)** shows that the decreasing particle size results in increasing solubility in the solvent. When recrystallization occurs, the ratio of surface area to cake volume increases, which therefore changes the surface energy of the solids. In order to maintain their surface energy, the unbound moisture in the wet cake becomes bound, impeding the solvent removal. Li [26] also reported that surface energy plays a key role in strengthening the solid-liquid bridges, leading to agglomeration. In addition, micronized material tends to have some degree of amorphous content, which also favours increased solubility. Therefore,

in micronised powder, recrystallisation counteracts the effect of decrease in drying time when the surface area increases.

$$X_{eq} = X_{eq\infty} \cdot \exp\left(\frac{2\gamma V_m}{rRT}\right) \quad \textbf{Eq. (2.6)}$$

where X_{eq} is the solubility of particles at radius r, $X_{eq\infty}$ is the normal solubility at equilibrium, γ is the surface energy, V_m is the molar volume, T is the temperature and R is the molar gas constant

2.1.4 Drying end point

The end point of drying may be monitored by determining the residual solvent content in the solids which can be measured through direct methods such as loss on drying (LOD), gas chromatography (GC) and Karl Fischer coulometric titration(KF) [5]. An LOD instrument is commonly used for quick measurements that are undertaken by simply heating up samples to a high enough temperature to vaporise any solvent which remains at 1bar (e.g. 120 ^{o}C is typically used) [27]. In this way, the mass loss is recorded and usually expressed as a percentage. GC also quantifies volatile compounds, but it demands a prior calibration using standards of known concentrations of the compounds to be measured. KF titration is another offline technique which is used specifically for water content in the samples and it can measure quite low concentration levels (down to parts per million). Other offline techniques include thermogravimetric analysis (TGA),

high performance liquid extraction (HPLC), nuclear magnetic resonance (NMR) and gravimetric analysis. When the sample is wet with multiple solvents it is desirable to use one of the analytical methods, which allow the identity of the released solvents to be known. Although these methods are simple to operate, there are many disadvantages related to offline measurements. For example, periodic sampling of the wet cake requires breaking in to the drying operation multiple times to snatch a sample and is time-consuming. Also, the sampling must be done carefully, since it may not be representative of the bulk cake depending on the location where the sample is taken. Additionally, if the substance to be dried is toxic, there is risk of exposure to the operator while sampling.

Therefore, particular attention is paid to replacing the conventional methods with modern online process analytical tools (PAT) [28]. By implementing on-line and in-line tools for monitoring drying, the cycle time and the cost are reduced allowing for advanced process control. Mass spectrometry is a popular technique for identifying various solvents in the vapor phase by continuously sampling from the outlet vent of the dryer. Its method relies on the molecular masses of the ionised species derived from the solvent and the solvent ratios are determined from the obtained mass spectrum. The solvent quantification is possible through

calibration with the use of standards. Such spectroscopic methods are near-infrared spectroscopy (NIR) [29] and Raman spectroscopy [30], which are beginning to be used in pharmaceutical manufacturing for monitoring drying operation units. These methods allow rapid quantification without sample preparation and can provide additional information associated with physical properties of the particles such as particle size and shape. Compared to NIR, Raman spectroscopy provides narrower spectra and simpler interpretation. However, its main drawback is that it requires chemometric models, which are typically system specific and require considerable development effort.

2.1.5 Contact drying kinetic models

Drying models have been developed to help understanding the systems behavior by using a set of equations, which correlate process parameters and material properties. Some of these models, namely penetration theory, discrete element method, pore networks and population balances are useful tools in optimizing drying processes.

2.1.5.1 Penetration theory

The penetration model was first proposed by Schlünder and coworkers [31], [20], back in 1980 and since then, it has been further developed and considered as present industrial standard. Their work was focused on contact drying in packed

beds as well as in mechanically stirred granular beds under vacuum or normal pressure. The findings on vacuum contact drying showed that the drying rate was a function of vapor pressure, heated surface temperature, stirring speed and moisture content. They showed as well that the supplied heat and vapor removal must overcome heat and mass transfer resistances (**Eq. (2.7) to Eq. (2.11)**). The heat transfer resistances include the contact resistance of the heated wall, the bulk and particle penetration resistance, while the mass transfer needs to overcome the permeation resistances of the particles and the bulk. For a static bed, all below resistances exist in series; however, this is not the case when it comes to agitated beds.

Heat transfer resistances

Contact:

$$\frac{1}{\alpha_{ws}} = \frac{T_w - T_o}{q_0} \quad \textbf{Eq. (2.7)}$$

Bulk penetration:

$$\frac{1}{\alpha_{sb}} = \frac{T_0 - T_b}{q_0} \quad \textbf{Eq. (2.8)}$$

Particle penetration:

$$\frac{1}{\alpha_p} = \frac{T_b - T_s}{q_{zT}} \quad \textbf{Eq. (2.9)}$$

where α_{ws} is contact heat transfer coefficient, ($Wm^{-2}K^{-1}$), α_{sb} is bulk heat transfer coefficient, ($Wm^{-2}K^{-1}$), α_p is particle heat transfer coefficient, ($Wm^{-2}K^{-1}$), q_{zT} heat flux into drying front, (Wm^{-2}), q_0 is heat flux into bed, T_w is hot surface temperature, K, T_b is bulk temperature, (K), T_s is saturation temperature, (K) and T_0 is interfacial temperature, (K)

Mass transfer resistances

Particle penetration:

$$\frac{1}{\beta_p} = \frac{p_s - p_b}{\dot{m}} \quad \textbf{Eq. (2.10)}$$

Bulk penetration:

$$\frac{1}{\beta_b} = \frac{p_b - p}{\dot{m}} \quad \textbf{Eq. (2.11)}$$

where β_p and β_b are particle and bulk permeation coefficient respectively, ($m\ s^{-1}$), p_s and p_b are saturation pressure at drying front and bulk pressure, bar, p is pressure in dryer, (bar) and $\dot{m}$ is drying rate,($kg\ m^2\ s^{-1}$)

In 1984, Schlünder and Mollekopf [19] further expanded the model considering the argument that the granular bed is randomly mixed. The penetration model is able to incorporate the random distribution of wet, partly wet and dry particles on the penetration heat transfer as illustrated in **Figure 2.2** [5]. According to the theory, the continuous mixing and drying process is switched between static and mixing periods. The bed is considered as a quasi-continuum with effective properties. The temperature at the heating surface is assumed to be known. The

heat penetrates from the heated wall to the bulk of the bed and is described as distinct front, **Figure 2.2 (b)**. Between the heating surface and the drying front, the particles are dry, while beyond that, the particles remain wet. In the wet part of the bed, the temperature is uniform and equal to the saturation temperature (T_s) of the liquid at the operating pressure. In the dry part of the bed, a temperature profile exists between the heating wall at T_w and the drying front at T_s. When the static period ends, perfect macro mixing is attained and the drying front penetration starts again **Figure 2.2 (c)-(e)** [32]. Even though, the penetration model has been known for quite a long time and is successfully used as an industrial standard, it fails to describe inter-particle interactions [20].

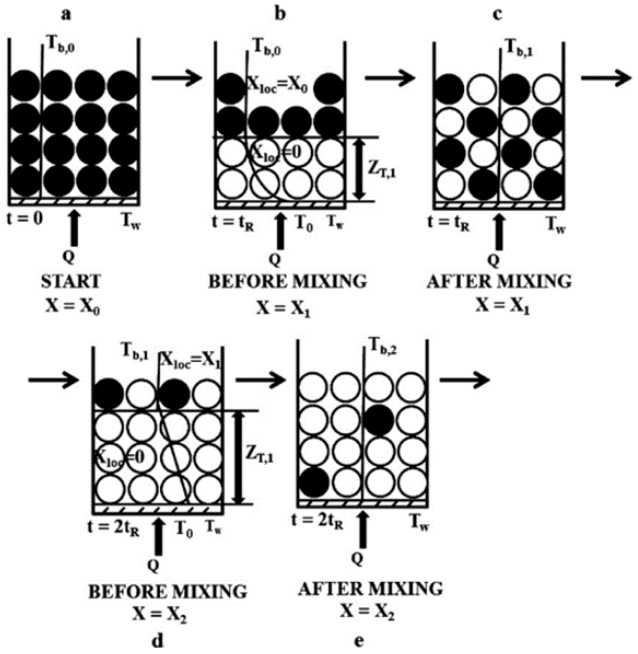

Figure 2.2. Graphical representation of the penetration theory

2.1.5.2 Discrete element method (DEM)

Condall and Strack [31], [33] were the pioneers of the discrete element method in late 1970s. This approach describes the dynamic behavior of individual particles such as particle positions, velocities and accelerations with the aim of modelling and optimizing the process. This information can then be used for calculating many parameters of interest including moisture content, local temperatures as well as study phenomena that are related to inter-particle interactions such as agglomeration or segregation [1]. DEM offers improved understanding of the process and reduces the number of experiments by providing accurate predictions outside the available experimental range. Other parameters such as equipment geometry, baffles design etc. can be modelled precisely, contributing significantly to process and product engineering using conduct dryers. Up until now, DEM approach was used either two-dimensional or in static granular beds due to limited computational power required to model more complex systems. However, with the assistance of supercomputers and other computing techniques, is possible to model larger and more complex systems with non-spherical particles.

2.1.5.3 Pore network

Pore network modelling is used to describe microscale flow and transport phenomena occurring during drying. Typically, they were helpful for simulating land drainage issues, however in the recent years they became very valuable in drying processes [1]. In a porous media, the network consists of randomly located pores, which are interconnected by throats. In order to produce realistic predictions, the selected networks should have representative size or a number of smaller network simulations are needed to get a general behavior. Pore network models can accurately predict for local transport (diffusion/permeation), and by varying the system's parameters such as pore space geometries, fluid properties, and boundary conditions, enables to assess their influence, that is difficult to be achieved experimentally [17].

2.1.5.4 Population balance models

Population balance modelling is an approach that provides an insight into the temporal change of particle property distributions with respect to internal and external variable spaces [34]. As particles go through a process, their external and internal coordinates change; the external because their physical location is altered and the internal because the particle characteristics such as size, shape, chemical composition etc. change through processing. Drying process simulations

have applied population balances to provide the time and spatial evolution of particle properties including temperature and moisture content. The applications of population balances to drying processes are discussed in the literature by various authors [34], [35].

2.2 Supercritical fluid technology

2.2.1 Supercritical fluids

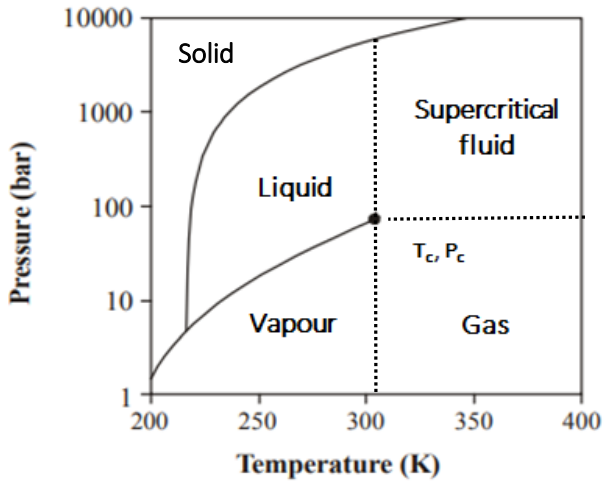

Figure 2.3. Pressure-Temperature phase diagram of CO_2.

Fluids where both temperature and pressure are above the critical point are defined as supercritical fluids (scF) [36]. As indicated in the phase diagram of pressure-temperature in **Figure 2.3,** the critical values T_c and P_c define the highest boundary where the vapour-liquid and liquid of the pure component are at phase equilibria. The dashed line area defines the supercritical region of the

substance. Within that area, no further condensation occurs increasing the pressure of the fluid. At these high pressures, the fluids combine liquid like and gas like properties. The density is similar to that of liquids but the diffusivity and viscosity are comparable to those of gases (**Table 2.1**). Hence, supercritical fluids have the solubilising power of conventional liquid solvents but with significantly better transport attributes [37]. Small modifications to the operating pressure or temperature can be used to fine-tune the solvation power of the fluid [38]. Additionally, the low surface tension enables the fluid to penetrate easily into porous materials, and even microporous materials [39].

Supercritical fluids are the most widely used industrial green solvents. They are characterised as environmentally benign, safe, cost efficient and recyclable. They offer a solvent-free and environmentally friendly alternative compared to conventional methods that often involve hazardous solvents. A particularly attractive characteristic is their ability to separate and dry a product by expansion where the gas can be easily recovered and reused directly [40]. In **Table 2.2** the critical conditions of some substances are presented.

Table 2.1. Characteristic properties of gas and liquid in comparison to those of supercritical fluids [41].

Properties	Gas	Supercritical Fluids	Liquid
Density (kg/m³)	1	100-800	1000
Viscosity (cP)	0.01	0.05-0.1	0.5-1
Diffusivity (m²/sec)	$1 \cdot 10^{-5}$	$1 \cdot 10^{-7}$	$1 \cdot 10^{-9}$

Table 2.2. Critical temperature, T_c and pressure, P_c of some substances [41].

Fluid	T_c (°C)	P_c (bar)
CO_2	31.1	73.8
H_2O	374.2	221
CH_3OH	239.9	80.8
C_2H_6	31.9	48.7
C_3H_8	96.7	42.5

2.2.2 Supercritical CO_2

The supercritical carbon dioxide ($scCO_2$) is the most widely used green solvent across the industry, due to its excellent properties [42]. It is chemically inert, non-flammable, non-toxic (though it can cause asphyxia) and it has low critical point (near ambient temperature 31 °C and pressure 73.8 bar) which is a very valuable characteristic in the case of thermally labile compounds. Also, because

it is a non-polar small linear molecule it has the ability to diffuse faster than the common liquid organic solvents. Additionally, it is cheap and readily available in bulk quantities with a high degree of purity.

One of the most notable properties that can be quite easily adjusted with slight changes in the supercritical region is the density. In the density-pressure phase diagram (**Figure 2.4**), the projection of CO_2 phase diagram is shown. Close to the critical temperature e.g. 310 K and around the critical pressure, the line is nearly vertical (highlighted in a red box in **Figure 2.4**). This means that a slight pressure increase in this region leads to a significant rise in the density of the supercritical phase [41]. In comparison to pressure, temperature has the opposite effects while keeping the pressure parameter constant. Many other physical properties also show large gradients with pressure near the critical point, e.g. viscosity and the solvent strength, which are all closely related to the density.

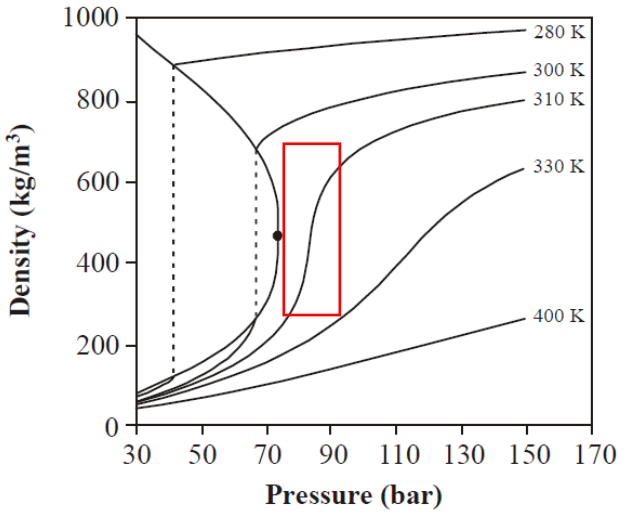

Figure 2.4. Density- pressure phase diagram of carbon dioxide.

2.2.3 Physical and chemical properties

Cubic equations of state are applied to estimate the physical and chemical properties of substances over a wide range of pressures and temperatures. In general, an equation of state is a thermodynamic expression that correlates the pressure with volume and temperature in order to describe the phase behaviour of pure components as well as mixtures. The name 'cubic' derives from the expanded equation which contains volume terms raised to the first, second and third power. The origin of cubic equations of state stems from the van der Waals equation, which was published in 1873 and was the first equation to represent qualitatively both vapour and liquid phases of mixtures [43]. Van der Waals equation accounts for the molecular volume and intermolecular forces of

attraction; parameters that were not included in the ideal gas law (PV=RT). Thereafter, several modifications of this equation have been suggested and are applicable in providing satisfactory predictions of vapour-liquid equilibrium of mixtures. Three well-known cubic equations are Redich-Kwong, Soave and Peng-Robinson [44].

Besides cubic equations of state, more sophisticated models based on statistical mechanics, such as the Statistical Associating Fluid Theory (SAFT) [45], [46] and Perturbed Chain-SAFT (PC-SAFT) [47], [48] have been developed to handle systems with hydrogen bonding compounds. However, they may not consistently surpass cubic equations of state, especially in high-pressure systems involving CO_2 and alkanes (12–14 carbon atoms) and alcohols [49]. The preference for cubic equations of state stems from their robustness and ease of implementation, making them suitable for initial modelling efforts concerning complex mixtures. Here, the Peng-Robinson cubic equation of state (PR-EOS) [50] is used to estimate the CO_2 properties at different pressures and temperatures. The PR-EOS is used since it requires little input information and little computational effort. The PR-EOS equation is written as:

$$P = \frac{RT}{V-b} - \frac{\alpha}{V\cdot(V+b)+b\cdot(V-b)} \quad \textbf{Eq. (2.12)}$$

For pure substances, the parameters α and b can be calculated by the critical properties and acentric factor.

$$\alpha = 0.457235 \cdot \frac{R^2 \cdot T_c^2}{P_c} \cdot \alpha \quad \textbf{Eq. (2.13)}$$

$$b = 0.077796 \cdot \frac{R \cdot T_c}{P_c} \quad \textbf{Eq. (2.14)}$$

$$\alpha = [1 + m \cdot (1 - \sqrt{\frac{T}{T_c}})]^2 \quad \textbf{Eq. (2.15)}$$

$$m = 0.37464 + 1.54226 \cdot \omega - 0.26992 \cdot \omega^2 \quad \textbf{Eq. (2.16)}$$

For mixtures, the van der Waals mixing rule is used; a and b are calculated from the equations:

$$\alpha = \sum_i \sum_j x_i . x_j \cdot \sqrt{\alpha_i \cdot a_j (1 - k_{ij})} \quad \textbf{Eq. (2.17)}$$

$$b = \sum_i \sum_j 0.5 \cdot x_i . x_j \cdot (b_i + b_j) \cdot (1 - I_{ij}) \quad \textbf{Eq. (2.18)}$$

where x_i is the mole fraction of the i component; α_i and b_i are the pure substance parameters defined by Peng and Robinson; and k_{ij} and l_{ij} are the binary interaction parameters for the (i, j) pair. The physical property information (Tc, Pc, and ω) used for the pure components are available in the literature (e.g. NIST library)

The binary interaction parameters k_{ij} and $l_{ij\ are}$ are empirical values that can be obtained by minimising the average absolute deviation for bubble and dew point pressures. Jaubert and coworkers [51] developed a group contribution method that allows the estimation of k_{ij} between two components at any temperature.

This method relies widely on PR-EOS and is a predictive approach, named PPR78 (predictive 1978, Peng Robinson EOS) [52]. For example, the PPR78 model could be used to calculate the k_{ij} between two components in any mixture containing paraffins, naphthenes, aromatics and CO_2.

2.2.4 Applications of supercritical CO_2

Supercritical fluid technology, particularly utilising carbon dioxide, has found diverse applications across various fields due to its advantages. Here is a summary of some of its applications along with a few examples:

a) **Aerogel Production:** Supercritical fluid drying is widely used in the production of aerogels, which are highly porous materials with applications in insulation, catalysis, and drug delivery systems [53], [54], [55], [56]. The advantage of using supercritical CO_2 lies in its ability to efficiently remove solvent from the gel matrix without causing structural collapse, resulting in aerogels with high porosity and low density.

b) **Extraction and fractionation**: Supercritical fluid extraction and fractionation are commonly employed in various industries [57]. Examples include the extraction of natural antioxidants from wine industry by-products [58], extraction of essential oils from various herbs and plants [59], [60], [61], [62], [63] and the extraction of bioactive compounds [64], [65], [66].

c) **Chromatography and analytical chemistry**: Supercritical fluid chromatography is a powerful technique for separating and analysing various compounds, including pharmaceuticals and natural products [67], [68]. It offers advantages such as rapid analysis and environmental friendliness.

d) **Crystal engineering and polymorph control:** Supercritical fluid processing is applied to control the crystalline form of drugs, enhancing their solubility and bioavailability. Techniques like rapid expansion of supercritical solutions (RESS) [69], [70], [71], [72] and supercritical anti-solvent (SAS) precipitation [73], [74], [75] are utilised for polymorph control.

e) **Food and beverage processing**: Supercritical CO_2 is utilised for the decaffeination of coffee and tea, extraction of flavours and fragrances, and the removal of lipids from food products [76], [77], [78], [76], [79]. It offers advantages such as mild processing conditions and solvent-free extraction. Additionally, supercritical CO_2 drying has emerged as an effective alternative to traditional drying methods, particularly for enhancing food safety and quality. This technique has been successfully applied to various food products, demonstrating both drying efficiency and microbial inactivation. For example, $scCO_2$ drying has been used for coriander leaves, apple slices,

strawberry slices, and carrots, achieving significant reductions in microbial contamination [80], [81], [82], [83].

f) **Environmental applications**: Supercritical fluids are applied in environmental remediation for the extraction of contaminants from soil and water [84], [85]. They offer efficient removal of pollutants while minimising the use of organic solvents and reducing waste generation.

g) **Drug encapsulation and delivery systems:** Supercritical fluids are employed in the encapsulation of drugs within carriers or matrices, enhancing drug stability and bioavailability [86], [87]. For instance, supercritical CO_2 is used to form lipid-based nanoparticles or liposomes for drug delivery [88].

h) **Sterilisation and cleaning:** Supercritical CO_2 is utilised for terminal sterilisation of pharmaceutical products, offering an effective and environmentally friendly alternative to conventional methods [89], [90], [91].

These examples illustrate the versatility and significance of supercritical fluid technology across various industries and research fields. Other possible uses of supercritical CO_2 can be found in a review by Ramsey et al. [45].

2.2.5 Supercritical fluid extraction (SFE)

This thesis reports an experimental investigation of the extraction of organic solvents from APIs with $scCO_2$; this can be seen as an extension of the supercritical fluid extraction (SFE) processes applied to natural products.

During a SFE process, the targeted compound is extracted from a fixed bed loaded into an extraction chamber by using supercritical or near-critical CO_2. The pressurised gas flows continuously through the bed, where CO_2 molecules diffuse into the pores and interact with the compound to be extracted. Then, the analyte is transferred in the pressurised CO_2 phase and carried over at the exit of the unit where the fluid is depressurised to a gaseous state and the solute precipitates in a collection vessel. Typically, the process is conducted until the mass of the accumulated solute remains constant.

2.2.5.1 Extraction curves

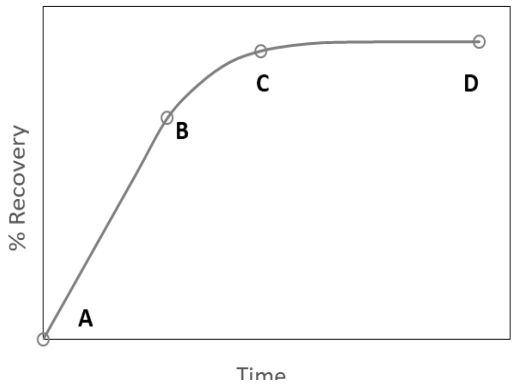

Figure 2.5. General extraction profile.

Overall extraction curves are generated by plotting the accumulated amount of the extract versus time. **Figure 2.5**, shows an example of a typical extraction curve, which consists of three extraction periods. At the early moments of the process (A-B), the extraction rate is constant as the easily accessible solute is extracted. Subsequently, the extraction is hindered (B-C) due to depletion of easily accessible solute, and at the later stages (C-D), it becomes diffusion-controlled process. This last stage continues until the entire solute is extracted and is represented by a flat line in the curve indicating the endpoint of the process.

2.2.6 Parameters that affect the supercritical CO_2 extraction

Many authors [92], [37], [93], [94], [95], [96] have discussed the parametric effects on $scCO_2$ extraction yield. The main parameters affecting the solute recovery are pressure, temperature, flow rate, bed length as well as the particle size of the solids. Other factors that have a great influence on the extraction yield of material extracted from a porous solid natural substrate are the pre-treatment of the substrates such as drying and milling, apparent density of solid loaded and initial analyte content in the substrate, which will not be discussed in the sections below.

2.2.6.1 Pressure and temperature

Pressure and temperature affect directly the physical properties of supercritical fluids including density, viscosity and diffusivity. High pressure increase the density and the solvation power of the fluid, which therefore result in better recovery yields [36]. On the other hand, temperature has an inconsistent effect on the fluids properties. High temperatures increase the diffusivity and the apparent volume; while at the same time reduce the "solvent" strength of the supercritical fluid. However, low temperatures decrease the vapour pressure of the solute and raise the density of the fluid [97]. These competing events result in a phenomenon called the "crossover effect" where high temperatures can result in low yields, while low temperatures exert the opposite effect. Previous studies have shown that close to the critical pressure the yield tends to decrease with increasing temperature [98], [99]. While at pressures >200 bar, the solubility of the substance to be extracted in the supercritical fluid phase becomes temperature independent [92].

2.2.6.2 CO_2 flow rate

By varying the gas flow rate, no changes to the physical properties of the supercritical fluid are expected [92]. A faster flow rate though, leads to a faster extraction particularly in the early stages of the process where the solute

concentration is high. Moreover, a sufficiently high flow rate is essential to overcome mass transfer resistance that limits the amount of solute transported into the fluid phase. However, very high flow rates reduce the $scCO_2$ residence time and the fluid exits the extractor without reaching saturation.

2.2.6.3 Bed height

Lu et al. [100] investigated the effect of different bed lengths on supercritical fluid extraction. It was observed that the increase of the bed length results in a noticeable increase in the extraction rate and recovery yield. The extended residence time of CO_2 in the case of longer beds explains the closer approach to the saturation limit and hence the improved extraction yield.

2.2.6.4 Particle size

Yin et al. [101] performed extraction experiments on samples with different sizes of particles. They concluded that extraction from smaller particles resulted in greater yields, since the decrease in the particle size enhances the mass transfer. The surface area available for extraction increases and there is more exposure and contact with the fluid allowing a higher extraction rate. However, the use of small particles is not always preferable, as agglomeration or channelling may occur in tightly packed beds especially in the case of fine particles, leading to a poor performance. On other hand, Ozkal et al. [102] reported that the mass

transfer coefficients decrease with large particles due to the decrease in the specific surface area.

2.2.7 Mathematical modelling for supercritical fluid extraction

Many mathematical models have been developed to describe the overall fixed bed behaviour during SFE and the most valuable ones are based on differential mass balance equations. Of these models, some are classified as hot sphere, broken and intact cells (BIC) and shrinking core (SC) models [103].

2.2.7.1 Hot sphere diffusion model

Bartle et al. [103] proposed the hot sphere model for describing the supercritical fluid extraction process by analogy to heat transfer phenomenon. This model assumes that the extracted particles are like hot spheres that cool down in the surroundings. The uniformly distributed solute diffuses through the matrix in a similar manner to heat diffusion following a number of stages in a sequence. Initially the CO_2 diffuses in the $scCO_2$ solution film that surrounds the spherical particle and then it is adsorbed on the particle surface and diffuses into the solid matrix. The analyte is dissolved in the solvent phase and diffuses out of the particle. Finally, the analyte diffuses through the $scCO_2$ solution film into the bulky solvent phase. The hot sphere model is useful for calculating diffusion coefficients, since up until now there is lack of available diffusivity data for solid

matrices. Many applications of the model on SFE processes can be found in the literature [104], [105].

2.2.7.2 Broken and intact cell (BIC) model

Sovova [106] introduced the broken and intact cells (BIC) model to mathematically describe $scCO_2$ extraction processes in natural materials that have been pre-treated by milling, grinding or crushing before being loaded into the extractor. This model is based on Lack's [103] plug flow model and is mainly applied for extraction of analytes from ruptured cells where some solute is easily accessible at the surface of particles while the rest is located in the solid matrix and less accessible. The easily accessible solute is extracted quickly by convection and diffusion in the solvent phase and the less accessible is extracted from the intact cells slowly due to the high mass transfer resistance. The BIC model finds many applications in oil extraction from seeds, leaves, flower roots and fruit peels [107], [108].

2.2.7.3 Shrinking core model (SCM)

The shrinking model assumes that the solute inside the particle is located within a core that shrinks as the extraction progresses. When the mass transfer rate of the solute in the non-extracted inner part is much slower than that in the outer part, where most of the solute has been extracted, or solute concentration is

much higher than the solubility of the solute in the solvent phase, a sharp boundary may exist between the outer and inner regions. These situations can be modelled using the SC model [103].

The model takes into account the resistance in one or both of the bulk phases. It includes particle and bed characteristics via porosity and diameter. Although the model implies many assumptions and/or determination of several coefficients involved in the equations, it reflects the various mechanisms that contribute to the overall behaviour of an extraction process. Some of its applications on natural matter extraction can be found in the literature [109], [110]. Moreover, Orlovic et al. used shrinking core models to simulate the diffusion of solvent through the pores of alumina/silica gels during drying [111], [112].

2.3 Summary

Agitated filter dryers offer a combined solution for filtration and drying in pharmaceutical manufacturing, enhancing process control, reducing contamination risks, and minimising product handling. Understanding the fundamentals of drying, including drying kinetics and parameters affecting performance, is crucial for optimising AFD operations. Key parameters such as temperature, pressure, bed height, agitation, and particle size significantly influence drying kinetics. Advanced techniques like online process analytical

tools (PAT) enable real-time monitoring and control of drying processes, reducing cycle time and enhancing product quality. Additionally, various drying kinetic models, such as penetration theory, discrete element method (DEM), pore network, and population balance models, provide insights into the complex phenomena occurring during drying processes.

Supercritical fluid technology has revolutionised various industries due to its unique properties and environmentally friendly nature. Supercritical fluids possess a balance of liquid-like and gas-like properties, offering enhanced solubilising power and excellent transport attributes. Among these, supercritical CO_2 stands out as the most widely used solvent due to its chemical inertness, low critical point, and availability. Moreover, the physical and chemical properties of substances in supercritical conditions can be accurately estimated using cubic equations of state, particularly the Peng-Robinson equation. This allows for precise modelling and prediction of extraction processes, essential for various applications. Supercritical CO_2 is extensively used in aerogel production, food processing, environmental remediation, and pharmaceuticals, excelling in extraction, fractionation, chromatography, and crystal engineering. Understanding the parameters affecting supercritical CO_2 extraction, such as pressure, temperature, flow rate, bed height, and particle size, is crucial for

optimising extraction processes. Mathematical models like the hot sphere, broken and intact cell, and shrinking core models aid in describing and predicting extraction behaviour, facilitating process optimisation and scale-up.

3 Agitated filter dryer (AFD)

This chapter demonstrates an experimental approach that utilises MODDE software for optimising the drying performance using a lab-scale agitated filter dryer. Given a fixed geometry setup, several parameters are varied to determine the desired process conditions for drying paracetamol powder filter cakes wet in dodecane. Such parameters are jacket temperature, drying mode, cake size and nitrogen flow rate. Their effect on the final product attributes is also investigated and the results obtained are used to support the research of $scCO_2$ extractive drying as a potential new drying technique.

3.1 Materials

Paracetamol powder (D_{10}=24 µm, D_{50}=64 µm and D_{90}=179 µm particle size and 1.24 g/cm^3 true density) was supplied by Mallinckrodt, propan-2-ol (≥ 99.5 % purity) by Sigma Aldrich and n-dodecane (≥ 99 % purity) by Alfa Aesar. All the materials are used without any further purification.

3.1.1 Active pharmaceutical ingredient (API)

Paracetamol powder, a pharmaceutical of major importance, was chosen as a model compound to study. Paracetamol, also known as acetaminophen, is a medicine used commonly as a pain killer and antipyretic [113]. The drug is commercially available in various forms including tablets, capsules, liquid suspensions, and suppositories [114].

It is slightly soluble in nonpolar and chlorinated hydrocarbons, whilst highly soluble in solvents of medium polarity. For instance, polar compounds such as alcohols are very good solvent candidates for the dissolution of paracetamol [115].

Because it is a widely used medicine, there is a large body of useful data available in the literature [116]. Additionally, paracetamol has low toxicity and is a relatively cheap compound, making it a good candidate for research purposes.

3.2 Apparatus

A lab-scale 500 mL agitated filter dryer was fabricated by Alconbury Weston Ltd (AWL) to perform conventional thermal drying under vacuum, **Figure 3.2**. The equipment is a copy of a common industrial dryer, designed to accommodate the cylindrical stainless-steel basket **Figure 3.1**, which was manufactured for the supercritical CO_2 setup. The basket is equipped with a 5-micron frit at the bottom enabling filtration, washing and drying to take place in a single container. Thus, API cakes of similar properties were formed by using the AWL kit and dried in two different ways. In the case of supercritical CO_2 extraction/ drying, the basket was transferred carefully in the high-pressure vessel, maintaining the cake structure untouched.

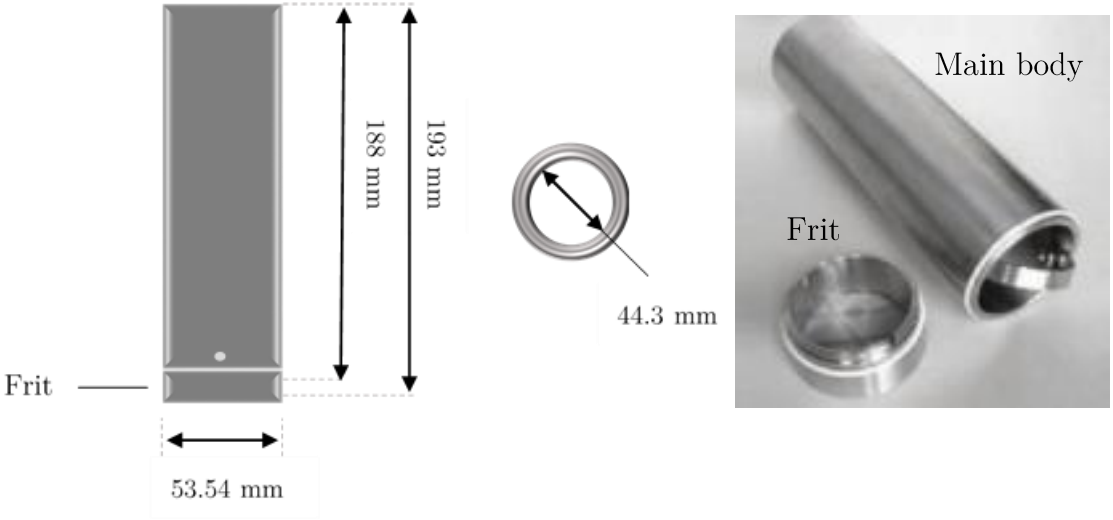

Figure 3.1. Stainless-steel extraction basket used for the supercritical CO_2 extraction/drying.

The main body consists of a heavy stainless-steel cylindrical chamber and a lid with an agitator (d=4.1 cm) that seals the vessel from the top. The chamber is heated through a water jacket that surrounds the surface of the vessel. This closed-loop heated jacket creates excellent heat transfer and rapidly achieves the required temperatures. By introducing agitation, it is possible to facilitate the heat exchange between the vessel and the particles within the filter cake due to the increased temperature homogeneity of the cake in the basket.

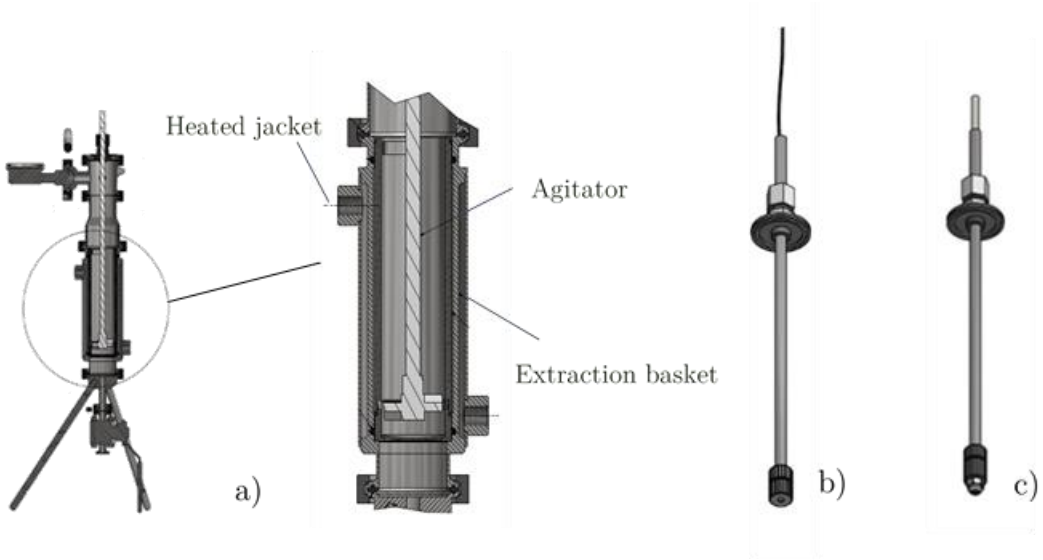

Figure 3.2. Agitated filter dryer constructed by AWL; (a) Main body (internal height ~ 200 mm and internal diameter ~56 mm), (b) USB-camera lid and (c) Nozzle-spay lid.

Moreover, two extra lids were designed to complement the existing one with the agitator; each lid used at different stages of the isolation process. The first one contains a spraying nozzle of 45^{o} degrees spraying angle. This permits gentle cake washing and uniform displacement of the mother liquor without disturbing the

packed bed of the cake. The second lid contains a USB camera that serves to select the filtration and washing endpoint to be dryland or breakthrough. On breakthrough, a deliquored cake is obtained, while on dryland the cake remains saturated with the solvent phase.

The chamber is connected to a vacuum pump and a house nitrogen supply that will be further discussed in the following subsections.

3.3 Methods

3.3.1 Selected filtration and washing conditions

Previous experimental studies have been conducted in the Centre for Continuous Manufacturing and Crystallization (CMAC) to develop best practice of the isolation process steps using a range of lab scale filtration technologies. The Biotage VacMaster is probably the simplest filtration design, and has been applied in many scientific projects that aimed to investigate the optimum separation conditions for a variety of systems. A reliable experimental database was created based on these projects, which covers a large number of factors for different combinations of crystallisation and wash solvents [17]. Acetaminophen has already been studied extensively in CMAC focusing on the upstream crystallization processes for the reasons mentioned in section **3.1.1.**

In this work, filtration and washing parameters were selected according to the experimental research that has been executed by a masters student, Martin Šimurda [17] whose thesis was focused on solvent selection for isolation processes. Specifically, he tested a wide spectrum of factors using a DOE methodology in order to investigate the agglomeration occurring under various operating filtration, washing and drying conditions. These factors included a number of crystallisation and wash solvents, different cake preparations regarding particle size and solid load, filtration/washing endpoints and drying methodologies. The main responses were the level of impurities in the final product, the extent of particle agglomeration and the agglomerate hardness with the latter being strongly related to the isolation process efficiency. Although he concluded that particle agglomeration could not be totally avoided, his research offers a complete and useful guideline for optimising the isolation process steps. **Table 3.1** shows the best combination of factors that resulted in high quality product using the Biotage VacMaster work station.

Table 3.1. Optimum combination of factors for the best isolation performance for 9 g, paracetamol cake.

Pressure (mbar)	500	**Number of washes**	2x
Crystallisation solvent	Ethanol	**Solid load**	30 vol%
Wash solvent	Cyclohexane	**Material grade**	Paracetamol powder
Volume of wash solvent	3 void cake volumes	**Filtration/washing end point**	Dryland

While Šimurda's findings delivered good isolation performance, some of these parameters have been adjusted to serve the purposes of this thesis. According to **Table 3.1**, cyclohexane displaces the mother liquor effectively and can be easily removed by means of conventional drying. Switching it though for dodecane, provides a challenge for both supercritical CO_2 extraction/drying and conventional drying. Dodecane is a high boiling point solvent with relatively low vapour pressure [117] which makes it extremely difficult to dry the wet filter cake. Additionally, dodecane is a competent wash solvent candidate and the amount of four cake void volumes is adequate for delivering a successful cake washing. Another adjustment related to API cake washing is the number of washing steps. In the present study, the entire amount of solvent is continuously pumped into the basket due to equipment limitations. The lab-scale agitated filter dryer is designed in a way that can fit only one lid mounted tool at a time.

Splitting the washing in two consecutive steps would require swapping the spraying nozzle with the USB camera multiple times. Hence, continuous washing is more practical and also, opens up new considerations for cake washing performance. Other alterations to Šimurdas' procedure involve the slurry preparation. Propan-2-ol is preferable crystallisation solvent, since it has very similar properties to ethanol and is commonly used in many CMAC projects. Lastly, the percentage of solids in the suspension was 25%, slightly less than 30 vol % of the saturated solution. A less dense slurry filters more rapidly giving a shorter cake formation time. Thus, the final filtration and washing factors are gathered together and presented in **Table 3.2,** as fixed parameters.

Table 3.2. Filtration and washing fixed parameters.

Pressure (mbar)	500
Crystallisation solvent	Propan-2-ol
Solid load	25 vol %
Wash solvent	n-Dodecane
Volume of wash solvent	4 void cake volumes
Number of washes	Continuous wash addition
Material grade	Paracetamol powder
Filtration/washing endpoint	Dryland

3.3.2 Selected drying conditions

The conventional way of drying used in this study, includes thermal drying under vacuum by using the agitated filter dryer showed in **Figure 3.2**. This way of drying is well established in the pharmaceutical sector and extensively researched in chemical engineering [26], [13], [22]. Experimental studies [1], [26] show that the efficiency of drying is not only closely related to the effectiveness of the previous process steps, but also to the selected operating drying conditions.

Parameters like temperature, gas flow rate, agitation and solid mass are the variables studied. The vacuum applied to the vessel could be also considered as a manipulated factor, but in practice, it was best to use a fixed moderate pressure $\sim$ 500 mbar for all the experiments, preventing in this way likely cake cracking at small solid volumes. Furthermore, achieving a vacuum of less than 500 mbar and simultaneously maintaining a flow of nitrogen posed challenges attributable to equipment leakages.

In most drying processes, vacuum drying is combined with a small flow of an inert gas, in this case nitrogen that removes the residual vapour from the sample. One factor that could affect drying is the gas flow rate that is worth to be investigated. Values taken from literature [26] are modified according to the

cross-sectional area of the cake (A=0.00154 m^2) formed into the extraction basket **Table 3.3.**

Table 3.3. Calculated nitrogen flow rates in lab scale.

Industry	**Laboratory**
500-1000 L/min/m^2	0.8-1.5 L/min

From preliminary experiments, the nitrogen flow rate of 1.5 L/min was found to be quite high, as the vacuum pump could not reach the set point; therefore values ranged between 0.2-0.8 L/min were used for investigation. A second factor that influences the drying performance is the temperature of both the heated nitrogen and vessel. Introducing heated nitrogen into the system is anticipated to increase the drying efficiency due to better heat and mass transfer rates. The nitrogen temperatures investigated varied between 50-70 ^oC and were the same as the ones chosen for supercritical CO_2 extraction/drying. In this way, it was possible to compare the effectiveness of the two drying methods under similar conditions. Agitation is another factor of significant importance; a downside of its application is the undesirable particle attrition. The simplest solutions to minimise this effect, is to use low stirring speed or reduce the time of the agitating period. Thus, continuous and intermittent agitation were examined

using the minimum rotational speed of 5 rpm. Finally, three different API cake sizes of 60 g (30 %), 105 g (50 %), and 150 g (70 %), were dried in order to observe the effect of solid load and solvent content on drying kinetics. The 150 g cake represents the maximum size that allows sufficient headspace for washing to be conducted, whereas the selection of 60 and 105 g was arbitrary.

3.3.3 Design of experiments (DOE)

After identifying the parameters with the most influential effect on drying, an experimental plan was carefully prepared using statistical analysis DOE methodology. DOE uses applied statistics to examine complex problems that involve a large number of variables. It is a useful tool for planning and executing a set of representative experiments that provide a detailed picture of the system by eliminating a number of possible combinations of factors. This strategy is a quick approach and less laborious, considering the cost for conducting each experiment [118].

There are many capable and user-friendly software packages for design of experiments. The University of Strathclyde provides access to MODDE Pro V11.0.1 software, which is developed by MKS Umetrics AB. The experimental screening is represented by factors and responses. Factors are the parameters to be varied such as; temperature, nitrogen flow rate etc., whilst responses are the

outputs acquired from the experiments (residual solvent content, drying time, LOD, ABI factor, extent of agglomeration). The next step is the selection of the DOE objective, which in this case is the optimisation of the process. Thus, a D-optimal design was selected to generate a worksheet of the subset of all possible combinations **Table 3.4**. When all the experiments had been performed and the responses were obtained, a series of steps of data analysis were followed to give an overview of the model performance and predictions of the most suitable operating conditions for optimising the drying process.

Table 3.4. A D-optimal experimental design produced using MODDE software.

Experiment No.	Temperature (°C)	Nitrogen Flow rate (L/min)	Solid mass (g)	Drying Mechanism
1	50	0.8	60	Static
2	70	0.8	60	Static
3	70	0.8	60	Continuous[†]
4	50	0.2	60	Continuous[†]
5	50	0.8	60	Intermittent[**,†]
6	70	0.2	60	Intermittent[**,†]
7	50	0.2	60	Intermittent[**,†]
8	70	0.8	60	Intermittent[**,†]
9	70	0.2	105	Static
10	50	0.5	105	Static
11	50	0.8	105	Continuous[†]
12	70	0.2	105	Continuous[†]
13[*]	60	0.5	105	Intermittent[**,†]
14[*]	60	0.5	105	Intermittent[**,†]
15[*]	60	0.5	105	Intermittent[**,†]
16	50	0.2	150	Static
17	70	0.8	150	Static
18	70	0.2	150	Continuous[†]
19	50	0.8	150	Continuous[†]
20	50	0.2	150	Intermittent[**,†]
21	50	0.8	150	Intermittent[**,†]
22	70	0.2	150	Intermittent[**,†]
23	70	0.8	150	Intermittent[**,†]

** Experiments 13, 14, and 15 serve as the central points in the Design of Experiments (DOE), and they will be utilised to assess the reproducibility of the process.*

***The cake is stirred for ten minutes and then left to dry in static motion for another ten minutes, following which a new round of stirring begins.*

[†]For experiments that involve agitation, the stirring speed is set at 5 rpm.

3.3.4 Experimental procedure

The experimental procedure was separated into four process steps; sample preparation, filtration, washing and drying, **Figure 3.3.**

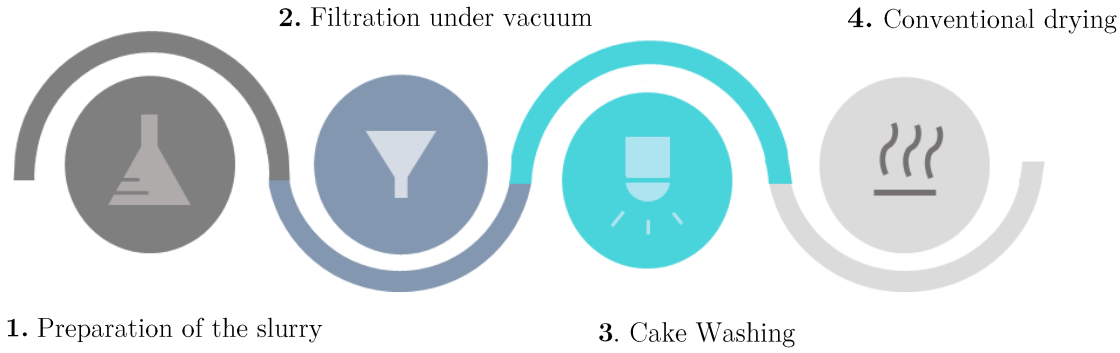

Figure 3.3. Experimental procedure of the isolation process.

3.3.4.1 Preparation of slurry

To begin with, fresh slurry was prepared from paracetamol/propan-2-ol saturated solution. Given the solubility of paracetamol in propan-2-ol at room temperature [119], an excess amount of material was introduced into the crystallisation solvent. After allowing the suspension to equilibrate overnight with stirring, the remaining solids were removed with a Buchner filter to isolate the saturated solution. Next, extra paracetamol was added to form cakes of different sizes, shown in **Table 3.5**. The solid load constituted approximately 25 vol %. of the saturated solution. Then, the suspension was stirred for five

minutes to ensure all the particles were well wetted and dispersed and then it was transferred into the stainless steel extraction basket, which had been placed into the AWL filter dryer body beforehand.

Table 3.5 The quantities used to prepare saturated solutions for the three different cake sizes.

		60 g cake		**105 g cake**		**150 g cake**	
	Density (g/cm^3)	**Mass (g)**	**Volume (ml)**	**Mass (g)**	**Volume (ml)**	**Mass (g)**	**Volume (ml)**
Propan-2-ol	0.786	180.4	230	316	402	452	575
Paracetamol	1.242	19.6	15.8	34.3	28.3	49	39.5

**The solubility of paracetamol powder in propan-2-ol at 20 °C, is 0.109 (g solute/g solvent).*

3.3.4.2 Filtration

The following step involved the isolation of particles from the mother liquor by filtering the slurry under vacuum at room temperature. A KNF diaphragm moist gas vacuum pump (N.860.3 FT.40.18) (1) with maximum pumping speed of 60 L/min was connected to the AWL unit as presented in **Figure 3.4.**

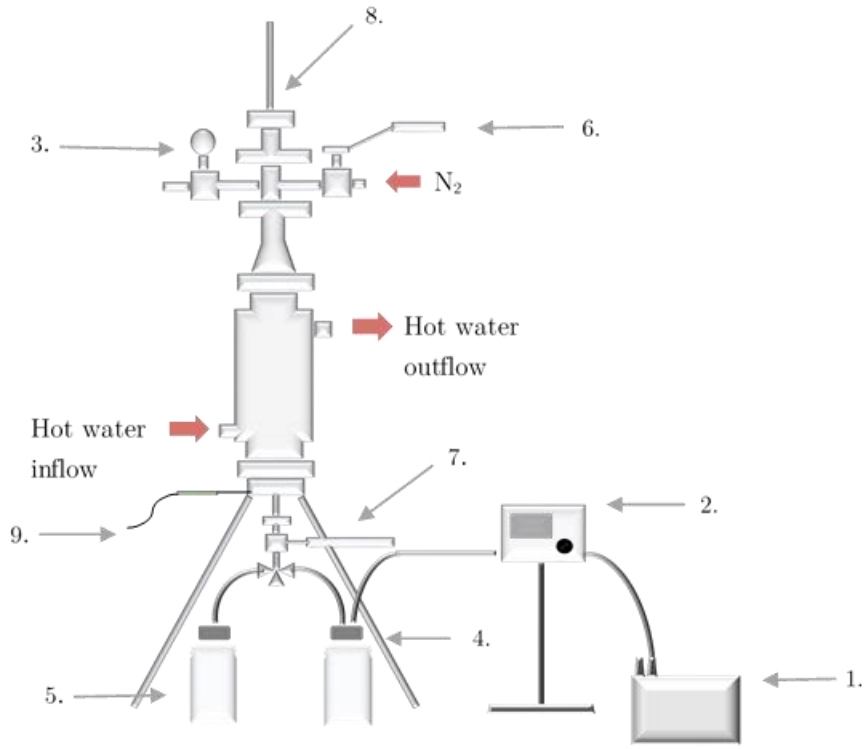

Figure 3.4. An illustration of the AWL pocket filter drier equipment connected to the vacuum pump; 1. Vacuum pump, 2. Vacuum controller, 3. Pressure gauge, 4. Mother liquor container, 5. Wash solvent/impurities container, 6. Valve-1/Nitrogen connection, 7. Valve-2/Vacuum connection, 8. Lid that contains a USB camera, 9.Thermocouple.

The pressure was set at 500 mbar through a regulator (2) that kept the vacuum level constant. When the total amount of slurry had been poured into the basket, the pump was switched on and the bottom valve (7) of the vessel opened, allowing the filtrate to flow through PTFE tubing into the collection container (4). During filtration, the particles settled in layers on top of the filter medium and after a while, the solid formed a cake. Only the layer adjacent to the filter underwent the entire amount of pressure while the top layer remained uncompressed. It was advantageous to leave the cake saturated before washing

in order to avoid cake cracking that would have had an effect on the subsequent stages. For this reason, the use of camera (8) was essential to observe from the top the cake evolution during filtration. When the surface of the cake was exposed to the air, the valve was shut within few seconds and the system was isolated from the vacuum pump. Both the sample and the collected filtrate were weighed with an electronic balance, which could be read with 0.01 g accuracy.

3.3.4.3 Washing

Any remaining mother liquor in the cake was removed during washing. An ample amount of dodecane slowly displaced the mother liquor that wetted the surface area of the particles or was occluded in the filter cake. This step was vital for the drying efficiency as particle agglomeration is associated with the presence of crystallisation solvent in the cake [13]. It is noteworthy to mention that the solubility of paracetamol in dodecane at room temperature is approximately 0.072 mg/g of solvent which means insignificant amount of API is lost during washing [120].

After filtration, the height of the formed bed was measured with a ruler inserted into the filter basket in order to determine its volume. This allowed the target quantity of the wash solvent to be estimated from **Eq. (3.1)**. One cake void volume is the space occupied by mother liquor (or partially by gas) in between

the particles and can be calculated by subtracting the volume of paracetamol powder added from the overall volume of the wet cake. As mentioned above (section **3.3.1**), the total amount of wash solvent refers to four times the wet cake's void volume.

$$V_{void} = V_{wet\,cake} - V_{solid} = \pi \cdot r^2 \cdot h_c - \frac{m_s}{p_s}, \qquad \textbf{Eq. (3.1)}$$

where r is the inner radius of the basket, h_c is the height of the cake m_s is the mass of the solid and ρ_s is its density

Table 3.6. The total amount of dodecane used for each cake size, calculated with **Eq. (3.1).**

Mass of cake (g)	60	105	150
Height of cake (cm)	5.5	9.5	13.5
One void cake volume (ml)	36	63	87
Total volume (ml)	144	252	350

The exact amount of wash solvent was made ready for use (13) (**Figure 3.5**), and it was introduced into the system through a peristaltic pump (11). A Tygon flexible tube was chosen for pumping the wash solvent as it has high chemical resistance towards dodecane. The speed of the pump rotor was tuned to achieve a smooth, consistent flow of the solvent, which was sprayed in fine mist through a nozzle (12) on the top of the cake.

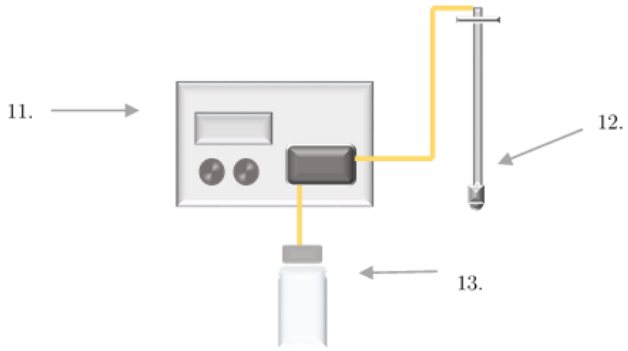

Figure 3.5. A peristaltic pump connected with spray nozzle for gentle cake washing; 11. Peristaltic pump, 12. Lid that contains a spray nozzle, 13. Wash solvent.

At the beginning of each washing step, approximately one cake void volume of dodecane was spayed into the basket. The surface of the cake was re-wetted with solvent and a layer of pure wash liquid was formed above it. Then, the bottom valve (7) was opened and vacuum was applied to the system. Mother liquor was slowly driven into the second container (5), and was simultaneously replaced in the cake by dodecane, which thereby kept the cake saturated without disturbing the inner packing. The rest of the solvent was constantly pumped, until the whole amount was added. Finally, the lid with the camera was used enabling the filtration to stop to dryland and the mass of the washed cake was recorded.

3.3.4.4 Conventional thermal drying under vacuum

The last step of the particle isolation process was drying. This experimental approach coupled conductive and convective drying means to achieve fast and effective solvent removal.

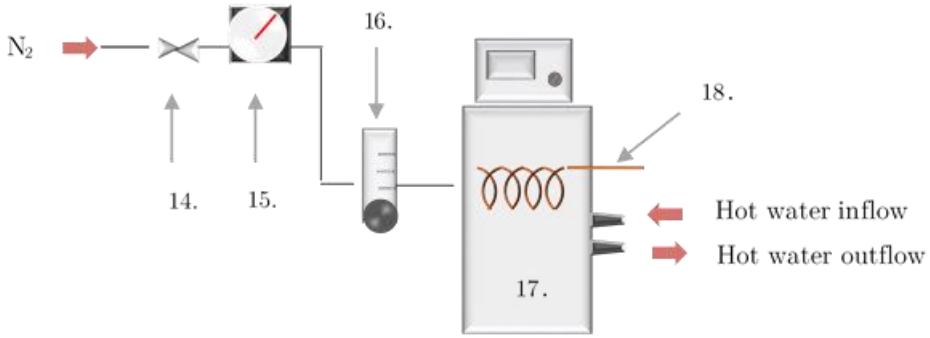

Figure 3.6. A schematic diagram of the heater unit connected with AWL kit; 14. Valve-3/nitrogen inlet, 15. Pressure regulator, 16. Air flow meter, 17. Water circulation system, 18. Copper coil.

A heater circulator unit (Lauda) (17) was assembled in the way it is illustrated in **Figure 3.6** and was connected through water piping with the AWL kit (**Figure 3.4**). The main heating source consisted of water circulation system that fed the jacket of the vessel with a closed water loop circuit. This unit contained an internal pump with a constant flow rate, a water bath of 5 L capacity and a thermostat, which sustained the temperature to set point. Also, nitrogen was introduced into the vessel after it was heated to the corresponding temperature of the equipment. The pressure and the flow rate of the gas could be easily manipulated with the use of a regulator (15) and a simple rotameter

(16) respectively, following the order presented in **Figure 3.6**. Moreover, a flexible thermocouple (9) was located close to outlet of the vessel (**Figure 3.4**) and was connected to a digital indicator. The displayed values represented temperature measurements of nitrogen throughout drying.

Before drying began, the wet cakes were preheated for approximately 30 minutes by circulating the heat transfer fluid through the filter jacket. When the nitrogen supply was opened, the valve (14) was turned, and nitrogen passed through the pressure controller (15) which reduced its pressure from 2 bar down to 0.5 bar. Then, the gas flow was adjusted to the chosen rate and the nitrogen passed through a heated copper coil (18) that was immersed in the water bath. The temperature of the gas reached the desired value and hot nitrogen entered directly into the filtration unit from the inlet valve (6). Once the bottom valve opened (7), the vacuum pump was connected back to the system. The pressure in the filtration kit was measured by a gauge (3) placed on the top of the vessel. In the early stages of drying, a significant amount of solvent was collected into the container within few minutes and the cake was almost completely deliquored. The rest of the solvent was carried away via heated nitrogen that flowed continuously through the bed. The outlet gas temperature was recorded at regular time intervals to generate a temperature profile of nitrogen throughout

the procedure. The completion of the process was determined by periodically tracking the mass loss of the cake with the use of a balance. In each measurement, the nitrogen supply and the vacuum pump were disconnected from the system in order to get the sample out for weighing.

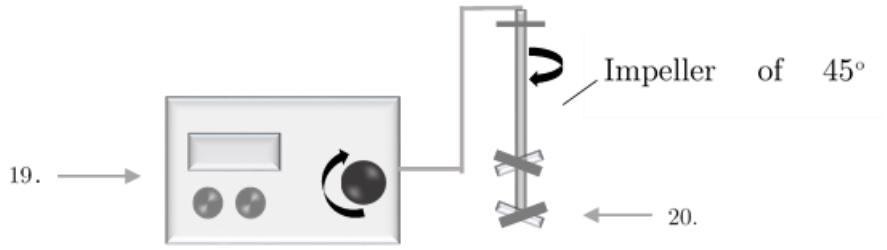

Figure 3.7. Agitation system; 19. Peristaltic pump motor, 20. Lid that contains an agitator.

Based on the DOE plan, there were sets of experiments that involved both continuous and intermittent agitation. An agitator shaft with two four-blade impellers (20) (**Figure 3.7**) was mechanically driven using a peristaltic pump motor which could be set to achieve suitably low rotation speeds (19). Before drying initiated, the stirrer was carefully positioned inside the cake while it was still wet with solvent. In each experiment, the impeller stirred the powder slowly at 5 rpm. In the case of intermittent agitation, the stirring period was switching every ten minutes from agitated to static drying and vice versa. Because particles tended to adhere to the impeller blades, making it challenging to detach the agitator and weigh the basket with the sample due to potential losses, it was

decided to measure the mass of the collected solvent within the predetermined period.

3.3.5 Dried cake analysis and mechanical properties

On completing the final stage of the isolation process, it was essential to check the quality of the drug substance. A number of factors with a major impact on the safety and efficacy of the API, included final impurity content, crystal morphology, particle size distribution and so on. Findings from previously published research [121], [122], [13], [123], show changes on crystal properties due to filtration, washing and agitated drying. For example, pressure filtration and agitated drying can decrease the size of large particles and increase the percentage of fines. This phenomenon is particularly observed on needle-shaped particles that undergo mechanical stresses through applied pressure or agitation. Agglomeration in contrast, enlarges the particle size and it is commonly reported to occur during drying. Additionally, incomplete removal of solvent and impurities during washing and drying can affect the product quality attributes.

In this study, there were no added impurities related to byproducts or reagents coming from the API synthesis. Therefore, attention has been paid on the crystallisation solvent removal and the residual wash solvent content in the final sample. Ideally, all the organic solvents should be completely removed from the

material, but this is almost impossible in real-life applications with current drying technologies. Thus, to evaluate the process efficiency, it was important the levels of residual solvents to meet the product specifications according to safety and stability requirements [124]. Additionally, powder characterization analysis was necessary to determine particle size distribution (PSD), aspect ratio, and extent of particle agglomeration. In this way, it was possible to identify the best operating conditions that would deliver the desired quality of the final material.

3.3.5.1 Selected-ion flow-tube mass spectrometry (SIFT-MS)

Selected-ion flow-tube mass spectrometry (SIFT-MS) is an analysis technique, which quantifies volatile organic compounds in the gas phase using chemical ionisation. Positive and negative reagent ions are produced by electrical discharge using a microwave water vapour source. These reagents are separated inside a quadrupole mass filter according to their mass per charge ratio and the selected cations or anions are transferred into the flow tube by a carrier gas, usually helium or nitrogen. In SIFT-MS three standard reagents, H_3O^+, NO^+ and O_2^+ are preferably used for the detection of a wide range of compounds. Each of these reagents reacts in different way with the analyte and gives a unique "fingerprint" that enables a variety of compounds to be easily defined. The

reactions take place in the flow tube where a continuous stream containing carbon dioxide and traces of solvents is injected. The product ions from the reactions including the reagents that do not interact with the analytes, enter to a second quadrupole where they are filtered and transmitted to a detector. There, the product ion analytes can be detected and quantified instantly with very high sensitivity. [125]

This analysis technique is very direct and simple as sub-samples from the bulk-dried product can be analysed without any preparation. Around 200 mg of the processed material were transferred in 20 mL headspace vial and sealed properly with a lid. The vial containing the sample was incubated at 80 ^{o}C for 20 minutes and then with the use of a 2.5 ml syringe that was held at 150 ^{o}C, vapour gas from the headspace was injected to the inlet of the instrument at 3 mL/min flow rate. An analysis scanning of the present components in the sample was generated and monitored for 90 seconds.

3.3.5.2 Particle size distribution and aspect ratio

The Morphologi G3 (Malvern) is one of the most reliable automated image analysis tools that provides high quality particle size and shape information. Its powerful microscopes have the capability to capture images of hundreds thousands individual particles ranging in size from 0.5 microns to several

millimeters. The system consists of the microscope itself, computer software that automatically stores images, analyses them, and gives statistically based measurements of morphological particle characteristics (circular diameter, aspect ratio, circularity, convexity).

Before starting the image analysis, a subsample (taken with a 15 mm^3 spatula) of dried powder was placed in the carrier of the instrument. The software was activated and ran a method, driven by SOP file (standard operating procedure) which contained adjusted parameters for dispersion conditions, sample focus, light intensity, magnification etc. Then, the carrier dispersed the particles on the slide and the area was scanned through microscope, which instantly produced digital images of each individual particle. The sample scanning procedure usually lasted from 10 to 30 minutes.

The raw input material was used as a reference sample to study the changes on the particle size and shape after experiments. The circular equivalent (CE) diameter describes the size of the particles, while image visualisation shows the presence of broken particles, aggregates, foreign particles and so on. In terms of agitated drying, it was expected that sheared particles with rough edges would be found along with an increased number of fines. Information related to attrition is also provided from the particle aspect ratio. The aspect ratio represents the

proportion between the width and length of a particle and it ranges from 0 to 1. For example, a needle-shape particle has very low aspect ratio compared to a spherical. After attrition occurs, needle-shape particles exhibit higher aspect ratios.

3.3.5.3 Loss on drying (LOD)

A quick and simple way to evaluate the moisture content of the processed material straight after drying is the LOD, **Eq. (3.2)**, methodology using MA160 Electronic Moisture Analyser (Sartorius). This device is an analytical balance that continually weighs whilst heating a sample for a rapid gravimetric moisture analysis. Compared to traditional methods such as oven drying, it has the advantage of time and automation. This technique is suitable for liquids, pastes and solid substances that contain volatile components for instance water, organic solvents, alcohols etc. Generally, the moisture analyser finds applications in the food, chemical and pharmaceutical industries since the moisture content affects the shelf-life and stability of many products.

$$\mathrm{LOD}(\%) = \frac{\text{Initial weight of the sample} - \text{Final weight of the sample}}{\text{Initial weight of the sample}} \cdot 100 \quad \textbf{Eq. (3.2)}$$

Following drying, approximately two grams of the processed material were uniformly distributed in a disposable aluminum pan of the moisture analyser equipment. For reliable results, it was better to take representative samples from different cake areas including surface, core and bottom. Next, a standard method of analysis was created based on the material and solvent properties. Paracetamol along with most pharmaceutical products is quite a heat sensitive compound so delicate heating at 40 °C was recommended. In the present analysis, the semi-automated mode stopped the method as soon as the weight loss per 24 seconds was below the defined detection limit (2 mg/24 s). After the end of each analysis, the current moisture percentage with the initial and the final weight of the sample were displayed on the screen. If the amount of moisture was high enough (with a maximum acceptable moisture content of 0.15% which corresponds to moisture of raw paracetamol), it often indicated significant residual solvent content in the sample. In other words, the drying process, which was performed, was incomplete.

3.3.5.4 Nuclear magnetic resonance (NMR) analysis

Subsamples from the washed material were obtained to examine how pure the product was after washing. For determining the content and the purity of these samples, Nuclear magnetic resonance (NMR) spectroscopy was chosen as an

appropriate analytical tool. Broadly speaking, NMR can provide information about structural and chemical composition of various components, which rely on their nuclei's unique behavior in a magnetic field.

The instrument comprises of a superconducting magnet, which produces high intensity magnetic field and a spectrometer for analysing the frequency of the electromagnetic radiation. Once the substance is exposed in the magnetic field, the nuclei are electrically charged and forced to move from lower to higher energy level. In the absence of radiation, they return to their initial state, which is followed by energy release. The transition between the two states of energy is described with a peak in the spectrum and is distinctive for each nucleus. Here, the ^{1}H-NMR type of spectroscopy was used to get signal information from different kinds of hydrogen present in the molecules. The intensity of these signals provided quantitative data related to proportions of different substances in the sample.

By adopting the previous methodology, standard cakes of 60 g, 105 g and 150 g were prepared after being washed with dodecane. A few milligrams from different cake levels, **Table 3.7**, were taken with the use of a micro spatula and transferred into NMR glass tubes. The samples were dissolved in 0.75 mL pure deuterated DMSO and placed carefully in the instrument. An AVII+600 NMR

Spectrometer BRUKER Advance 2+ (Bruker, UK) was used to collect proton NMR spectra. Each sample was analysed in duplicate. NMR spectra were recorded and processed using Topspin3.5 (Bruker). **Figure 3.8** shows an example of a spectrum obtained from paracetamol measurements and displays the chemical shifts of the compounds present. The plot was calibrated using as a reference the d-DMSO peak seen at 2.5. From the spectrum, it was possible to identify the types of protons and calculate the ratios of each compound by integrating the area under the peak.

Table 3.7. Subsampling from different levels of a 150 g cake.

Cake levels	**Mass of subsamples (mg)**
(1) Surface	10.6
(2) Few cm below surface	20.9
(3) Middle	13.9
(4) Few cm above the frit	14.9
(5) Bottom	10.2

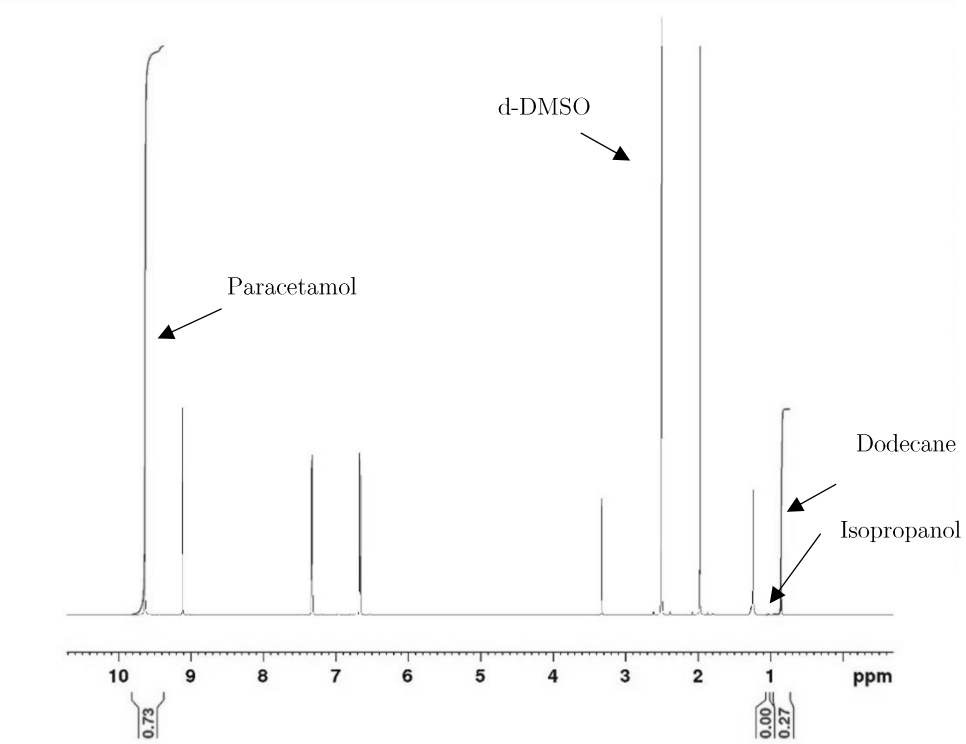

Figure 3.8. H-NMR spectra of paracetamol and its impurities dissolved in d-DMSO solvent.

Previous investigations on similar cakes (up to 9 g) subjected to washing with four void cake volumes of dodecane revealed a ratio of 99.8% for the wash solvent and 0.2 % for the crystallization solvent [11]. Likewise, in this case, the four void cake volume protocol is anticipated to maintain efficient cake washing, yielding similar or slightly higher isopropanol ratios, given the larger size of the cakes. It is important to mention here that there are no added impurities, meaning that there is not an acceptable impurity limit to achieve during washing. However,

the reduction of propan-2-ol to nearly zero aims to minimise undesirable interparticle bridge formation resulting from recrystallization during drying [7].

3.3.5.5 Extent of agglomeration and calculation of agglomerate brittleness (ABI) index

Particle clustering is strongly linked with the presence of mother liquor in the sample at the start of drying. Even a tiny amount of it is enough to fuse two or more particles together with a crystalline bridge of material deposited producing unwanted lumpy material. This phenomenon typically occurs during drying although it is a consequence of a combination of factors which also impact the size and brittleness of the clusters. There are many techniques used for testing the agglomerates mechanical properties [17]; the most popular and reliable one is sieving. Here, sieving was used for determining the extent of agglomeration and checking the friability index.

Initially, the dried product was visually inspected to characterise the agglomerated parts. It is very common to find a blend of cluster sizes in the samples varying from very small pieces to large solid blocks. There is no standard size for classifying a particle cluster as an agglomerate. Since, the particle size distribution of paracetamol powder was smaller than 1mm it was arbitrarily decided that clusters of maximum length greater than this size were considered

as agglomerates. Medium scale sieves of 200 mm diameter and 50 mm depth, were used to separate the agglomerated material into three size categories; the original size of paracetamol (A $<$ 1 mm), small to medium size agglomerates (1 mm $\leq$ B $\leq$ 20 mm) and large paracetamol lumps (C $>$ 20 mm). When the processed sample was removed from the carrier basket, it was transferred to 1 mm mesh sieve, which was attached to the collection pan. The material that could not pass through the sieve was reported as agglomerated and was manually split in two additional fractions, B and C. An example of agglomerated paracetamol is demonstrated on **Figure 3.9**. The mass of A, B and C fractions was recorded and the extent of agglomeration was calculated by simply divide the mass of the agglomerates (B and C) by the total mass of the sample (A, B and C).

Figure 3.9. Agglomerated paracetamol separated into three size categories. The material was dried with supercritical CO_2.

For friability analysis, this project followed the Birch and Marziano approach [23]. As a first step, the agglomerated material (B and C) was put into the 1 mm mesh sieve, which was placed onto the collection pan. The sieve set with the sample was covered with a clamping lid on the top and fastened on a digital sieve shaker (Fritsch) to accomplish consistent sieving. Through experimental trials, the vertical oscillation amplitude was set to 1.1 mm, as higher amplitudes were breaking the agglomerates quite rapidly. Measurements were performed by activating the sieve shaker and executing four consecutive shaking cycles each of 1-minute duration. In each cycle, the agglomerates were constantly subjected to vibration and shattered into fragments due to collisions (**Figure 3.10**). The smallest pieces passed through the sieve and were accumulated in the sieve pan, while the material retained on the sieve was weighed after the defined period of sieving cycle. The acquired data were plotted and fitted using power curve where

the exponent value of the power function indicated the agglomerates brittleness index. Samples with high index number were soft agglomerates.

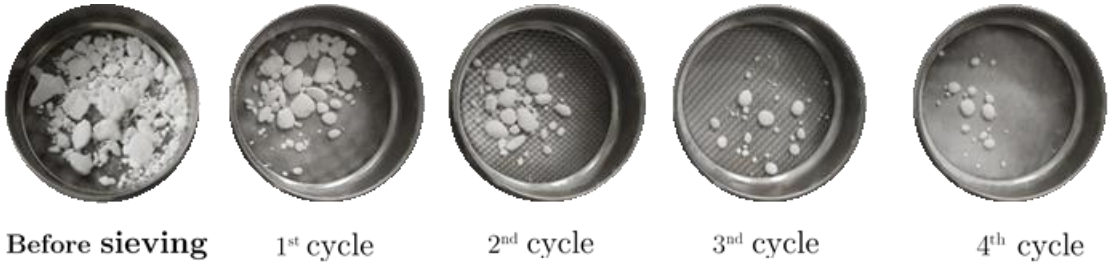

Figure 3.10. Four shaking one-minute cycles for measuring the brittleness index of the paracetamol agglomerates.

3.4 Results and discussion

Table 3.8 shows an updated version of the design of experiments created by using MODDE. The experiments 19 to 23 that involved continuous and intermittent agitation of 150 g of cake were removed from the experimental plan. These changes were made to address issues encountered with the agitation of large wet cakes. An extra experiment involving drying 105 g of cake under higher flow rate was added to investigate further the effect of nitrogen flow.

Table 3.8. Updated design of experiments.

Experiment No.	Temperature (°C)	Nitrogen Flow rate (L/min)	Cake size (g)	Drying Mechanism
1	50	0.8	60	Static
2	70	0.8	60	Static
3	70	0.8	60	Continuous[†]
4	50	0.2	60	Continuous[†]
5	50	0.8	60	Intermittent[**,†]
6	70	0.2	60	Intermittent[**,†]
7	50	0.2	60	Intermittent[**,†]
8	70	0.8	60	Intermittent[**,†]
9	70	0.2	105	Static
10	50	0.5	105	Static
11	50	0.8	105	Continuous[†]
12	70	0.2	105	Continuous[†]
13[*]	60	0.5	105	Intermittent[**,†]
14[*]	60	0.5	105	Intermittent[**,†]
15[*]	60	0.5	105	Intermittent[**,†]
16	70	0.8	105	Static
17	50	0.2	150	Static
18	70	0.8	150	Static
19	70	0.2	150	Continuous[†]

[*]*Experiments 13, 14, and 15 serve as the central points in the Design of Experiments (DOE), and they will be utilised to assess the reproducibility of the process.*

[**]*The cake is stirred for ten minutes and then left to dry in static motion for another ten minutes, following which a new round of stirring begins.*

'For experiments that involve agitation, the stirring speed is set at 5 rpm.

3.4.1 Filtration and washing efficiency

Table 3.9 to **Table 3.14** present the results of the ^{1}H-NMR analysis for assessing the washing efficiency. Clearly, the amount of dodecane used for mother liquor displacement can ensure effective cake washing, since only small quantities of propan-2-ol were detected in the samples after washing. The presence of IPA solvent shows consistency across the cake's vertical profile with the exception of the surface, where the quantity of crystallisation solvent was a little bit higher. This could be due to the immiscibility between the two solvents. At the early moments of washing, it is assumed that a portion of the mother liquor located on the cakes surface, was disturbed and suspended on the top of the layer of the solvent [120]. However, the obtained solvent ratios are comparable to previous experimental measurements taken for the same model system of much smaller cake sizes [17]. Post filtration, the solvents occupied approximately the 20 wt.% of the wet cake. This percentage aligns with typical moisture content values (20-25%) obtained after filtration using an AFD [126]. Also, from **Table 3.10, Table 3.12** and **Table 3.14,** the solvent phase in the sample increases from the top to the bottom part of the cake due to applied vacuum and gravity forces.

Table 3.9. Wash and crystallisation solvent ratios after 60 g paracetamol cake washing according to ^{1}H-NMR spectroscopy.

Cake levels	**% of dodecane**	**% of propan-2-ol**
(1) Surface	99.54	0.46
(2) Middle	99.6	0.4
(3) Bottom	99.75	0.25

Table 3.10. Ratios of each compound in the subsamples taken from 60 g cake.

Cake levels	**% of dodecane**	**% of propan-2-ol**	**% of paracetamol**
(1) Surface	4.79	0.02	95.19
(2) Middle	5.22	0.02	94.76
(3) Bottom	7.41	0.02	92.57

Table 3.11. Wash and crystallisation solvent ratios after 105 g paracetamol cake washing according to ^{1}H-NMR spectroscopy.

Cake levels	**% of dodecane**	**% of propan-2-ol**
(1) Surface	98.99	1.01
(2) Few cm below surface	99.92	0.08
(3) Few cm above the frit	99.84	0.16
(4) Bottom	99.79	0.21

Table 3.12. Ratios of each compound in the subsamples taken from 105 g cake.

Cake levels	% **of dodecane**	% **of propan-2-ol**	% **of paracetamol**
(1) Surface	5.34	0.06	94.60
(2) Few cm below surface	5.88	0.03	94.09
(3) Few cm above the frit	6.06	0.03	93.91
(4) Bottom	10.11	0.03	89.85

Table 3.13. Wash and crystallisation solvent ratios after 150 g paracetamol cake washing according to ^{1}H-NMR spectroscopy.

Cake levels	**% of dodecane**	**% of propan-2-ol**
(1) Surface	87.16	12.84
(2) Few cm below surface	97.66	2.34
(3) Middle	99.51	0.49
(4) Few cm above the frit	98.59	1.41
(5) Bottom	99.73	0.275

Table 3.14. Ratios of each compound in the subsamples taken from 150 g cake.

Cake levels	% **of dodecane**	% **of propan-2-ol**	% **of paracetamol**
(1) Surface	2.91	0.43	96.66
(2) Few cm below surface	1.35	0.03	98.62
(3) Middle	6.5	0.02	93.48
(4) Few cm above the frit	1.74	0.03	98.23
(5) Bottom	8.77	0.02	91.21

3.4.2 Drying results

The main goal of this study is to identify the best combination of factors that yields a high-quality product in short drying times. Even if the highest applied temperatures and long agitation drying periods facilitate the drying rates, the final product's physical properties might be severely affected. Thus, a big part of the experimental results is focused on the investigation of the effects of the operating conditions on drying performance.

3.4.2.1 Drying kinetics

To better understand drying kinetics, the use of mathematical models is essential for describing the systems behaviour at a microscopic level. Since various types of materials are dried by different drying means, there is not such a simple

modelling approach that could explain the drying phenomena. In a recent survey the contact vacuum drying is consider one of the most complex drying processes [6]. This way of drying entails heat transfer from the heated surfaces and the nitrogen-drying medium to the wet particles, heat and mass transfer within the bed and transport properties that change as drying proceeds. By introducing mechanical agitation these phenomena can be further complicated. At the moment there is a number of applied models for contact vacuum drying in the literature [127], [31], [18], [128] each one constitutes of specified set of equations and has a degree of complexity depending on process parameters and systems properties addressed.

In order to describe the present drying curves gathered under different experimental conditions, two simple mathematical equations **Eq. (3.3)** and **Eq. (3.4)** were used to find a correlation with the experimental drying data, regardless of the equipment, drying mode and cake characteristics.

The linear fall equation, **Eq. (3.3)**, was used at the beginning of the drying curve, where most of the solvent was depleted. This period was quite short compared to the next one and it could be neglected. The slow drying step which was the most important step here, is expressed by a falling exponential equation,

Eq. (3.4), that serves to describe the decrease in the rate of drying which usually leads to long drying times [129].

$$y = 1 - a \cdot t \quad \textbf{Eq. (3.3)}$$

$$y = a' \cdot \exp(-b' \cdot t) \quad \textbf{Eq. (3.4)}$$

where y is the normalised residual solvent $\frac{x_t}{x_0}$, x_0 is the initial mass of solvent in the cake and x_t is the mass of the residual solvent at time t during drying; a, a' and b' are adjustable parameters, which are estimated through a Matlab curve-fitting tool

Typically, in conventional drying operations, the drying cycle is divided in three stages; the initial, constant rate and falling rate periods. Here, the drying process is separated in two periods instead. Initially, abundant solvent drained pretty quickly by cake deliquoring through nitrogen blow down under vacuum. While in the second stage, the mass transfer rate reaches very low values as most of the solvent has been removed.

The differences between the stages of drying described above are linked to drying operation mode. Generally, the most common filter dryers have a vapour line leaving the top of the drier, which is connected to the vacuum pump to remove the solvent from the system. They often have an inert gas line providing a slow flow of nitrogen to ensure that the vaporised solvent is carried away. However, the available lab-scale setup was connected to a vacuum point beneath the wet

cake held on the filter. Simultaneously hot nitrogen flowed through the bed in the same direction as the filtrate, possibly increasing the solvent removal rate.

3.4.2.1.1 Fitted data using an exponential function

The recorded mass values of residual solvent were normalised by the initial amount of solvent and plotted against time to establish drying curves. Normalising the solvent content enables comparison across different factors since the initial solvent content deviated for similar cakes. In the following subsections, the role of wall temperature, solid load, drying mode and nitrogen flow on the the evaporation rate are discussed. Additionally, the variable parameters of the fitted equations provided valuable information for further analysis. **Table 3.15** shows the identified parameters a , a' and b' of the mathematical equations **Eq. (3.3) and (3.4)**. The intercept parameter a' is the initial value of the function **Eq. (3.4)** and here, expresses the critical residual solvent in the cake with respect to the initial solvent content in the sample. The critical solvent content refers to the average residual solvent when the fast drying period ends. The a and b' parameters determine the rate at which the solvent content decreases. The statistical parameter predictions of **Eq. (3.4)** exhibit R^2 and RMSE values between 0.952-0.997 and 0-0.036 respectively, which indicate the equation fits quite well.

Table 3.15. Obtained values of the drying rate constants by fitting the experimental data in **Eq. (3.3)-(3.4)**.

	$y = 1 - a \cdot t$			$y = a' \cdot \exp(-b' \cdot t)$			
Exp. No	a	**RMSE**	R^2	a'	b'	**RMSE**	R^2
1	0.095	0	1	0.699	0.017	0.032	0.985
2	0.082	0.128	0.823	0.535	0.036	0.011	0.996
3	0.293	**0**	1	0.439	0.026	0.009	0.997
4	0.102	0.182	0.766	0.432	0.068	0.015	0.974
5	0.123	0.255	0.689	0.134	0.024	0.014	0.908
6	0.231	0	1	0.395	0.115	0.016	0.971
7	0.174	0	1	0.134	0.010	0.007	0.973
8	0.201	0	1	0.425	0.032	0.010	0.996
9	0.087	0.133	0.832	0.399	0.020	0.016	0.980
10	0.098	0.165	0.793	0.365	0.032	0.016	0.993
11	0.182	0	1	0.537	0.075	0.012	0.988
12	0.088	0.108	0.892	0.393	0.008	0.014	0.962
13	0.147	0.209	0.761	0.566	0.048	0.035	0.976
14	0.115	0.209	0.761	0.289	0.068	0.009	0.961
15	0.107	0.179	0.795	0.243	0.024	0.015	0.952
16	0.171	0.125	0.829	0.441	0.032	0.035	0.975
17	0.082	0.125	0.822	0.408	0.021	0.022	0.974
18	0.083	0.132	0.815	0.403	0.019	0.020	0.981
19	0.148	0	1	0.518	0.014	0.027	0.994

3.4.2.1.2 Effect of temperature

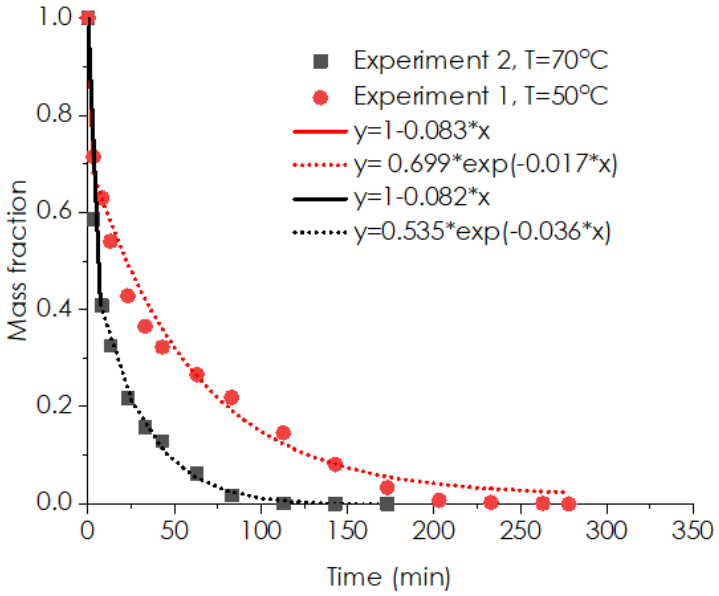

Figure 3.11. Effect of temperature on drying rate for a 60 g paracetamol cake at 0.8 L/min nitrogen flow rate and static drying mode.

The effect of two different drying temperatures was investigated at 60 g fill load, 0.8 L/min flow rate and static mode. From **Figure 3.11,** it is shown that the solvent content drops to 20% after 40min drying for the highest wall temperature of 70 °C. The time required to achieve 20% residual solvent in a similar cake at 50 °C is 110 min. Hence, higher wall temperature increases the drying rates due to greater heat transfer between the medium and the cake, resulting in shorter drying times. The effect of temperature is also noticeable on the exponent b' drying constant, which is higher at 70 °C (0.036 vs 0.017).

3.4.2.1.3 Effect of cake mass

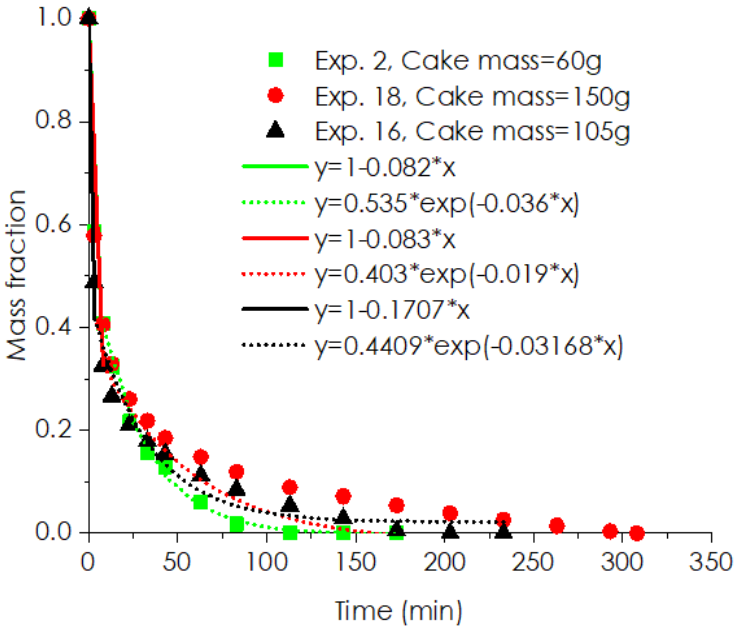

Figure 3.12. Effect of cake mass on drying time at 70 °C, 0.8 L/min nitrogen flow rate and static drying mode.

The influence of cake mass, i.e. fill level on drying behaviour of paracetamol has been investigated at 70 °C and 0.8 L/min nitrogen flow rate. As shown in **Figure 3.12,** faster solvent removal is observed for a lower fill load of 60 g as compared to 105 g and 150 g. This is mainly due to the presence of a smaller mass of particles for the 60 g fill load, which more quickly attain a uniform temperature. As the fill load increases, provides more resistance to both heat and mass transfer through the bulk, resulting in longer drying times. By observing the drying constants, the b' value decreases with an increase of cake mass. However, it is

important to highlight that the model fit is poor at the later stages of drying, especially evident in experiments 16 and 18.

3.4.2.1.4 Effect of drying mode (static or dynamic)

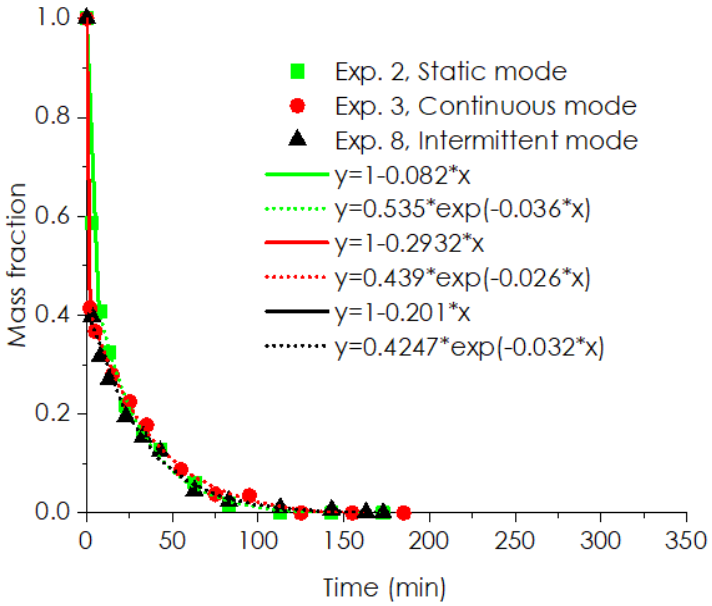

Figure 3.13. Static and dynamic drying modes compared for 60 g paracetamol wet cakes at 70 °C and 0.8 L/min nitrogen flow rate.

For 60 g cakes, the differences between the measured drying curves with and without mixing are not as obvious as expected. When deliquoring the samples in the first ten minutes of the drying cycle, it seems that agitation speeds up the removal of the unbound solvent and this is reflected in the fast period of the drying curve, which is very steep. Moving to the slow drying period, all three drying modes, continuous, intermittent and static give similar curves. In **Figure**

3.13, the samples are fully dry approximately at the same time. The parameter b is slightly higher in static drying than in the other two modes.

Generally speaking, for large filter dryers, agitation is known to facilitate both heat and mass transfer rates through mixing, ensuring temperature homogeneity across the cakes. However, in most of the experiments reported here the samples that dried in the static mode, have shorter drying times and a lower moisture content when compared to the agitated samples of the same solid load. This could be a result of many factors that affect the heat transfer rate through thermal conduction, which is assumed to be the dominant drying mechanism here. One possible factor is the geometry of the vessel and therefore, of the formed cake. The high ratio of height to diameter is greater than 1 as seen in **Figure 3.2**. This effect becomes more prominent when the solid load increases. In static drying the particles are in close contact with each other (**Figure 3.14**) and this results in greater heat transfer rate through conduction. In this equipment, the distance from the wall to the centre of the wet cake is relatively small, around 22 mm. In a more typical scenario where the height to diameter ratio is < 1, it would be expected the opposite effect where mixing would result in lower drying times compared to static drying mode. Another factor could be granulation occurring through mixing. When filter cakes are substantially wet

and agitation is introduced, agglomerates/large granules can be formed as a consequence of the combination of agitation and evaporation depositing dissolved product achieved by the heating. Such granules are likely to be more difficult to dry and therefore, extend the drying times. Additionally, the generation of transient voids in the cake during agitation would offer further resistance to the heat transfer between particles. However, the negative effect of mixing on the rate of solvent removal will be further evaluated through MODDE software where all the obtained values will be assessed.

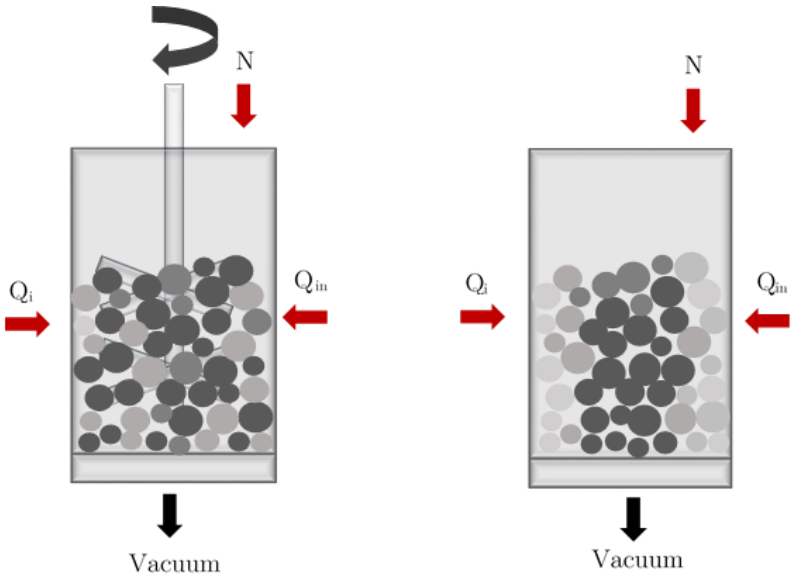

Figure 3.14. Particle arrangement in agitated and static drying.

3.4.2.1.5 Effect of nitrogen flow rate

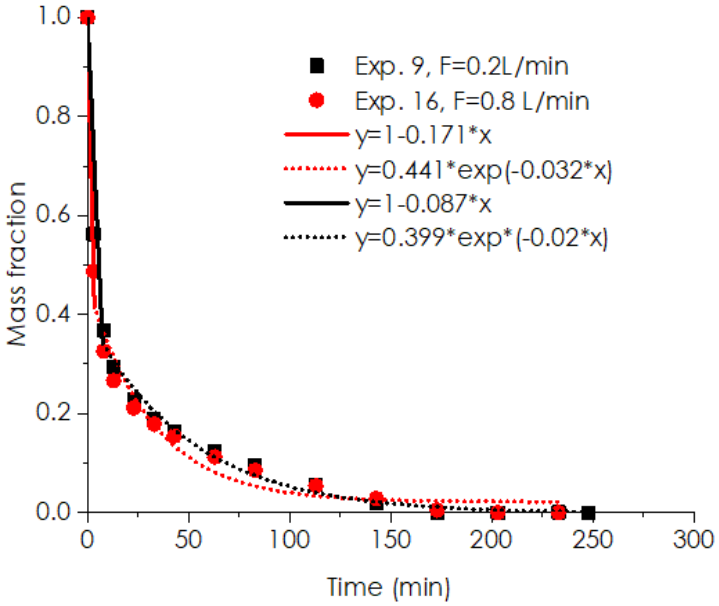

Figure 3.15. Effect of nitrogen flow rate on 105 g paracetamol cake drying at 70 °C and static drying mode.

As shown in **Figure 3.15**, the comparison of the drying curves does not show any significant deviation in the rate of solvent removal achieved by varying the nitrogen flow rate. This is because the dominant heating mechanism here is conduction. However, the parameter b is greater at the highest flow rate. Generally, it is expected that high velocity of gas flow around the particles reduces the diffusion limitations and the evaporated solvent is carried away more rapidly.

3.4.2.2 Statistical evaluation of the experimental data using MODDE

This approach of examining the drying curves give only qualitative understanding of the effects of different operating conditions on drying kinetics. To gain a further insight into the current system, it is necessary to use specialised software to describe better the experimental results and investigate regions for design space of high experimental performance. MODDE software provides an array of useful tools for data analysis, optimisation and prediction. By simply adding the collected data in the DOE worksheet, MLR models can be fitted for each response. The model evaluation is described through model fit R^2, precision of prediction Q^2, reproducibility and validity. If the model shows good fit and reliability, a robust optimal point can be predicted using the software's optimizer tool.

In order to analyse the results, regression coefficient plots were used to observe factors with great influence on the two responses. Each bar represents an important factor and illustrates the average effect on each response. A significant term is one with a large distance from y=0 as well as having an uncertainty level that does not extend across the y=0 value. The error bar represents the 95 % confidence interval related to the coefficient. **Figure 3.16** summarises the main

takeaways from drying paracetamol cakes with the use of a lab-scale agitated filter dryer.

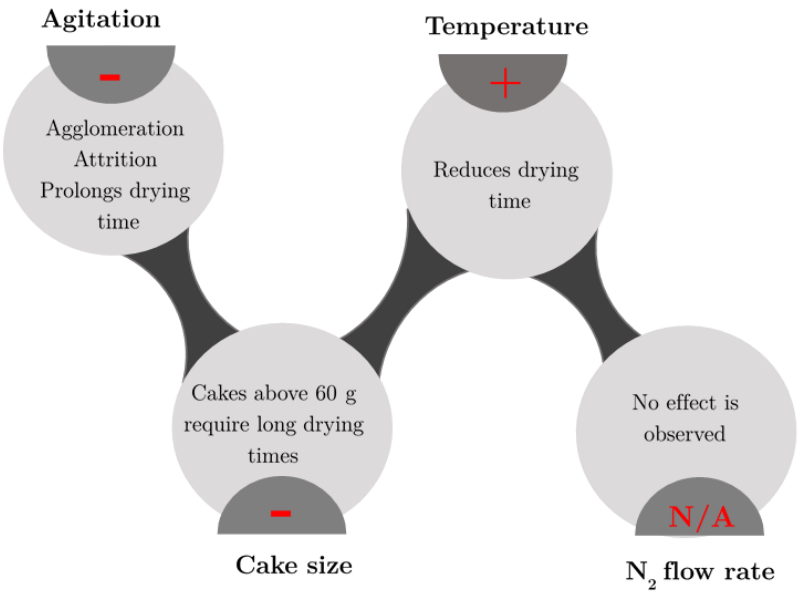

Figure 3.16. Summary of key findings from drying paracetamol cakes wet in dodecane at different drying modes and experimental conditions.

3.4.2.2.1 Loss on drying (LOD)

From overall data observation, **Table 3.19**, it seems that 60 g paracetamol samples dried in static mode, have the lowest values of moisture content, approximately 0.05%. More than half of the runs in the experimental design present moisture levels above 0.2%, which technically they are considered low. However, knowing the relatively low volatility of dodecane and the gentle operating conditions used during LOD methodology, it is expected these numbers

to be quite small. Raw paracetamol measurements taken at 40 °C of gentle drying show approximately 0.15% moisture content. Thus, when compared to untreated material, experimental samples with moisture less than 0.15% are identified as completely dried. This could be verified from the headspace results using SIFT-MS analysis.

The effects of the varied operating parameters on the final moisture content are assessed by applying an MLR model through MODDE software. **Figure 3.30**, demonstrates a bar graph of R^2 (model fit), Q^2 (predictive indicator), reproducibility and model validity. For a model of high significance, the bar values should be greater than 0.5 which in this case they are, with the exception of the reproducibility bar. The variance of LOD measurements between replicas is justified since the samples did not dry completely and the initial amount of wash solvent deviated slightly from each experiment. The regression coefficient plot, **Figure 3.17**, shows that many factors affect drying efficiency, three of which have stronger influence. The increase in temperature as well as drying in static mode, yield the targeted LOD values, whereas the increase of cake size impedes the drying process.

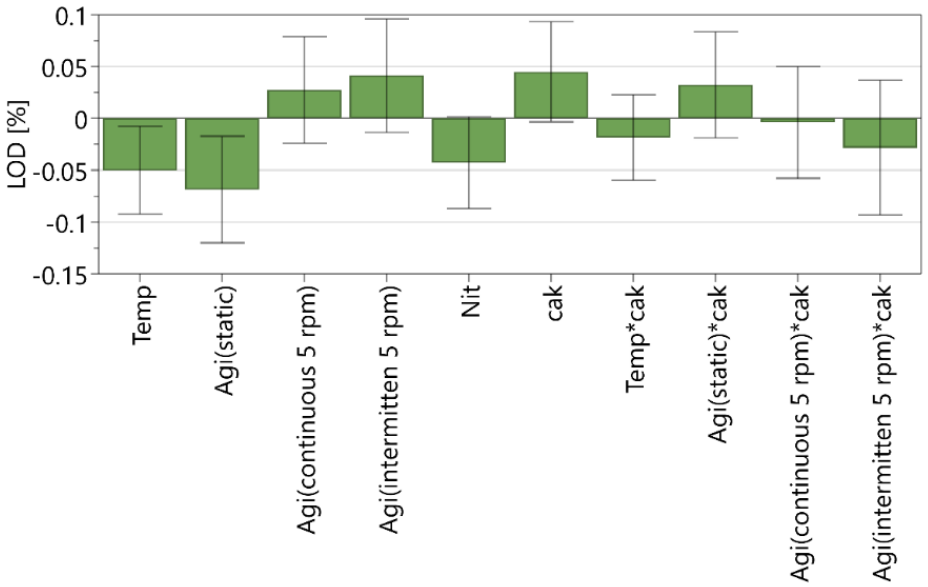

Figure 3.17. Regression coefficients of LOD after removing no-significant terms from the model (Temp=Temperature, Agi=Agitation, Nit=Nitrogen, Cak=Cake size).

3.4.2.2.2 Residual solvent content (SIFT-MS)

The removal of dodecane is quite challenging particularly for cakes above 60 g. **Figure 3.18** presents concentration levels of dodecane and IPA, detected in the samples headspace after drying. For less than half of the experiments, the dodecane residues vary from 0.008 to 1.15 mg/g, while the rest exhibit more than 9mg/g. Samples equal to or above 9 mg/g of dodecane have reached the saturation point that the equipment can measure, therefore the results obtained for the experiments 4, 5, 7, 11, 13, 14, 15, 17, 18 and 19 are not representative values of the actual dodecane concentration in the headspace. However, this limitation does not impact the overall results including the model validity, since

they are considered as wet samples. At the same time, propan-2-ol concentrations are very low and range within 1-6.10^{-3} mg/g in all the cases.

Based on the ICH guidelines, the daily exposure concentration limit for alkanes of similar properties with dodecane, such as heptane, is 5000 ppm, which is equivalent to 50 mg per day or less. Similarly, propan-2-ol is classified as Class 3 solvent with the same permitted exposure level. Considering that the maximum allowed daily dose of paracetamol is 4 g, then the concentration upper-limit of both dodecane and propan-2-ol should be around 12.5 mg of solvent per g of API. Thus, only 10 out of 20 samples meet the ICH criteria.

By modelling the dodecane concentrations using MLR regression model, resulted in a very good fit with high prediction power, model reproducibility and validity. The resulting regression coefficient plot, **Figure 3.19**, shows that many process parameters influence the residual solvent. Generally, high temperatures, static drying, and small cake sizes ensure low solvent content of the powder.

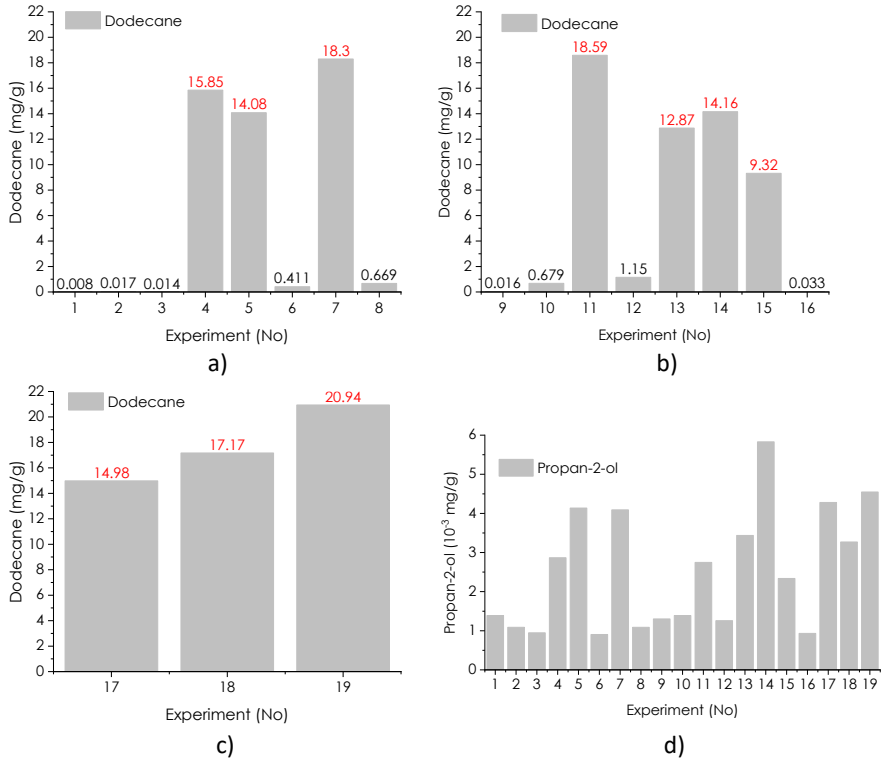

Figure 3.18. Dodecane and propanol levels measured in the headspace of samples after drying using SIFT-MS analysis (number of repetitions, n=1).

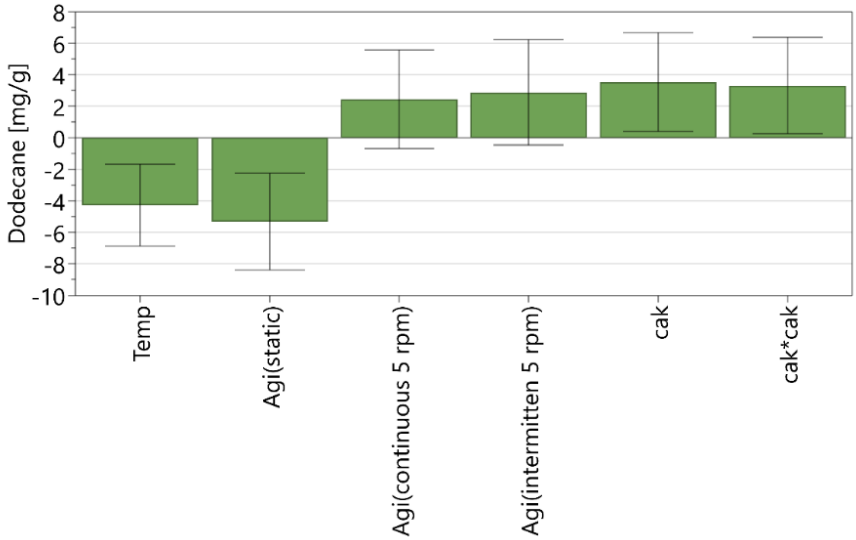

Figure 3.19. Regression coefficients of dodecane residues after removing no-significant terms from the model (Temp=Temperature, Agi=Agitation, Cak=Cake size).

3.4.2.2.3 Drying time

The influence of drying process parameters on drying time was assessed. At first sight, the shortest drying times (~ 180 min) are reported for 60 g cakes dried at highest temperature, 70 °C and nitrogen flow rate, 0.8 L/min. Increasing the solid load and therefore the dodecane content in the cake, prolongs the drying times which sometimes exceeded the 350 min without reaching the upper residual solvent limits. Agitation seems to significantly speed up the removal of the unbound solvent in the first minutes of the drying cycle; however, its influence on drying time during the falling rate period is not as beneficial as expected for the reasons mentioned on subsection **3.4.2.1.4.**

Fitting the MLR regression model in the experimental data results in a good fit regarding the prediction power, validity, and model reproducibility. The obtained regression coefficient-fitting plot, **Figure 3.20,** comes in agreement with our first assumptions, as cake size and temperature are the two most influential factors. Thus, low solid loads and high temperatures facilitate the drying kinetics.

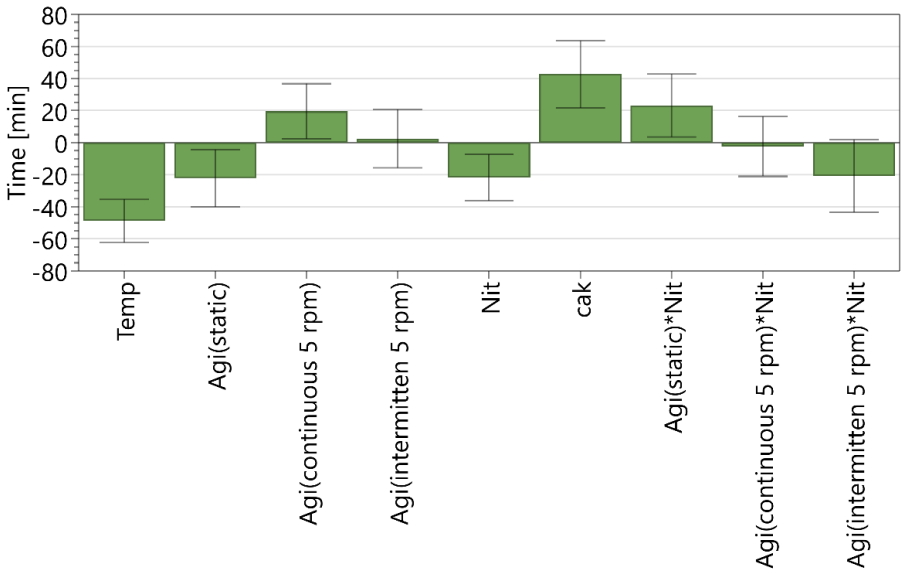

Figure 3.20. Regression coefficients of drying time after removing no-significant terms from the model (Temp=Temperature, Agi=Agitation, Nit=Nitrogen, Cak=Cake size).

3.4.2.2.4 α' and b' parameters

The experimental data points fit quite well in the mathematical equation; however, the dependence of parameters $\boldsymbol{\alpha'}$ and $\mathbf{b'}$ on DOE factors is not so clear by comparing a few experiments only. A wider picture of the impact of different factors on the drying rate and critical moisture content in the bed can be obtained through MODDE software. For the adjustable parameter $\boldsymbol{\alpha' = x_{t,}}$ the actual mass of the solvent remaining in the cake at the beginning of the falling rate period is used, as estimated through experimental data. From the summary fit plot **Figure 3.30** (page **112**), the model fit, and prediction power are above 0.5 and their difference is less than 0.3 for both responses. At the same time,

the values of reproducibility and model validity are sufficient resulting in a good model. The coefficient regression plots show the relationships between the input factors and the adjustable parameters $\boldsymbol{\alpha'}$ and $\mathbf{b'}$.

Regarding the parameter $\boldsymbol{\alpha'}$, **Figure 3.21**, it seems to increase at high solid loads and static drying mode. The higher the bed size, the more solvent residues it contains. Compared to static drying, intermittent and continuous agitation reduces the initial unbound solvent more effectively in the first drying period resulting in less critical solvent in the cake. For instance, the critical moisture content for cakes in experiments 1 and 5, as presented in **Table 3.19**, is 7.6 g under static conditions and 1.4 g during intermittent agitation.

The parameter $\mathbf{b'}$ is observed to have greater values under the presence of intermittent agitation and at high temperatures. Whilst static drying seems to have negative impact on the drying rate, and this is opposed to our first assumptions. As it is observed from the drying curves, the exponential equation fits quite well in the first data points of the falling rate period and this first stage seems to determine the value of the adjustable parameter $\mathbf{b'}$. However, in some cases, at the later stages of drying where diffusion dominates and the drying times are long, the data points are a bit far from the curve. Hence, the exponential equation might not be ideal for describing the later stages of the

falling rate period and this could lead in wrong interpretation of the experimental data.

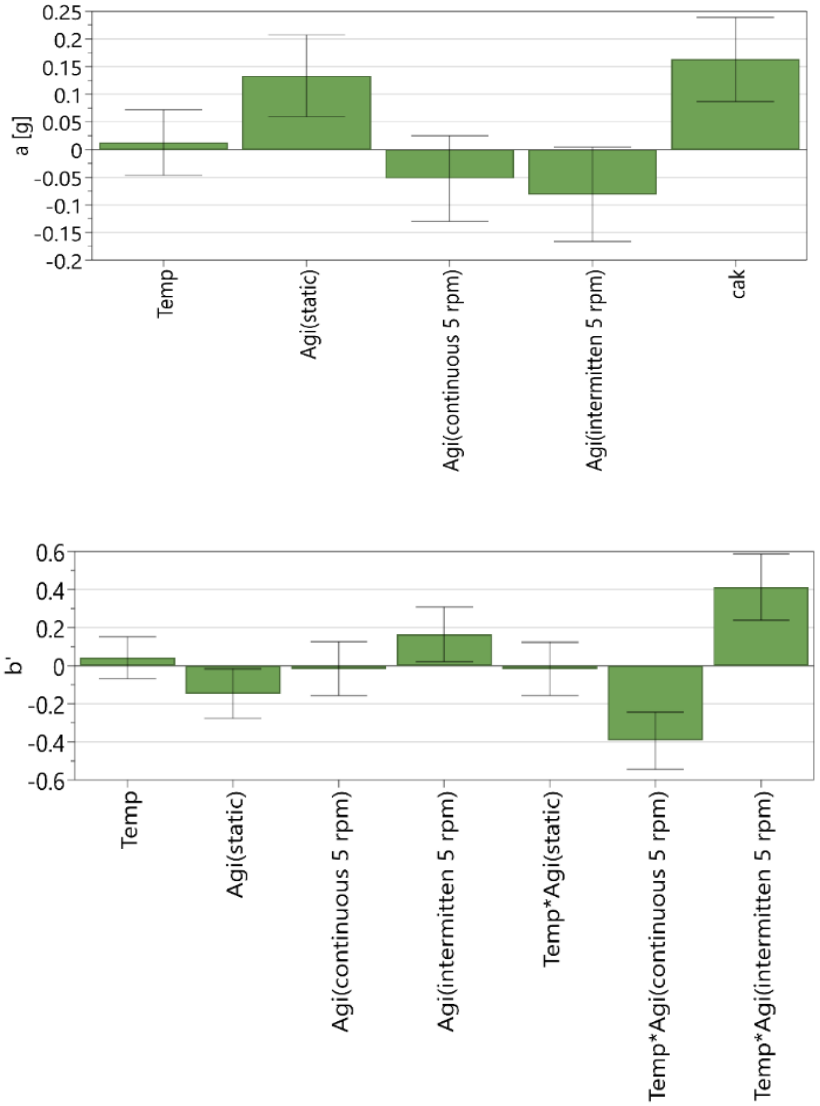

Figure 3.21. Regression coefficients of a' and b' parameters after removing no-significant terms from the model (Temp=Temperature, Agi=Agitation, Cak=Cake size).

3.4.2.2.5 Extent of agglomeration and attrition

Agglomeration was present in all the dried samples and ranged between 30% and 76%. As it is shown in the obtained regression coefficient plot, **Figure 3.22**, it is mainly dependent on two factors; cake size and drying mode. Cakes dried under static mode display a substantial degree of agglomeration, ranging from 55% to 76%, whereas cakes subjected to agitation during drying show lower percentages, approximately 33% to 40%. As anticipated, the introduction of agitation, leading to increased mechanical collisions within the bed, mitigates the agglomeration phenomenon. Conversely, by increasing the size of the bed appears to promote the formation of clusters. This may be attributed to the slightly higher residual amounts of crystallization solvent in the larger cakes after washing. In addition, nitrogen flow is observed to reduce agglomeration as it might be connected with the quick removal of propa-2-nol during drying. Generally, the summary fit plot shows a good fit of the MLR regression model to the data which means it is a rather useful model for agglomeration predictions in this case.

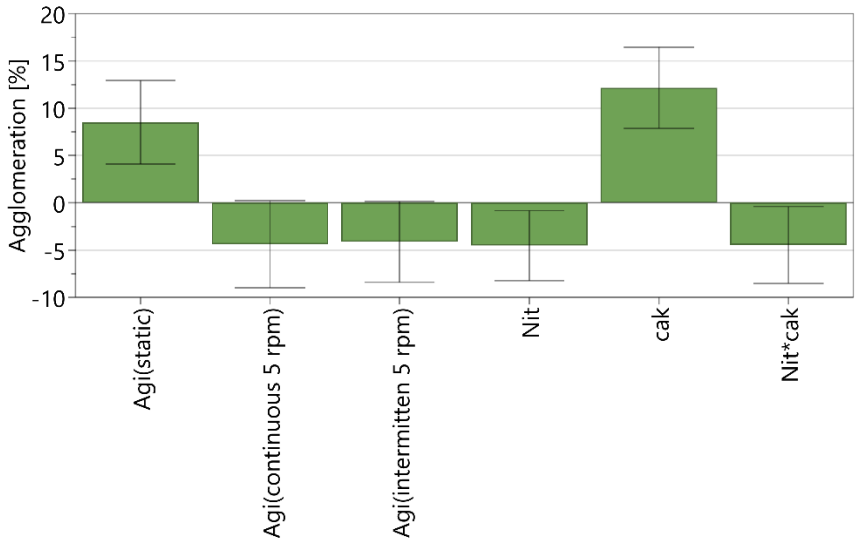

Figure 3.22. Regression coefficients of agglomeration extent after removing no-significant terms from the model (Temp=Temperature, Agi=Agitation, Nit=Nitrogen, Cak=Cake size).

In this section it is worth to mention particle attrition as it counterbalances the rate of agglomeration. It is predominant at the later stages of the drying as most of crystals are aggregated by liquid-bridges when more solvent is present at the beginning of drying. To comprehend the impact of agitation in the studied conditions, the final particle aspect ratio and the particle size distribution were measured in the way described before. As illustrated in **Figure 3.23**, particles with low aspect ratio have a needle-like shape.

Figure 3.23. Aspect ratio of needle-shape untreated paracetamol particles.

The collision between the particles and the impeller leads to the breakage of needles into smaller fragments which therefore increases the aspect ratio of the particles.

Figure 3.24, shows the particle aspect ratio distribution of samples that dried at the three different drying modes, along with a reference sample corresponding to raw paracetamol (blue line). **Figure 3.21 (a)** and **(b)** correspond to 60 g samples which present very low moisture content at the end of drying. As observed in the distribution plots, there is a small shift to the right in the experiments where agitation is applied, suggesting that a number of particles have a relatively less elongated shape, which normally occurs due to the breakage of needles. **Figure 3.24 (c)** compares aspect ratio distribution plots of 105 g samples. Particle attrition in agitated experiments, is less profound here due to relatively high solvent content in the samples after drying. At low moisture levels, the attrition increases in the cakes, while high solvent content acts as

lubricant [130]. However, it can be concluded that particle attrition is not so prominent in these experiments since the stirring speed was really low.

This is also confirmed from **Figure 3.25** which shows the variations in particle size for all percentile values, D_{10}, D_{50} and D_{90} using as a reference point the raw paracetamol (dashed line). As it is seems, the particle size deviates from the reference value in all the cases, but within an acceptable limit.

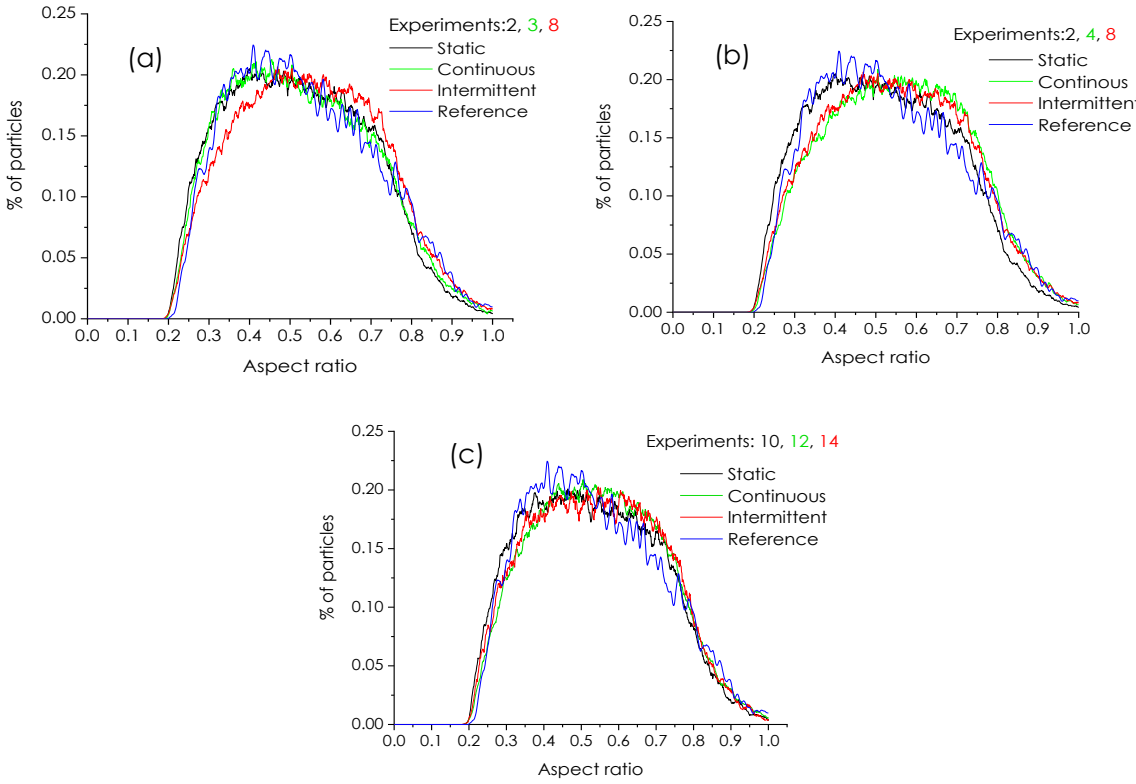

Figure 3.24. Aspect ratio distribution plots: (a) and (b) 60 g paracetamol cakes dried at three different modes, (c) 105 g paracetamol cakes dried in three modes (number of repetitions, n=1).

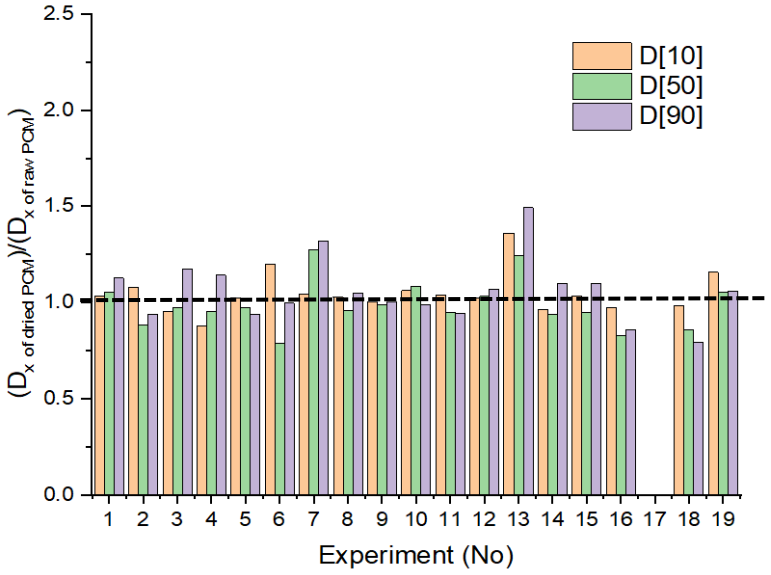

Figure 3.25. Changes in particle size after drying; the dashed line corresponds to raw paracetamol and is used as a reference point (data for sample 17 is missing, number of repetitions, n=1).

3.4.2.2.6 Agglomerate brittleness index (ABI factor)

At the moment there is not any precise technique used for measuring the agglomerates mechanical properties. Birch and Marziano are the first to publish a valid appoach that can test the agglomerate hardness. Based on this method, the % of the initial mass retained on the sieve is recorded after four shaking cycles and then plotted against the number of cycles. By fitting power equation to the experimental data points, the ABI factor is obtained from the power value b. The bigger this value is, the softer the agglomerated material and vice versa.

Although this method provides quite satisfactory data, there are cases where the results are questionable. One of the pitfalls in measuring the agglomerate britleness index is the large deviation between individual agglomerates within the same sample. Since clusters are formed in different parts of the cake this feature is inevitable and is reflected on the average agglomerate hardness of the sample. In experiments where the majority of the agglomerates are totally shattered at the beginning of the analysis, only a small percentage define the average brittleness index of the material. Such an example is experiment 6, where the 68% of the agglomerates are soft, while the rest of the material constists of much harder pieces, which therefore determine the ABI. Compared to experiment 6, experiment 12 has less soft agglomerates (36%), but the loss of mass in the last three cycles is higher resulting in greater ABI value (**Figure 3.26**). The same issue is observed between samples 7 and 14 in **Figure 3.27**. By using the power function to model the data, the b value is independent of the initial amount of agglomerates which leads to inaccurate results. Additionally, for agglomerates that show weak fragmentation in the first cycle followed by strong ones, the curve demonstrates quite low quality fit to the data.

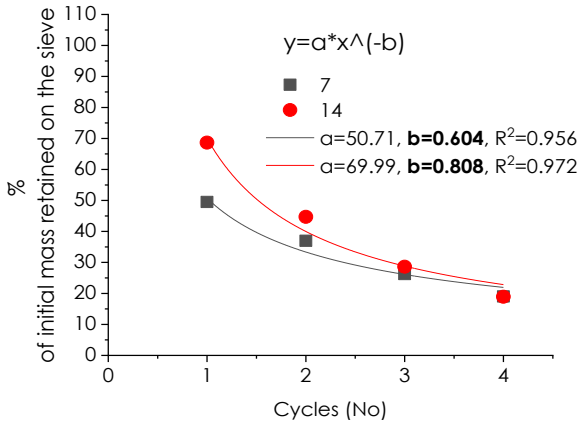

Figure 3.26. Power function fit for samples 7 and 14.

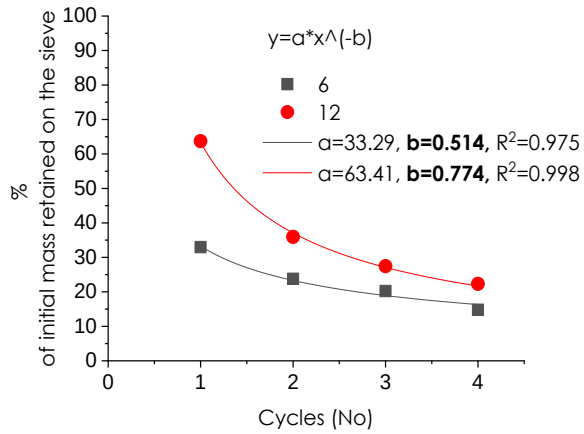

Figure 3.27. Power function fit for samples 6 and 12.

As an alternative, this study uses an exponential decay equation **Eq. (3.5)**. In mathematics, this formula is used to describe a process where the initial amount a is reduced by a decay factor b over time x. In this case, factor b is the average percentage rate that the original amount of agglomerates decreases during four identical cycles.

$$y = a \cdot (1 - b)^x \quad \textbf{Eq. (3.5)}$$

Comparing the two equations, the exponential decay results in more reliable ABI data and in most of the cases it has similar or greater R^2 values, **Table 3.16**. Furthermore, by ranking the b values from higher to lower, there are major differences on the agglomerate softness based on the equation is used. This is demonstrated on the **Example 1** below, where the experiments from **Figure 3.26Figure 3.27**, highlighted with red colour, are placed in different orders. Particularly, experiment 6 appeared to have soft agglomerates in case A, contrary to case B where it exhibits hard clusters.

Example 1

A) Exponential decay

5>**6**>10>**7**>4>15>13>**12**>**14**>9>3>1>2>8>11>18>16>17>19

B) Power function

5>15>10>**14**>3>13>4>**12**>1>8>**7**>11>9>**6**>2>18>16>17>19

Table 3.16. R^2 values obtained by fitting the experimental points to power function and exponential decay.

	R^2		b factor	
Exp. No	$y = a \cdot x^{-b}$	$y = a \cdot (1-b)^x$	$y = a \cdot x^{-b}$	$y = a \cdot (1-b)^x$
1	0.786	**0.893**	0.73	0.26
2	0.905	**0.983**	0.51	0.25
3	0.846	**0.927**	0.81	0.28
4	0.917	**0.993**	0.79	0.38
5	0.995	0.993	1.23	0.74
6	0.975	0.924	0.51	0.52
7	0.956	**0.963**	0.60	0.38
8	0.874	**0.967**	0.62	0.24
9	0.983	0.973	0.52	0.29
10	0.967	**0.997**	1.04	0.48
11	0.75	**0.932**	0.54	0.23
12	0.998	0.986	0.77	0.35
13	0.991	0.987	0.80	0.36
14	0.972	**0.999**	0.81	0.33
15	0.998	0.984	1.05	0.37
16	0.857	**0.977**	0.40	0.17
17	0.861	**0.946**	0.39	0.15
18	0.989	0.988	0.43	0.22
19	0.989	**0.991**	0.26	0.11

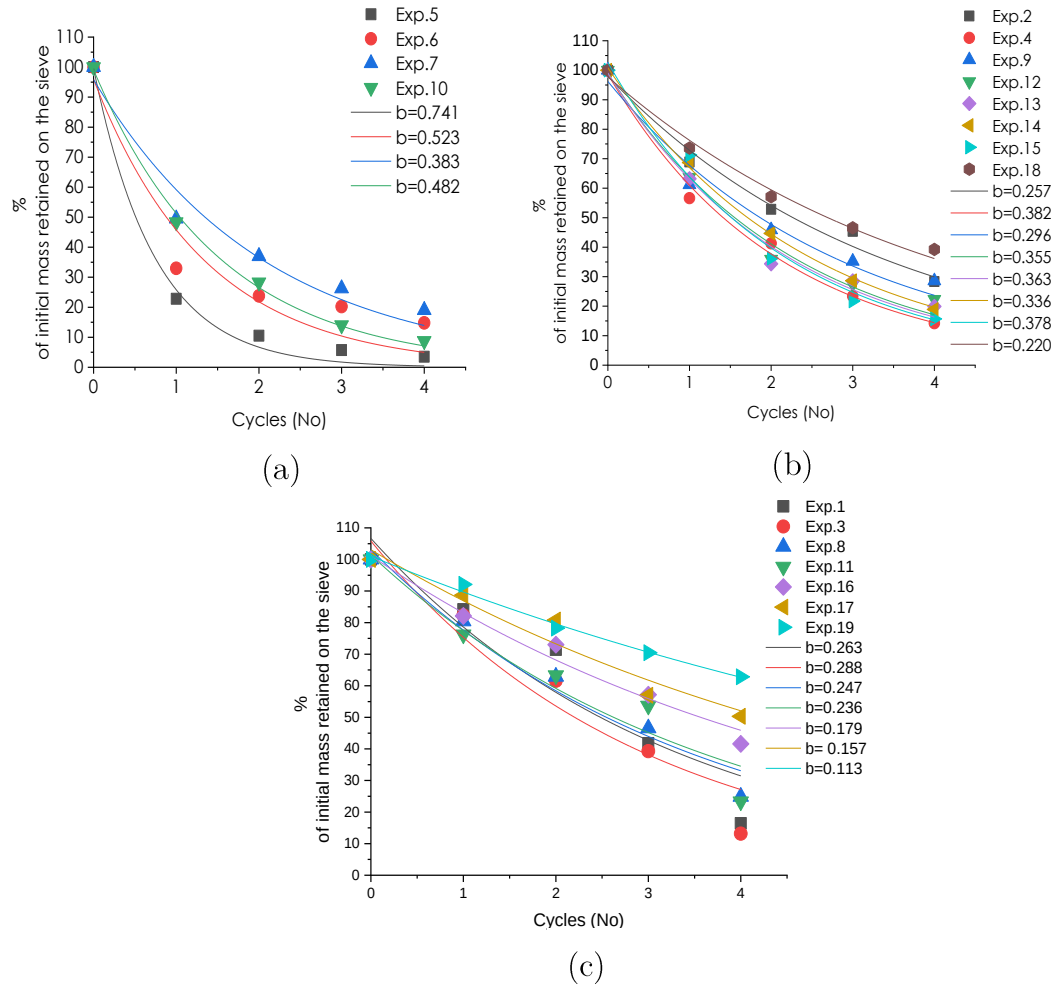

Figure 3.28. Exponential decay fit to the experimental data points obtained from sieving. The b parameter indicates the softness index of the agglomerated sample. The higher this value, the softer the agglomerates in the samples and vice versa.

According to **Figure 3.28**, only three out of nineteen samples display relatively high ABI values ranging between 0.48 and 0.74. In these three cases, a rapid breakup was observed in the initial cycle, resulting in 50 % of the initial mass of agglomerates being retained on the sieves. The subsequent cycles showed small amount of material left, not exceeding 20% of the initial mass, **Figure 3.28 (a)**.

The rest of the experiments exhibit ABI values in the range of 0.113-0.38. The notably low ABI values of samples 17, 18, and 19 are closely linked to the presence of solvent residues (above the SIFT-MS quantification limit), as the agglomerates were slightly damp before sieving.

In order to correlate the b factor with the varied parameters, MLR model is fitted to the experimental data and **Figure 3.30** presents a summary of the fit. For a robust model, the R^2 should be higher than 0.5 and the difference between R^2 and Q^2 should be preferably less than 0.3. Additionally, the model validity should be larger than 0.25 to avoid lack of it. Hence, the model shows poor fit to the ABI data. This could be a result of an incorrect model or due to the large variation in brittleness of individual agglomerates within the same sample. The latter leads to incostistent measurements that are impossible to be predicted by modelling.

After tuning and removing the insignificant terms, the model consists of three significant parameters with the most influence on the ABI factor, **Figure 3.29**. By far the most important parameter here is the cake size, followed by agitation and temperature. It was expected that continuous agitation would have the opposite effect on the ABI. Its contribution on forming strong agglomerates in the bed might be a result of granulation through mixing and inefficient thermal

conduction between the particles and the jacketed walls. At the same time, temperature tends to increase the agglomerates hardness. A possible explanation might be that the solubility of paracetamol in propan-2-ol could increase with higher temperatures [115], thus formation of solid bridges may be more likely.

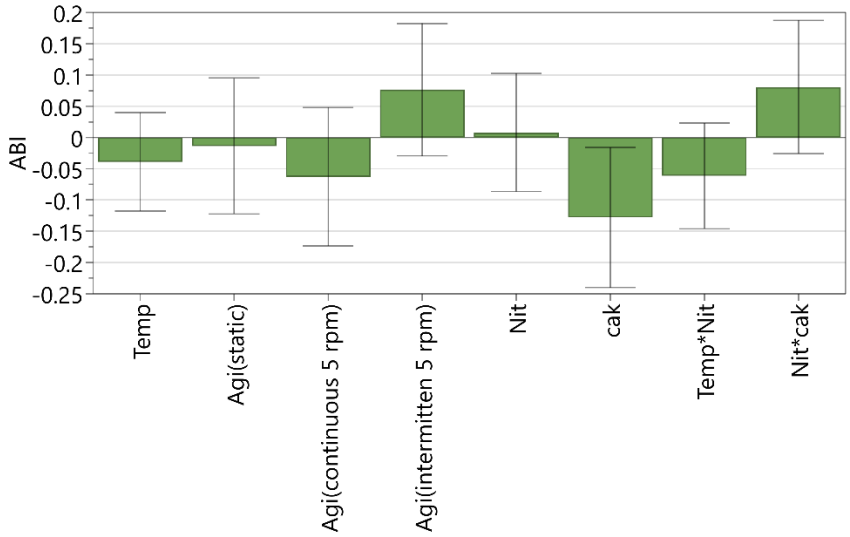

Figure 3.29. Regression coefficients of ABI index after removing no-significant terms from the model (Temp=Temperature, Agi=Agitation, Nit=Nitrogen, Cak=Cake size).

3.4.2.3 Model optimisation

MODDE software provides an Optimiser toolbox that finds and analyses the optimal conditions for maximising the drying performance considering the final product quality. To calculate the best combination of factors, all four parameters were included within the limits that set before and the targeted/desired values are specified for each response. The best combination of factors and the models' predicted values are shown in **Table 3.17** and **Table 3.18** respectively. The

optimiser's results are confirmed experimentally, as small cakes that dried intermittently at the highest temperature resulted in low dodecane levels with relatively low extent of agglomeration.

Table 3.17. Best combination of factors selected by optimiser tool.

Factors	Values
Temperature (°C)	70
Mass cake (g)	60
Drying mode	intermittent
Nitrogen flow rate (L/min)	0.8

Table 3.18. Quality targeted and predicted product profile.

Responses	Objectives	Predicted values
LOD (%)	Minimise	0.20
Dodecane (mg/g)	Minimise	1.47
Time (min)	Minimise	166
Agglomeration (%)	Minimise	39
ABI	Maximise	0.31

Table 3.19. Overall experimental results fitted to the MLR regression model.

Exp.	Temperature	Nitrogen Flow rate	Cake size	Drying Mechanism	LOD	Dodecane	Time	Agglomeration	ABI	b	a
No	(°C)	(L/min)	(g)		(%)	(mg/g)	(min)	(%)			(g)
1	50	0.8	60	Static	0.05	0.008	278	53.7	0.263	0.017	7.56
2	70	0.8	60	Static	0.05	0.017	173	54.08	0.257	0.032	9.12
3	70	0.8	60	Continuous	0.1	0.014	185	36.67	0.288	0.026	6.41
4	50	0.2	60	Continuous	0.37	15.856	350	40.64	0.382	0.068	6.99
5	50	0.8	60	Intermittent	0.25	14.084	350	33.73	0.741	0.024	1.43
6	70	0.2	60	Intermittent	0.29	0.411	253	35.45	0.523	0.115	6.64
7	50	0.2	60	Intermittent	0.35	18.30	350	33.01	0.383	0.010	1.97
8	70	0.8	60	Intermittent	0.25	0.669	173	36.52	0.247	0.032	8.54
9	70	0.2	105	Static	0.05	0.016	233	74.21	0.296	0.020	17.02
10	50	0.5	105	Static	0.27	0.679	233	40.1	0.482	0.032	16.05
11	50	0.8	105	Continuous	0.26	18.593	350	44.57	0.236	0.075	11.25
12	70	0.2	105	Continuous	0.32	1.149	263	30.62	0.355	0.008	6.6
13	60	0.5	105	Intermittent	0.21	12.869	300	55.5	0.363	0.048	13.3
14	60	0.5	105	Intermittent	0.31	14.159	350	54.37	0.336	0.068	8.2
15	60	0.5	105	Intermittent	0.41	9.319	270	59.38	0.378	0.024	6.54
16	70	0.8	105	Static	0.15	0.033	233	60.16	0.179	0.031	16.89
17	50	0.2	150	Static	0.48	14.499	350	76.27	0.157	0.021	20.14
18	70	0.8	150	Static	0.21	17.170	350	62.88	0.22	0.019	21.22
19	70	0.2	150	Continuous	0.31	20.943	350	73.12	0.113	0.014	15.89

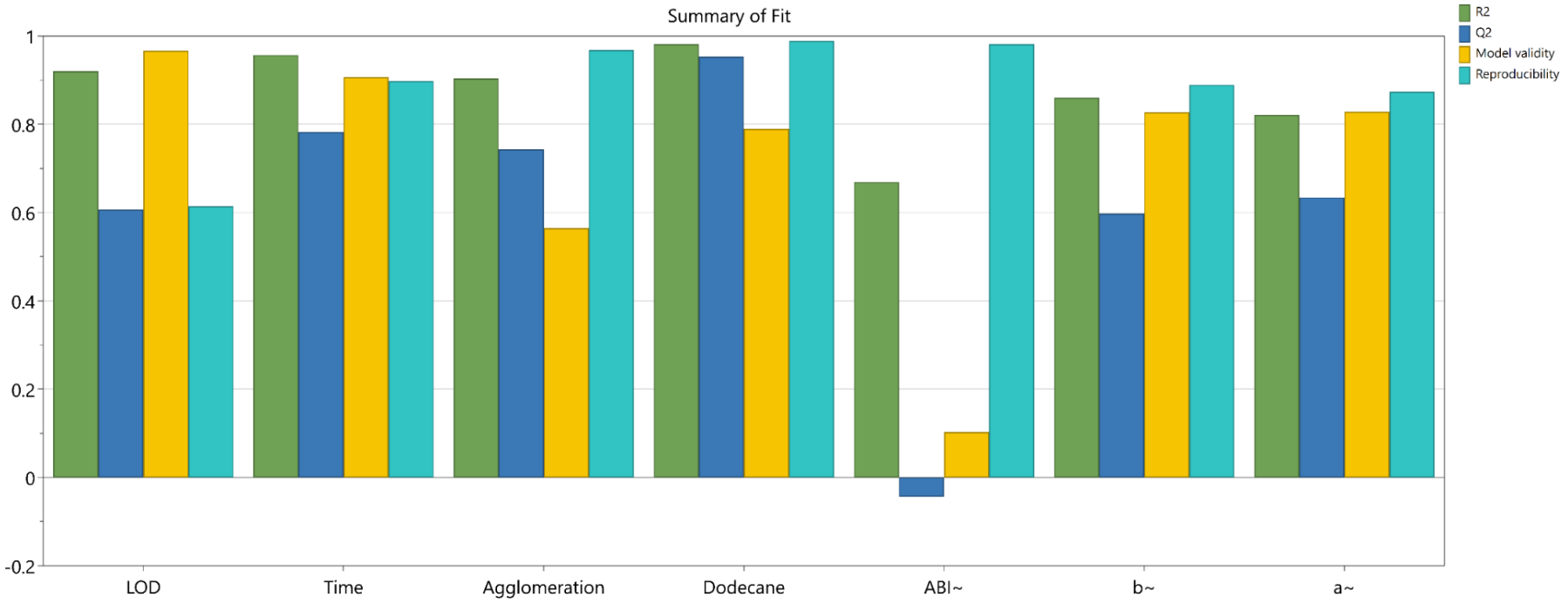

Figure 3.30. Summary fit plot for all the responses.

3.5 Conclusions

The current study successfully demonstrated the optimisation of conventional drying using a lab scale filter dryer. To achieve this a DOE methodology was implemented and a descriptive model was developed through MODDE software. Along with this, the influence of key process parameters such as temperature, nitrogen flow rate, mass of cake and drying mode was examined extensively. From overall observations, the parameters with the highest contribution factor in determining the drying performance were the mass of cake and the temperature of jacketed walls. Cake sizes of 60 g dried completely at 70 ^{o}C with minimum drying time, 180 min. Moreover, the geometry of the setup favoured the static drying mode. It is assumed that greater heat transfer rates were achieved through static as compared to agitated drying (see **sections 3.4.2.1.4** and **3.4.2.2.4**). On the other hand, mechanical agitation eliminated agglomeration and when it occurred intermittently, increased the brittleness index of the clusters. The effect of nitrogen flow rate is yet to be understood, as there was not a clear correlation with the drying kinetics. Finally, the developed descriptive model was suitable to select the best combination of factors for generating dry paracetamol samples with predefined characteristics, as confirmed experimentally. The selected optimised process conditions for the studied system

were 60 g paracetamol cakes, intermittent drying mode, 70 °C wall temperature and 0.8 L/min nitrogen flow rate. The results of this chapter support a bigger objective of this work and are used for the investigation of $scCO_2$ extractive drying as an alternative drying technology of APIs.

4 Supercritical CO_2 extraction/drying coupled with Selected Ion Flow Tube Mass Spectrometry (SIFT-MS) analysis

In this chapter, supercritical CO_2 extraction is used as an alternative way of drying paracetamol particles after being washed with dodecane. To determine a satisfactory drying endpoint, Selected Ion Flow Tube Mass Spectrometry is coupled with the extraction/drying process. SIFT-MS is a sensitive analysis technique that has the capability to track concentration changes of VOC in real-time. By using online probe sampling at the later stages of the extraction/drying, the endpoint of the process can be monitored, allowing for the final solvent concentrations in the product to be minimised.

A core aim of this chapter is to demonstrate the use of online monitoring by SIFT-MS as a tool for optimising solvent extraction using supercritical CO_2. A set of preliminary experiments were conducted to examine the cake preheating effect on the extraction kinetics along with the SIFT-MS capability and reliability to be used as an online analysis method. To validate both techniques being coupled, the supercritical CO_2 treated samples were analysed at the end

using SIFT-MS headspace analysis to determine the final concentrations of solvents in the product.

4.1 Why SIFT-MS is an important online analytical tool for the $scCO_2$ extraction/drying process

The maximum allowable daily solvent intake set out in ICH Q3C [124] translates into maximum allowable solvent concentrations in the API when the dose is taken into account. This makes it important to define an acceptable extraction/drying endpoint and measure the residual solvent concentration during the drying process. Conventional monitoring by gravimetric methods such as periodic offline weighing does not provide real time information, is not sensitive enough to reliably determine solvent residues at the required levels and hence the true extraction/drying endpoint. For this reason, Selected Ion Flow Tube Mass Spectrometry (SIFT-MS) analysis has been investigated as a novel, online process analytical tool to support the investigation of supercritical CO_2 extraction technology used as a drying method. To achieve the goal of online monitoring a SIFT-MS system with a 250 ms-sampling rate was coupled to the exit of the supercritical CO_2 extraction vessel during the later stages of process. During the early stages of process, the solvent loading exceeds the maximum threshold for the instrument. SIFT-MS has the ability to detect and accurately quantify concentrations of solvent down to between 100 ppm to a few parts per billion in the gas phase. The technique has been implemented in several fields of

research including biomedicine [131], health and safety [132], food technology [133] and environmental science [134], [125], [135]. Gas Chromatography (GC) is also being used broadly across industries as an analytical tool for identification of various compounds and as a separation method of multicomponent mixtures. However, SIFT-MS has the advantage of time and simplicity since no reference standard samples are required for the quantification of the compounds of interest. As compared to other spectroscopic methods, it offers ability to detect and quantify multiple solvents off-line and real-time without using chemometric models that require considerable data, time and expertise (i.e. NIR and MIR).

4.2 Materials and methods

4.2.1 Materials

Paracetamol powder (D_{10}=24 µm, D_{50}=64 µm and D_{90}=179µm particle size and 1.24 g/cm^3 true density) was supplied by Mallinckrodt, propan-2-ol (≥ 99.5 % purity) by Sigma Aldrich, n-dodecane (≥ 99 % purity) by Alfa Aesar and liquid CO_2 (> 99.8 % purity) by BOC. All the materials were used without any further purification.

4.2.2 Experimental procedure

The experimental procedure includes the preparation of the slurry, filtration/washing and supercritical CO_2 extraction/drying (**Figure 4.1**). For the first three steps, similar methodology to that of the AFD experiments was followed (see sections **3.3.4.1, 3.3.4.2**, and **3.3.4.3**). In the last step of the experimental procedure, the basket containing the dodecane-soaked cake was filled with glass wool to reduce dead volume and was mounted in the supercritical CO_2 rig where the wash solvent was extracted.

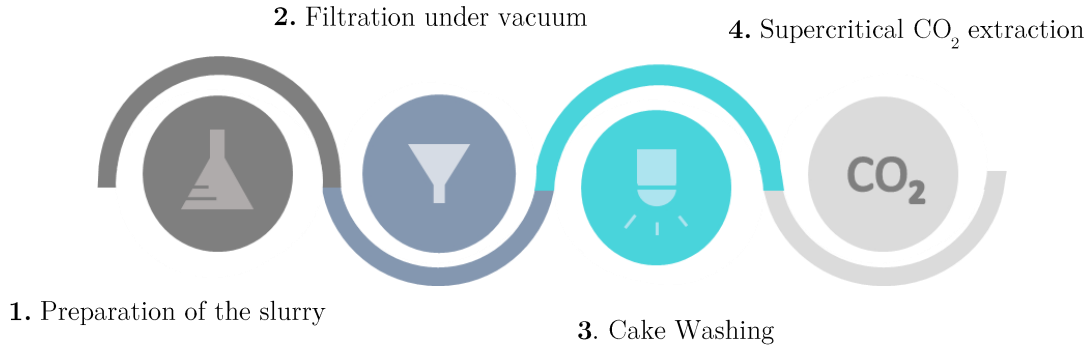

Figure 4.1. An illustrative example of the experimental procedure.

4.2.3 Supercritical CO_2 extraction/drying

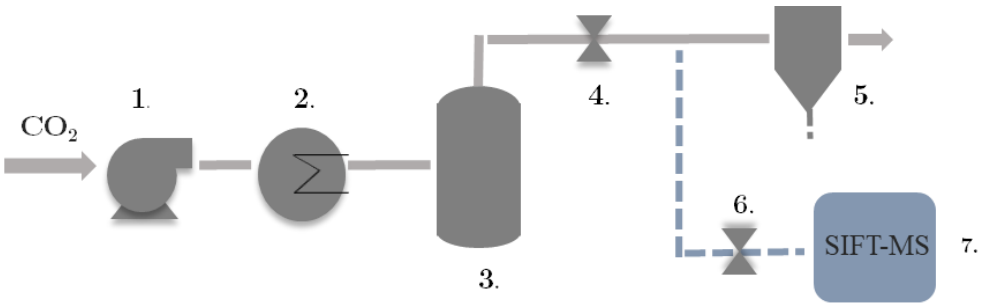

Figure 4.2. Schematic diagram of the supercritical CO_2 extraction/drying process coupled with SIFT-MS; (1) High pressure pump (Flow rate= 20 g/min), (2) Electrical heat exchanger (Temperature= 60 °C), (3) Temperature controlled pressure vessel, (4) Back pressure regulator (Pressure= 140 bar), (5) Cyclone (Temperature=25 °C and Pressure= 7 bar), (6) Metering valve (Pressure= 1 bar and Flow rate = 30 mL/min), (7) SIFT-MS equipment.

An overview of the extraction process coupled with SIFT-MS is presented in **Figure 4.2** Liquefied carbon dioxide was pumped (1) at controlled flow rate through a heat exchanger (2) in the pressure vessel (500 mL) (3). There is a backpressure regulator (4) that held the pressure inside the vessel to the set point while CO_2 was continuously flowing through the cake at a constant rate. The CO_2-solvent mixture was throttled to 7 bar pressure into a cyclone to separate the two phases. As a result, the solvent precipitated in the cyclone and the gas went to the exhaust. The exhaust was constantly sampled via a side stream to the SIFT-MS (7). A metering valve (6) was connected to the stream

to reduce the pressure to 1 bar and control the flow rate of sampling for reliable measurements.

4.2.4 Selected Ion Flow Tube Spectrometry, SIFT-MS

Previous papers have described in detail the SIFT-MS technology [136–138]. The principles of the technique are briefly summarised in section **3.3.5.1**.

In the present work, SIFT-MS Voice200*ultra* equipment was provided by Anatune. Before each experiment, the flow rate of sampling was regulated to 30ml/min and the method was validated by using standard analytes of known concentrations, for accurate measurements. The temperature of the sample inlet was set to 120°C to maintain a vapour phase of the sampled mixture.

4.2.5 Online monitoring of the supercritical CO_2 extraction/drying endpoint by using SIFT-MS

To determine the endpoint of drying by supercritical CO_2 extraction, extraction curves were generated by measuring the amount of solvent collected at the exit of the cyclone at different time intervals. An example of them is illustrated on **Figure 4.3 (a)** where the percentage of the extracted solvent, in this case dodecane, is plotted versus time. When most of the solvent was removed from the cake, the extraction/drying rate became slow and the quantity of solvent

precipitated in the vessel was so small that was difficult to be collected and measured with a balance. As it is shown from the **Figure 4.3** (a) a rough approximation of the extraction/drying endpoint was given gravimetrically at around 110 minutes and this was where online SIFT-MS analysis was applied.

A shut off valve connected to the stream after the backpressure regulator opened and continuous sampling took place with the use of SIFT-MS online probe. Solvent concentration changes were tracked in real time in the gas phase and data concentration points were recorded every 3 seconds. **Figure 4.3 (b)** gives a graphical representation of dodecane concentrations in ppm obtained from SIFT-MS analysis. At the beginning of the graph, the amount of dodecane in the CO_2 phase decreased over time and after around 170 minutes of extraction/drying the curve reached a plateau, which means no more solvent was removed and indicated the end of the process. In many instances, solvent precipitation and accumulation in the sampling line occurred during extraction, leading to inaccurate measurements. As a result, the concentrations recorded by the instrument do not accurately reflect those in the extraction vessel, explaining why the concentrations at the end of the $scCO_2$ extraction/drying often differ significantly from offline measurements. Furthermore, as stated earlier in section **4.1**, the instrument's limit of detection ranges from 100 ppm to a few parts per

billion in the gas phase. This signifies that measurements above 100 ppm may not be reliable. Nevertheless, from **Figure 4.3 (b)**, it can be concluded that once the concentration stabilises, the extraction/ drying process is complete. In this experiment, the extraction/drying stopped at around 180 minutes and the system was depressurized gradually obtaining at the end the solvent free sample. The cake was weighed before and after the extraction/drying allowing for the total amount of the solvent removed from the sample to be estimated (shown in blue colour **Figure 4.3 (a)**). After the extraction/drying, offline SIFT-MS headspace analysis was used for rapid quantification of the actual solvent concentrations remained in the cake.

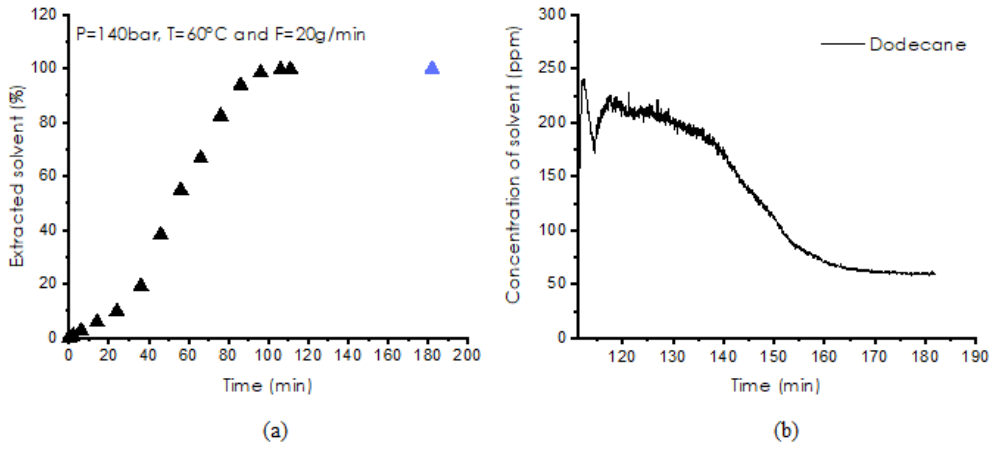

Figure 4.3. (a) Percentage of extracted dodecane versus time; at P=140 bar, T= 60 °C and F=20 g/min (b) Dodecane concentration changes over time obtained from SIFT-MS online analysis.

4.3 Results and discussion

Samples of 120 g paracetamol powder wet in dodecane, were dried at P=140 bar, T=60 ^oC and F=20 g/min. The supercritical conditions were chosen with respect to the critical point of CO_2. From previous initial experiments, it was noticed that at the beginning, the extraction/drying of dodecane was quite slow. It was assumed that the main cause could be the time taken for the system to reach the desired temperature and achieve a single phase. Since the formed cake is at room temperature before it is introduced into the chamber, heat is transferred from the preheated vessel to the wet cake. An approximation of time for the cake to reach the 60 ^oC was estimated experimentally to confirm this assumption.

Three out of four samples were preheated for different periods before the supercritical CO_2 extraction/drying started. In the first experiment, the system was pressurised straight after the cake was placed in the chamber while in the rest of the cases, the samples were left for 30, 60 and 90 minutes to reach the predefined temperature. Due to limitations of the technique and the design of the equipment, it was difficult to obtain the temperature profile of the cakes during preheating. For example, the structure of the equipment does not allow the use of thermocouples inside the vessel and potential modifications might affect the sealing of the vessel. Any cake disturbance caused by locating the

thermocouples inside the sample, should be avoided for even and efficient extraction/drying.

From the experimental measurements, extraction curves were produced in the way that was described in the subsection **4.2.5**. **Figure 4.4** shows clearly the differences between the four cases. In the first two experiments, (1) and (2), the fast extraction/drying zone where easily accessible solvent is removed, started after 40 minutes, whereas in the experiments (3) and (4) slow extraction/drying occurs for the first 20 minutes. Furthermore, the endpoint is significantly shifted to the left when preheating the cake for at least 60 minutes and the total time to carry away the solvent from the sample is reduced by half.

Table 4.1 presents the total time taken for the solvent removal including the amount of CO_2 spent for the experiments (1)-(4). When considering the total time of both the preheating and extraction/drying stages, the time taken for all solvent to be removed was comparable to that without the pre-heating stage. Through pre-heating, it was found that the amount of carbon dioxide required was greatly reduced. In addition to this, it is less energy intensive than the extraction/drying process, leading to less energy being expended. This results in lower operating costs while increasing the efficiency of the process, highlighting

the potential of including a pre-heating stage. There are few published examples of preheating the substrate prior to commencing supercritical extraction none of them relate to extractive drying as exemplified here [139], [140], [141].

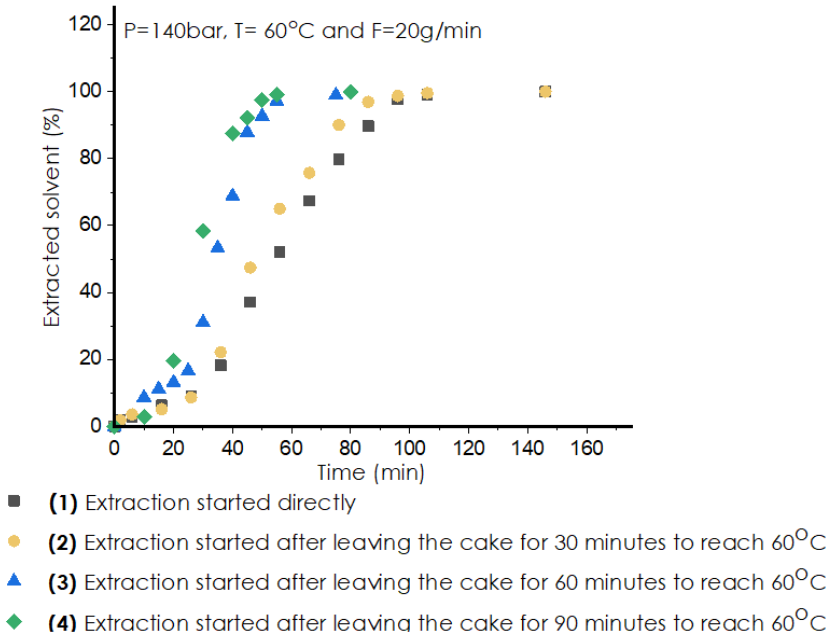

Figure 4.4. Extraction curves showing the effect of preheating the cake before extraction on the kinetics. The final point was determined using on-line SIFT-MS analysis.

Table 4.1. Total extraction/drying time and amount of CO_2 spent for the experiments (1)-(4).

Exp. No	Total mass of removed solvent (g)	Extraction/drying time (min)	Preheating period (min)	Total time for solvent removal (min)	Total mass of CO_2 (g)
(1)	37	152	0	152	3021
(2)	37	146	30	176	3098
(3)	34	76	60	136	1768
(4)	37	80	90	170	1754

4.3.1 Samples analysed using offline SIFT-MS headspace analysis

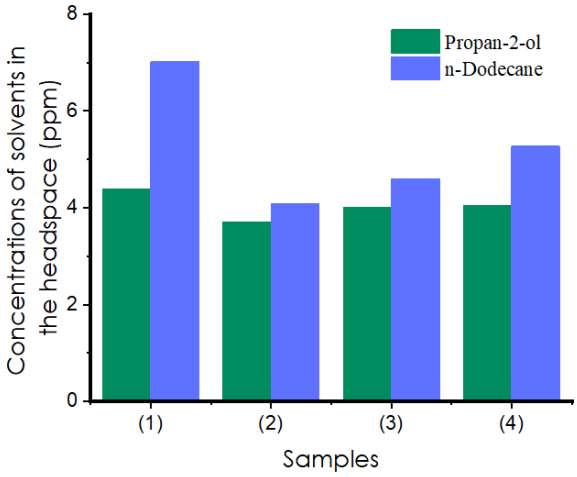

Figure 4.5. Dodecane and propan-2-ol concentrations in the headspace given by SIFT-MS for samples (1)-(4) (number of repetitions, n=1).

For the validation of the endpoint, the processed samples were analysed using SIFT-MS headspace analysis to determine the final solvent concentrations in the product. The solvent residues in experiments (1)-(4) were within the range 4-7 ppm in the headspace, (shown in **Figure 4.5**). These measurements represent the relative solvent concentrations in the samples and in all cases, the solvents had been removed to a satisfactory level. At the moment, there is no provided data in the literature for allowable concentration limits of dodecane per daily dose. For this purpose, an assumption was made considering the hazards and the properties of the solvent. According to the ICH [142], solvents of similar properties with dodecane such as heptane, are classified as Class 3 solvents and the permitted daily exposure is 5000 ppm. Thus, these values verify that the product is successfully dried and indicate the feasibility of SIFT-MS to monitor online the supercritical CO_2 extraction/drying endpoint. Furthermore, **Figure 4.5** shows the capacity and consistency of both techniques separately and being coupled.

4.4 Conclusions

The work presented in this chapter shows that supercritical CO_2 extraction is a very promising technique for the removal of organic solvents from APIs. When coupled with SIFT-MS online analysis, the process can be monitored in real time

at the later stages of the extraction/drying to a scale of scrutiny not possible by existing techniques, allowing for the solvent residues in the final product to be reduced down to a few ppm, whilst minimising process time and CO_2 consumption. This has been proved through the experimental work conducted, in which four paracetamol cakes were successfully dried after being washed with dodecane. The dry cakes were analysed using SIFT-MS headspace analysis, which showed negligible amount of residual solvents ranged within 4-7 ppm in headspace. The narrow range of final concentrations indicates the reliability and reproducibility of the coupled techniques.

At the same time, the effect of pre-heating prior to extraction/drying process was investigated. It was concluded that leaving the cake to reach the defined temperature enhances the efficiency of the process by reducing significantly the extraction/drying time. This lowers both the amount of CO_2 required for the removal of dodecane and the energy consumption of the process. In the next step, a parametric study for optimising the process was carried out.

5 Optimisation of supercritical CO_2 extraction/drying

Chapter 5 presents an experimental parametric study which aims to optimise the extraction/drying process for solvent removal as proposed in chapter 4, by evaluating important variables including pressure, temperature, CO_2 flow rate and mass of substrate in the wet cake. A simple mathematical model is applied to the measured extraction/drying data in order to generalise the experimental results and understand the behavior of the system. Moreover, the influence of the operating variables on the extraction/drying process including the final particle characterisitics is investigated using MODDE software. The experimental procedure as well as offline and in-line analytical and characterisation techniques are thoroughly descibed in the previous chapters and are not mentioned here.

5.1 Experimental design

For the experimental design, four factors were selected: pressure, temperature, CO_2 flow rate and mass of the substrate in the wet cake. The pressure and temperature values investigated represent a relatively broad range of operating conditions within the supercritical CO_2 region. The lowest pressure and temperature conditions were defined by the CO_2 critical point, while the highest conditions were arbitrarily chosen. Although more extreme values could have been selected due to the low solubility of paracetamol in $scCO_2$ [143], the purpose of the study was to perform supercritical CO_2 extraction/drying over a wide range of operating conditions, but not necessarily the most forcing conditions possible. The CO_2 flow rate ranged between 10-30 g/min and the mass of cake varied between 60-150 g, to achieve similarity with the AFD experiments reported in chapter 2. The CO_2 flow rate was determined in accordance with the equipment's capacity (maximum flow rate 50 g/min), with careful consideration given to both upper and lower limits. For example, excessively high flow rates can lead to insufficient contact time between the CO_2 and wet particles. Conversely, excessively low flow rates may prolong the extraction/drying process. The preheated periods for 60, 105 and 150 g cakes

were 60, 90 and 120 min respectively. All the ranges of operational variables evaluated are illustrated in **Table 5.1**.

Table 5.1. Investigated parameters using supercritical CO_2 technology.

Pressure (bar)	80 -200
Temperature (°C)	50 -70
CO_2 flow rate (g/min)	10 -30
Mass of cakes (g)	60- 150

Following the same methodology as reported previously, MODDE Pro V11.0.1 software was used to optimise the extraction/drying process and to determine which process inputs have the most significant influence on the process outputs. A D-optimal method was selected to create a reduced number of extraction/ drying experiments including 3 repetitions to evaluate the reproducibility of the process (**Table 5.3**). The measured responses were; residual solvent content, extraction/drying time, C_{fL^*} concentration (see section **5.2.1**), extent of agglomeration, agglomerate brittleness index (ABI) and particle size. **Table 5.2** lists all the responses and the corresponding offline techniques used for evaluating the process efficiency.

Table 5.2. Offline techniques used for cake analysis and mechanical properties.

Residual solvents in the dried cake	Offline SIFT-MS
Extent of agglomeration	Birch and Marziano's method
ABI index	Birch and Marziano's method
Particle size	Morphologi G3 (Malvern)

Table 5.3. A D-optimal experimental design produced using MODDE software.

Exp. No.	**Temperature (°C)**	**Pressure (bar)**	**CO_2 flow rate (g/min)**	**Cake size (g)**
1	50	200	10	60
2	50	140	10	60
3	70	200	10	60
4	60	140	20	60
5	50	80	30	60
6	70	80	30	60
7	60	200	30	60
8	70	80	20	60
9	70	200	20	60
10	50	80	10	150
11	70	80	10	150
12	60	200	20	150
13	50	200	30	150
14	70	200	30	150
15	60	80	30	150
16	60	140	20	150
17	50	200	10	105
18	70	140	10	105
19	50	80	20	105
20*	60	140	20	105
21*	60	140	20	105
22*	60	140	20	105

* *Experiments 20, 21, and 22 serve as the central points in the Design of Experiments (DOE), and they will be utilised to assess the reproducibility of the process.*

5.2 Results and discussion

The experimental design of experiments, **Table 5.3**, was modified by removing experiments involving the lowest pressure due to very slow extraction/drying rates. As it is seen from **Figure 5.1**, small mass fractions of solvent (0.15-0.3) were removed after 2 hours of extraction/drying at 80 bar. A possible explanation is that the solubility of dodecane near the critical point of CO_2 is quite low. Thus, the experiments 4, 5, 6, 10, 11 and 15 were excluded from the experimental design and an extra one involving drying 60 g of cake at conditions similar to the DOE middle point was added. In this way, it was possible to compare different cake sizes and to investigate the effect of solid load on extraction/drying process. The updated version of the DOE is presented on **Table 5.4**.

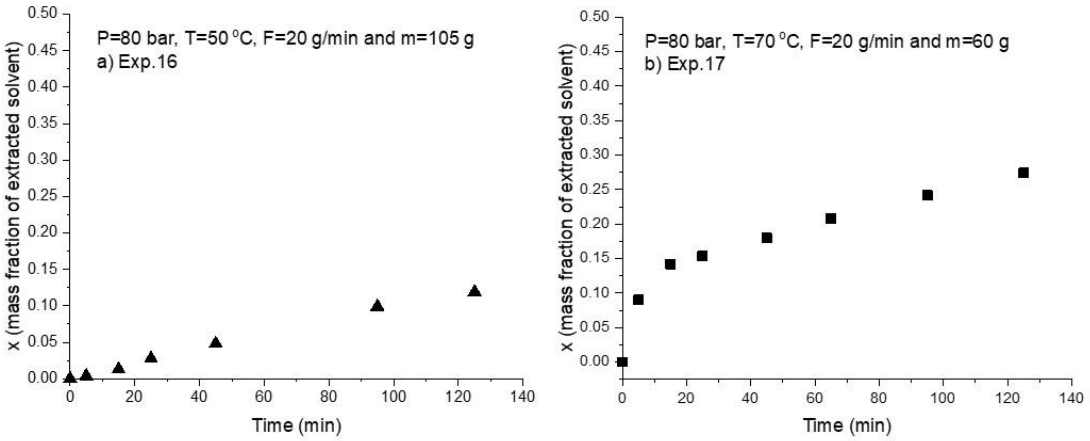

Figure 5.1. Extraction/drying curves at low supercritical CO_2 conditions.

Table 5.4. The updated version of the experimental design.

Exp. No.	**Temperature (°C)**	**Pressure (bar)**	**CO_2 flow rate (g/min)**	**Cake size (g)**
1	50	200	10	60
2	50	140	10	60
3	70	200	10	60
4*	60	140	20	60
5	60	200	30	60
6	70	200	20	60
7	60	200	20	150
8	50	200	30	150
9	70	200	30	150
10	60	140	20	150
11	50	200	10	105
12	70	140	10	105
13†	60	140	20	105
14†	60	140	20	105
15†	60	140	20	105

**This experiment was added to the DOE in order to investigate the effect of solid load.*

† Experiments 13, 14, and 15 serve as the central points in the Design of Experiments (DOE), and they will be utilised to assess the reproducibility of the process.

5.2.1 Applying an existing mathematical model to the CO_2 extraction/drying experimental data

There are a variety of published models that differ from mathematical and mass transfer mechanism point of view [144]. Many papers characterise the supercritical fluid extraction of liquids as a drying procedure [106] while others relate it to gas absorption or solvent-extraction mass transfer. Generally, the initial extraction rates are dominated by the solubility of the solute in the supercritical fluid phase and from the aspect of maths, all the equations rely on differential mass balance integration of **Eq. (5.1)** with some assumptions. The main differences between these models lie in phase equilibrium description, fluid flow mode, and solute diffusion in matrices [144].

$$\frac{dC_f}{dt} + u \cdot \varepsilon \cdot \frac{dC_f}{dz} = D \cdot \frac{d^2C_f}{dz^2} + \frac{(1-\varepsilon)}{\varepsilon} \cdot \alpha \cdot k \cdot (C_f^* - C_f) \quad \textbf{Eq. (5.1)}$$

where C_f is the concentration of solute in the supercritical CO_2 phase, u is the interstitial velocity of the fluid, ε is the void fraction of the bed, D is the axial dispersion coefficient of the solute in the supercritical CO_2 phase, α is the effective solid – fluid contact area for mass transfer, k is the mass transfer coefficient for the solute and C_f^* is the concentration of solute in the fluid phase that is in equilibrium with the solid surface

The current model system deals with the extraction of dodecane from paracetamol powder particles in a packed bed by using supercritical CO_2. This system differs from the common SFE processes since the extract is an organic

solvent, held up within an API filter cake. Considering that at relatively mild conditions, the solubility of paracetamol in the supercritical CO_2 phase is low [143] and the solid-solvent interactions are negligible, the extraction is mainly driven by the solubility of the organic solvent in the fluid phase relative to its value at saturation. In this study, the behaviour of the extraction process under investigation is described using a mathematical model proposed by Pardo-Castaño et al. [93]. This model, which is based on the Brunauer-Emmett-Teller (BET) adsorption theory (see section **5.2.1.3**), is characterised by one simple equation with three adjustable parameters, as opposed to Sovová's model, which comprises three conditional equations. The proposed model not only correlates information on the kinetics of SFE but also predicts the apparent solubility, as indicated by the slope of the extraction yield versus time curve. Even though the model has been used for correlating experimental data on the supercritical extraction of natural matter such as germ corn oil and striped weakfish oil, it performs relatively well for the system being investigated and it is quantitatively and qualitatively useful for investigating solvent extraction rates under different operating conditions.

5.2.1.1 Assumptions

In order to simplify the differential balance equation **Eq. (5.1)** and reach the simple mathematical model proposed by Pardo-Castaño et al., it is necessary to make some assumptions considering the differences between the present system and the one reported in the paper by Pardo-Castaño et al. [93].

- It is assumed that the organic solvent is uniformly distributed across the bed.
- The physical properties of the supercritical CO_2 remain constant throughout the extraction process.
- The bed void fraction is constant ($\varepsilon = 0.32$).
- It is considered as a packed bed of equally sized spheres based on the median particle diameter D_{50} of the crystalline paracetamol.
- At t = 0, pure carbon dioxide is continuously introduced at the bottom of the cake where pressure, temperature and flow rate are kept constant at their set point. As the flow stream diffuses into the pores of the cake, liquid (solvent) is extracted and carried away by the CO_2 molecules.
- The accumulation of the solvent in the fluid phase is negligible.
- The axial dispersion is not considered. This approximation is valid for long vessels or when high superficial velocities are applied [145]. The first

criterion can be evaluated by the ratio [146] between the length of the extractor and the average particle diameter.

$$\frac{L_E}{D_p} \geq 50$$

Under the above assumptions, which satisfactorily describe the removal of dodecane from paracetamol particles packed in fixed bed, the conservation equation **Eq. (5.1)** for the solvent in the fluid phase is simplified as below **Eq. (5.2).**

$$u \cdot \varepsilon \cdot \frac{dC_{sf}}{dz} = k \cdot (C_f^* - C_f) \quad \textbf{Eq. (5.2),}$$

$$z=0,\ C_f = 0 \text{ and } z=L,\ C_f = C_{fL}$$

$$\text{and } k = (1-\varepsilon) \cdot \alpha_{sf} \cdot k_{sf}$$

where k_{sf} is the external mass transfer coefficient for the solvent evaporated in the supercritical phase around the solid particles (m/s) and a_{sf} is the specific surface area of the particles (m^{-1})

By integrating the equation **Eq. (5.2)** and considering the initial conditions for the extractor, the concentration of solvent in the fluid phase at the outlet of the bed is given by **Eq. (5.3).**

$$C_{fL} = C_{fL}^* \cdot \left[1 - \exp\left(-\frac{k \cdot L}{u \cdot \varepsilon}\right)\right] \quad \textbf{Eq. (5.3)}$$

where L is the length of the packed bed (m)

5.2.1.2 Overall material balance in the packed solid

Now, a material balance of the solute in the solid packed into the extractor is employed, as provided by:

$$\frac{dm_s}{dt} = -\dot{m}_f \left[\frac{m_{fL}}{m_{fT}-m_{fL}}\right] \textbf{Eq. (5.4)}$$

where m_s is the mass of the solute in the solid at time t, $\dot{m}_f$ is the flow rate of the supercritical fluid, m_{fL} is the mass of solute in the supercritical fluid phase at the exit of the vessel and m_{fT} is the mass of solute and supercritical fluid

It is assumed that $m_{fT} \gg m_{fl}$ and the **Eq. (5.4)** can be represented as follows:

$$\frac{dx_s}{dt} = -\frac{\dot{m}_f}{m_0} \cdot C_{fL} \quad \textbf{Eq. (5.5)}$$

where x_s is the solute mass fraction in the solid at time t, and m_0 is the initial extractable mass of the solute in the packed bed. It is assumed that changes in x_s do not occur considerably in the axial direction, given that the amount of extracted solute from the solid matrix in the differential element is minimal and significantly lower than the solubility of the solute in the supercritical fluid

By replacing **Eq. (5.4)** into **Eq. (5.5)** the following relationship is obtained:

$$\frac{dx_s}{dt} = -\frac{\dot{m}_f}{m_0} C_{fL}^{*} \cdot \left[1 - \exp\left(-\frac{k \cdot L}{u \cdot \varepsilon}\right)\right] \textbf{Eq. (5.6)}$$

5.2.1.3 BET- type equilibrium equation

The interaction of solute with the solid and fluid phase can be described by the BET adsorption isotherm formula:

$$\frac{x_s}{x_m} = \frac{K \cdot x}{[1 - x] \cdot [1 + (K - 1) \cdot x]} \quad \textbf{Eq. (5.7)}$$

where x is the ratio between the solute mass fraction in equilibrium, C_{fL}^*, and the solute mass fraction the saturated supercritical phase, C_{sat}. The solute mass fraction in the first monolayer (m_m/m_0) is x_m and K is the sorption equilibrium coefficient which indicates the strength of interaction between solute and solid.

Eq. (5.7) can be written and solved as follows:

$$(1 - K) \cdot x^2 + \left[K \cdot \left(1 + \frac{x_m}{x_s}\right) - 2\right] \cdot x + 1 = 0 \quad \textbf{Eq. (5.8)}$$

$$x = \frac{-\left[K \cdot \left(1 + \frac{x_m}{x_s}\right) - 2\right] \pm \sqrt{\left[K \cdot \left(1 + \frac{x_m}{x_s}\right) - 2\right]^2 - 4 \cdot (1 - K)}}{2 \cdot (1 - K)} \quad \textbf{Eq. (5.9)}$$

Considering the scenario where the supercritical fluid is saturated with the solute, resulting in a substantial number of molecules being adsorbed on the solid ($m_0 \to 0, x_s \to \infty$), an expression for x as a function of K is derived:

$$x = \frac{2 - K \pm K}{2 \cdot (1 - K)} \quad \textbf{Eq. (5.10)}$$

Since K>1 and 0 ≤ x ≤1, the root with the negative sign in the **Eq. (5.10)** is physically valid and therefore x=1. By replacing **Eq. (5.8)** in **Eq. (5.6)**, the following relationship is obtained:

$$\frac{dx_s}{dt} = -\frac{\dot{m}_f}{m_0} C_{fL}^{*} \cdot \left\{ \frac{-\left[K\left(1+\frac{x_m}{x_s}\right)-2\right] \pm \sqrt{\left[K\left(1+\frac{x_m}{x_s}\right)-2\right]^2 - 4(1-K)}}{2(1-K)} \right\} \quad \textbf{Eq. (5.11)}$$

5.2.1.4 Simple BET-based model

Solving the **Eq. (5.11)** allows the model to represent the extraction of the solvent as a function of time and is given below **Eq. (5.12)** [93].

$$t = \frac{m_0}{Q_{CO2} \cdot C_{fL}^{*}} \cdot \left(x_0' + x' + (2-K) \cdot \left[x - x_m \cdot \ln\left(\frac{\alpha'}{\beta}\right)\right] + K \cdot x_m \cdot \ln\left[\frac{\alpha''}{\beta' \cdot (1-x)^2}\right]\right) \quad \textbf{Eq. (5.12)}$$

and

$$a = K^2 \quad \textbf{Eq. (5.13)}$$

$$b = 2 \cdot (2-K) \cdot K \cdot x_m \quad \textbf{Eq. (5.14)}$$

$$c = (K \cdot x_m)^2 \quad \textbf{Eq. (5.15)}$$

$$x_0' = \sqrt{a+b+c} \quad \textbf{Eq. (5.16)}$$

$$x' = \sqrt{a \cdot (1-x)^2 + b \cdot (1-x) + c} \quad \textbf{Eq. (5.17)}$$

$$a' = x' + K \cdot (1-x) + (2-K) \cdot x_m \quad \textbf{Eq. (5.18)}$$

$$a'' = x' + (2-K) \cdot (1-x) + K \cdot x_m \quad \textbf{Eq. (5.19)}$$

$$\beta = x_0' + K + (2-K) \cdot x_m \quad \textbf{Eq. (5.20)}$$

$$\beta' = x_0' + (2-K) + K \cdot x_m \quad \textbf{Eq. (5.21)}$$

$$C_{fL}^{*} = C_{sat} \cdot \left[1 - \exp\left(-\frac{k \cdot L}{u \cdot \varepsilon}\right)\right] \quad \textbf{Eq. (5.22)}$$

$$k = (1 - \varepsilon) \cdot \alpha_{sf} \cdot k_{sf} \quad \textbf{Eq. (5.23)}$$

where x is the mass ratio between the amount of solvent measured at time t (s) and the overall extractable mass of solvent (kg/kg); m_0 is the initial mass of solvent in the packed bed (kg); Q_{CO2} is CO_2 flow rate (kg/min); C_{sat} is the solvent concentration in the saturated supercritical CO_2 phase (kg/kg)

The K_{sf} coefficient is expressed by the dimensional Sherwood number as follows:

$$K_{sf} = \frac{Sh \cdot D_m}{D_p} \quad \textbf{Eq. (5.24)}$$

where D_m (m^2/s) is the binary diffusion coefficient of the solvent and the supercritical CO_2

The Sherwood number can be estimated by several relationships depending on the hydrodynamic conditions (laminar or turbulent flow) and the geometry of the solid surface [147]. Here, this parameter is calculated using equations **Eq. (5.25)** [103] and **Eq. (5.26)** [145] taken from the literature.

$$Sh = 0.135 \cdot Re^{0.5} \cdot Sc^{0.33} \textbf{ Eq. (5.25)}$$

valid for Re (0.169—1.292) & Sc (6 -25)

$$Sh = 0.3 \cdot Re^{0.83} \cdot Sc^{0.33} \textbf{ Eq. (5.26)}$$

valid for Re (2—40) & Sc (2 -20),

where the dimensionless parameters Re and Sc in the aforementioned equations are determined through the following expressions,

$$Re = \frac{\rho \cdot u \cdot d_p}{\mu} \quad \textbf{Eq. (5.27)}$$

$$Sc = \frac{\mu}{\rho \cdot D_m} \quad \textbf{Eq. (5.28)}$$

The adjustable parameters in the equation **Eq. (5.12)** include the solubility, C_{fL}^*, of the solvent in the supercritical CO_2 phase corrected by transport limitations such as diffusion (kg/kg), the x_m solvent mass fraction (kg/kg) of solvent in the first monolayer or the less accessible solvent ($m_{inaccessible}/m_0$) and the K ratio between the adsorption equilibrium constants in the first monolayer and that in the next layers (kg/kg).

In the present work, the x_m parameter is not influenced by the operating conditions and since it represents the least accessible amount of solvent in the cake it can be considered constant for all the experiments of the studied system. Additionally, the equilibrium adsorption ratio K, is around one as the solid-solvent interactions are weak and the adsorption constants are approximately the same for all the layers including the solvent retained in the inter-particle spaces and within the crystal lattice. Hence, the equation **Eq. (5.12)** is converted to a simpler model **Eq. (5.29)** with two adjustable parameters C_{fL}^* and x_m.

$$t = \frac{m_0}{Q_{CO2} \cdot C_{fL}^*} \cdot [x - x_m \cdot \ln(1 - x)] \quad \textbf{Eq. (5.29)}$$

The C_{fL}^* and x_m are determined by fitting the model to the extraction data using a global optimization algorithm which is implemented through Python. As the

objective function for minimisation, the average squared deviation (ASRD) **Eq. (5.30)** is used, where N are the experimental data points in each run, t_j is the extraction time (s) for the experiment j, and subscripts exp and cal refer to experimental and calculated, respectively.

$$F(C_{fL}^{*}, x_m) = \frac{100}{N-1}\sum_{j=1}^{n}\left(\frac{t_j^{exp} - t_j^{cal}}{t_j^{exp}}\right)^2 \quad \textbf{Eq. (5.30)}$$

According to Pardo-Castaño et al.'s paper [93], the time is normalised by rescaling the values in the range 0 to 1. In this way, the model performs better, reducing the number of iterations required for fitting the routine. Furthermore, the initial guess for the solubility of the solvent in the supercritical CO_2 phase was approximated according to the experimental data obtained at the beginning of the extraction. The highest amount of solvent removed in the fast extraction zone divided by the CO_2 mass spent for the extracted solvent gives an estimated value at the specific operating conditions. Finally, for the experiments where the cakes required longer preheating periods and resulted in slow extraction rates at the early stages of the process, the obtained extraction curves were modified by excluding one or two initial experimental data points. Thus, the model could give valid information about the solubility and the extraction kinetics at the defined operating conditions.

The fluid physical properties at the selected operating conditions are based mainly on the pure carbon dioxide as described in the paper and are calculated by equations of state and published correlations, found in literature [149], [150], [151]. All the mathematical relationships including the calculations are reported in the **Appendix B** section of this chapter and the most significant parameters used for the BET based model are presented in **Table 5.5** The density results derived from the Peng-Robinson equation of state closely match with the data obtained from the NIST Chemistry Webbook (see **Table B 3**). Likewise, the viscosity values taken from A.Fenghour et al. paper exhibit a similar level of proximity. The calculated Reynolds number changes slightly across different conditions, and in all cases, the values are below or close to 1, which correspond to laminar flow. The external mass transfer coefficient K_{sf} ranges from 0.6 to $2.6 \cdot 10\text{-}5$ m/s with lower values observed at smaller CO_2 flow rates (10 g/min). The binary diffusion coefficient ($\mathbf{D}_m$) falls within the range of 4.6 to $6.2 \cdot 10^{-9}$ m^2/s. It seems to rise with temperature under constant pressure conditions, while showing a slight decline with increasing pressure at constant temperature. The Schmidt number, which represents the ratio of momentum diffusivity to mass diffusivity, varies between 11.1 and 20.5. The lowest value corresponds to the

experimental conditions of 140 bar and 70 °C, where the kinematic viscosity is at its minimum and the diffusion coefficient is at its maximum.

Table 5.5. The required parameters estimated for modelling the experimental data of the current system.

Exp. No.	**$D_m \cdot 10^{-9}$ ↾ (m^2/s)**	**$K_{sf} \cdot 10^{-5}$ (m/s)**	**Re**	**Sh**	**Sc**	**$\mu \cdot 10^{-6}$ * (Pa · s)**	**ρ** ** **(Kg/m^3)**
1	4.6	0.5	0.2	0.2	19.8	71.7	787
2	4.8	0.6	0.3	0.2	20.5	60.1	606
3	5.9	0.7	0.3	0.2	14.0	54.8	657
4	5.5	2.2	0.8	0.6	14.3	40.2	511
5	5.3	2.3	0.9	0.7	14.4	54.8	721
6	5.9	1.8	0.6	0.5	14.0	54.8	657
7	5.3	1.6	0.6	0.5	14.4	54.8	721
8	4.6	1.8	0.7	0.6	19.8	71.7	787
9	5.9	2.6	0.9	0.7	14.0	54.8	657
10	5.5	2.2	0.8	0.6	14.3	40.2	511
11	4.6	0.7	0.2	0.2	19.8	71.7	787
12	6.2	1.6	0.5	0.4	11.1	30.3	438
13	5.5	2.2	0.8	0.6	14.3	40.2	511
14	5.5	2.2	0.8	0.6	14.3	40.2	511
15	5.5	2.2	0.8	0.6	14.3	40.2	511

**The viscosity of the CO_2 above the critical point was obtained from A.Fenghour, et al.'s (1997) paper* [152]
***The density of the supercritical CO_2 was estimated by Peng Robinson equation of state (1976)* [149]
↾ Binary diffusion coefficient was calculated using S.P. Cadogan etal. correlation (2016) [151]

5.2.2 Mathematical modelling results

The simpler form of the BET based model contains two parameters fitted in the equation by minimising the difference between experimental and predicted values. As it is stated previously, the x_m value illustrates the amount of solvent that is less accessible and is independent from the operating conditions. A similar case for the x_m is reported by other authors but for different studied systems [153]. Because the mass of the easily accessible solvent is much greater than the amount of solvent that is difficult to remove, this number is expected to be small. As it can be seen from **Table 5.6** the parameter x_m is 0.0909 for all the data sets, while the C_{fL}^* varies with the operating conditions. In terms of solubility, the fitted C_{fL}^* value is equal to C_{sat} calculated by equation **Eq. (5.22),** meaning that the diffusional limitations are negligible. In other words, the amount of free unbound solvent deposited in the pores of the cake is substantial and is easily removed with minimal mass transfer resistance. Additionally, the size of the particles results in large surface area to be exposed in the supercritical CO_2 phase and the diffusion path into the crystal lattice is quite short through which negligible mass of trapped solvent is extracted. **Table 5.6** presents the results obtained for all the experiments including the ASRD calculated values. The average mean squared deviation between the experimental and the predicted

data is within the range 10 to 35 percent. These errors are considered quite large and in most of the cases, occurred at the initial points of extraction/drying curve. A big deviation is observed as well between the final experimental and calculated extraction point. The endpoint of the process is the final measurement and relies on the sensitivity of the SIFT-MS instrument, which is used to optimise the extraction by minimising the solvent residues to a few ppm. When the extracted solvent reaches 98%, the kinetics are mainly controlled by diffusion, in which case other models could be applied on the data recorded with the use of SIFT-MS online analysis. The dependency of the C_{fL}^{*} value on the operating conditions will be discussed in the following sections by comparing experiments which differ by one factor.

Table 5.6. The C_{fL}^* and x_m values procured by fitting the experimental data to the BET based model.

Exp. No.	C_{fL}^* (kg/kg)	x_m	ASRD%
1	0.092	0.0909	19.5
2	0.030	0.0909	10.8
3	0.045	0.0909	12.9
4	0.032	0.0909	17.2
5	0.051	0.0909	24.6
6	0.061	0.0909	22.3
7	0.175	0.0909	34.9
8	0.075	0.0909	25.8
9	0.090	0.0909	17.4
10	0.114	0.0909	30.7
11	0.100	0.0909	10.4
12	0.036	0.0909	13.1
13	0.054	0.0909	19.1
14	0.077	0.0909	21.6
15	0.045	0.0909	20.9

5.2.2.1 Effect of process parameters on the extraction kinetics

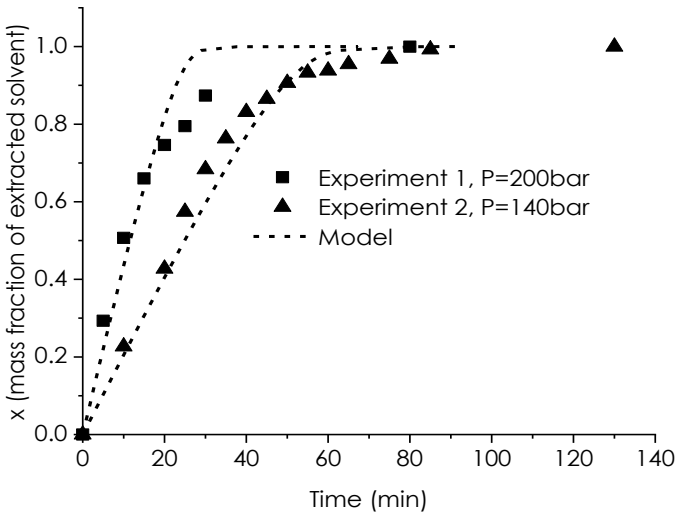

(a)

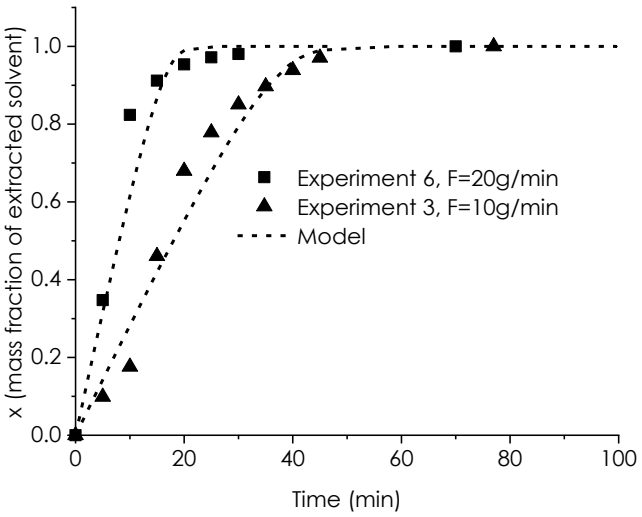

(b)

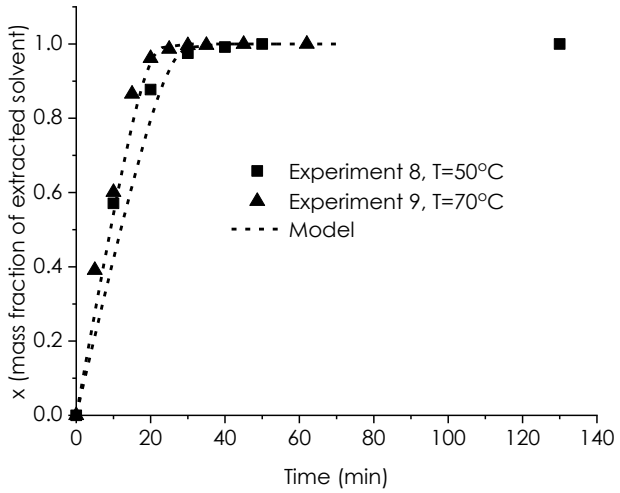

(c)

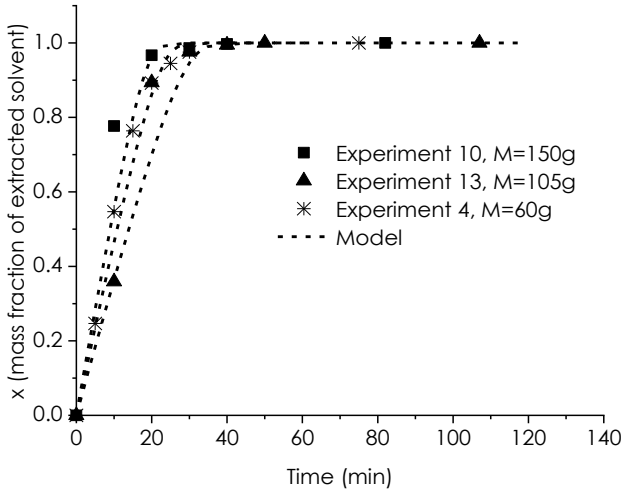

(d)

Figure 5.2. Effect of key factors on extraction kinetics: (**a) Pressure effect** for 60 g cake, T=50 °C and F=10 g/min: P=200 bar and C_{fL}^* =0.092 kg/kg, P=140 bar and C_{fL}^* =0.03 kg/kg; (**b) Flow rate effect** for 60 g cake, T=70 °C and P=200 bar: F=20 g/min and C_{fL}^* =0.061 kg/kg, F=10 g/min and C_{fL}^* = 0.045 kg/kg, (**c) Temperature effect** for 150 g cake, P=200 bar and F=30 g/min: T=70 °C and C_{fL}^* =0.090 kg/kg, T=50 °C and C_{fL}^* =0.075 kg/kg; (**d) Cake size effect** for P=140 bar, T= 60 °C and F=20 g/min: M=60 g and C_{FL}^* =0.032 kg/kg, M=105 g and C_{fL}^* =0.077 kg/kg, M=150 g and C_{fL}^* =0.114 kg/kg.

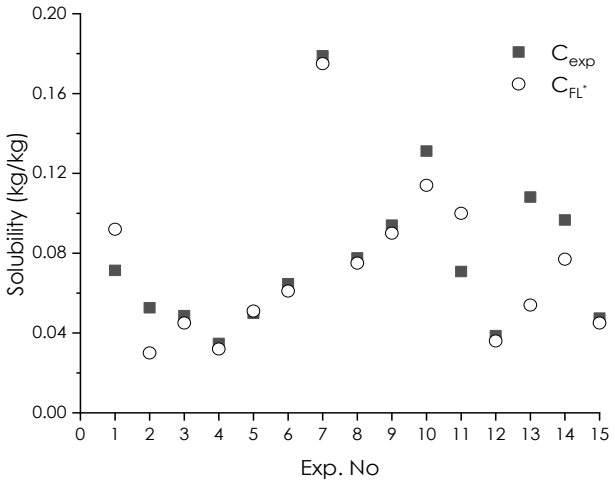

Figure 5.3. The differences between experimental and predicted concentration values, where C_{exp} is the highest solvent concentration extracted in each experimental run and C_{fL}^{*} is the fitted parameter in the BET model.

Figure 5.2 presents the results obtained for various cases where the predicted extraction rates at bed exit are compared with the observed ones. The kinetic curves obtained from the extraction of dodecane illustrate clearly two phases. In the first phase, the unbound free solvent is removed quickly and the extraction rate increases linearly. While in the next phase, there is more gradual decrease in solvent content and the path for interparticle diffusion increases resulting in slow extraction rates. Speaking of the modelled data, in most of the cases compare satisfactorily with the experimental data and the C_{fL}^{*} results bring confidence in using the BET based model for giving an approximation of the solubility of the involved component (dodecane) in the carbon dioxide phase, **Figure 5.3.**

5.2.2.1.1 Effect of pressure

Figure 5.2 (a) investigates the pressure variable for 60 g cakes by keeping constant the rest of the factors. As it can be seen, there is a noticeable difference between the curves at 140 and 200 bar with the latter resulting in higher extraction rates. This is also reflected on the results obtained from the model, where the C_{fL}^* value is three times bigger at 200 bar. By increasing pressure, the density of the fluid is greater and therefore its solubilisation power as solvent also increases. Many authors observed the same behavior for different systems and consider the pressure as the most significant term with the most positive effect in the SFE processes.

5.2.2.1.2 Effect of flow rate

By increasing the flow rate, a faster extraction rate is anticipated, particularly in the initial stages of the process, as depicted in the extraction runs in **Figure 5.2 (b)**. To assess potential mass transfer limitations, the experimental data are normalised by multiplying the time by the CO_2 flow rate. As observed in the **Figure 5.4**, the experimental data points from the two extraction runs are well-aligned, indicating the absence of any mass transfer limitations. Consequently, the C_{fL}^* values should be the same for both experiments; however, in this

instance, they differ slightly, which may be attributed to the model's performance.

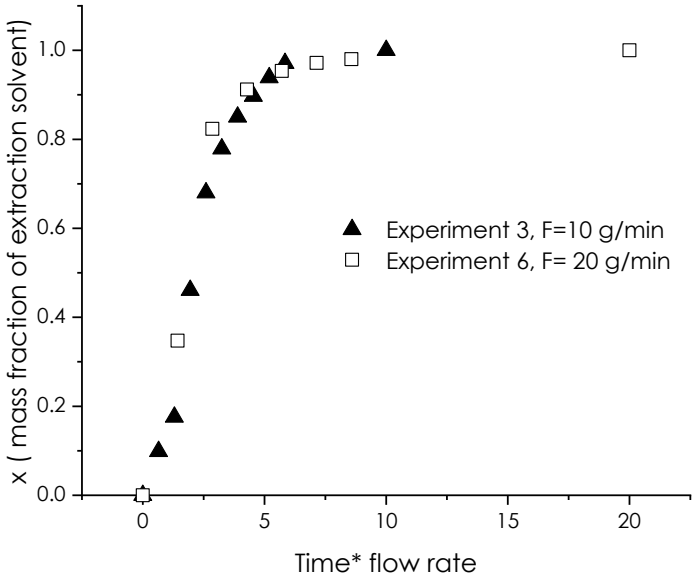

Figure 5.4. Normalised data by multiplying time by CO_2 flow rate.

5.2.2.1.3 Effect of temperature

On the other side, the temperature factor is more complex. At pressures close to the critical point and at constant fluid velocity, the solubility of the substance to be extracted decreases by increasing the temperature. This phenomenon is called retrograde vaporization and it disappears at the so-called crossover pressure where the system becomes temperature independent [97]. As it is shown in **Figure 5.2 (c)** the curves procured at two different temperatures 50 °C and 70 °C are similar and the resulted C_{fL}^* values are relatively close to each other (0.075 kg/kg and 0.09 kg/kg respectively). Hence, in this case, the pressure factor

seems to prevail over temperature and in order to prove this, different pressures should be tested for the same temperature to determine the crossover pressure. However, a slightly different effect is observed for 60 g cakes. **Figure 5.5**, shows deviations between the extraction points at the early stages of the two processes. An interpretation of this variation could be the initial amount of solvent, which differs a lot (28 g and 14.6 g) for the two experiments and/or the large headspace above the 60 g cakes that may introduce errors in the measurements. It should be noted that the pressure and temperature conditions are same in **Figure 5.2 (c)** and **Figure 5.5** therefore it is anticipated the resulted graphs to show similar trends.

Additionally, parity plots illustrating the model's predictions for extraction/ drying time are presented in the **Figure 5.6**. It is evident that a significant number of predicted data points exhibit a deviation of more than ±10%, indicating poor performance of the model in this case.

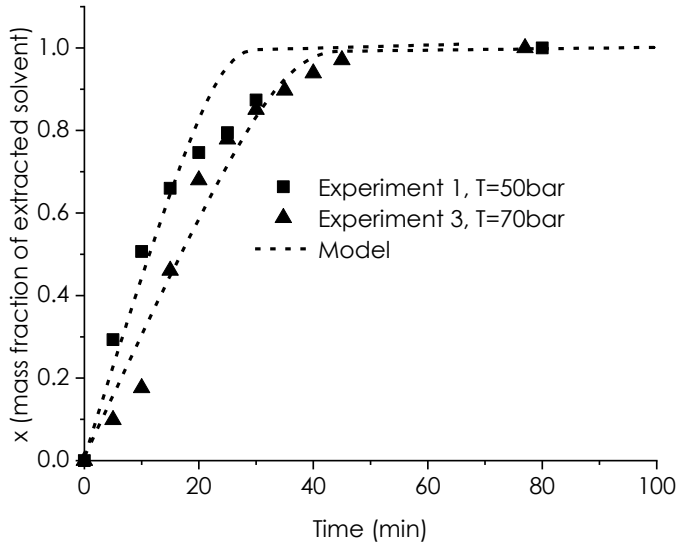

Figure 5.5. a) **Temperature effect** for 60 g cake, P=200 bar and F=10 g/min: T=50 °C and C_{fL}^* = 0.092 kg/kg, T=70 °C and C_{fL}^* =0.045 kg/kg.

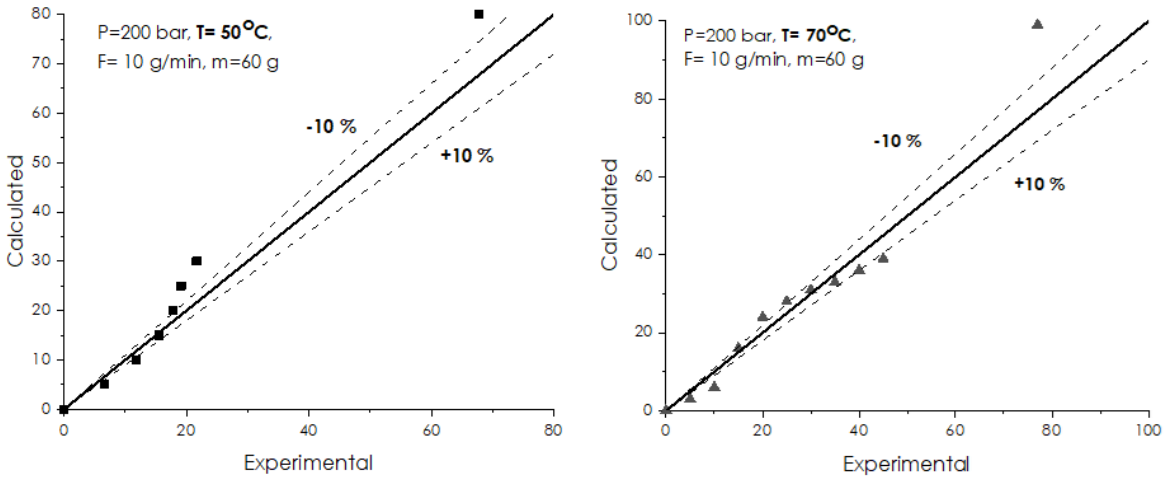

Figure 5.6. Parity plots corresponding to experimental and model calculated extraction/drying time data for experiments 1 and 3. Dashed lines indicate ±10 % error intervals.

5.2.2.1.4 Effect of cake size

In the last case, **Figure 5.2 (d),** three cake sizes that differ in the initial solvent content are investigated. Likewise, in this situation, it is expected the predicted C_{fL}^* values to be similar. However, it is obvious that the larger cakes result in higher concentration values due to reduced dead volume, higher amount of the available solvent and greater residence times within the paracetamol bed.

5.2.2.1.5 Overall results of the model

In summary, pressure, flow rate and cake size are the most influential factors for the extraction kinetics and this is also reported in previous studies [92]. When it comes to temperature though, the results are controversial for the current experiments. For instance, the effect of temperature at 200 bar is slightly different in **Figure 5.2 (c)** and **Figure 5.5,** which makes it hard to decide if it is positive or negative.

Generally, the quite large variance in the solvent content of similar cakes complicates the comparison of experiments that differ by one factor. This issue is also depicted in the three center points **Figure 5.7**. The cake with the less amount of solvent at the beginning of the extraction resulted in low C_{fL}^* data. On the other hand, points CP (1) and CP (2) have very similar $C_{exp,}$ and CP(1) value seems to be closer to the C_{fL}^*, **Table 5.7.**

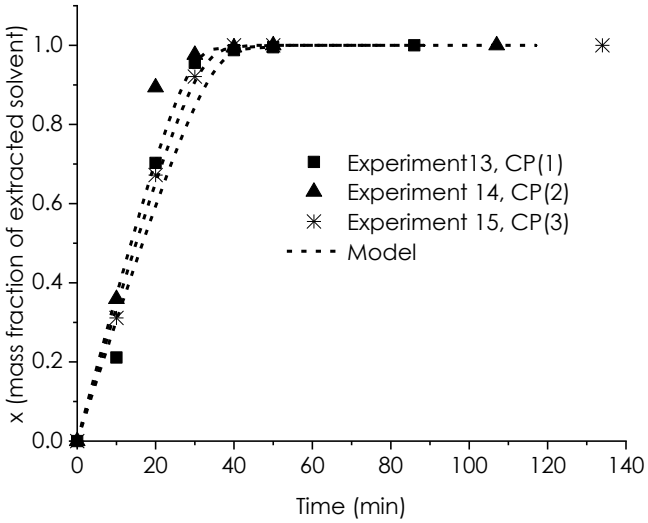

Figure 5.7. Reproducibility for 105 g cake, P=140 bar, F=20 g/min and T=60 °C: CP (1) C_{fL}^* = 0.054 kg/kg, CP (2) C_{fL}^* =0.077 kg/kg and CP (3) C_{fL}^* =0.045 kg/kg.

Table 5.7. The deviation of the initial solvent content between the three centre points and its affect on the solubilty data.

Exp. No	**Initial solvent content (g)**	**C_{exp} (kg/kg)**	**C_{fL}^* (kg/kg)**
13-CP(1)	32.1	0.108	0.054
14-CP (2)	24.1	0.097	0.077
15-CP (3)	16.6	0.047	0.045

Speaking of the predicted solubility, in most of the extraction runs particularly the ones involving 60 g cakes, the C_{fL}^* has not reached C_{sat}, even if it is theoretically possible according to the BET model, **Eq. (5.22)**. In reality, there are a few factors that prevent this from happening. The most important are the

headspace above the cakes and the inconsistent initial amount of solvent as discussed previously. Filling up the extraction basket enhances the solvent mass transfer rates **Figure 5.2 (d)** and gives better measurements. The maximum cake size that can be experimentally prepared for the given system is 150 g, which occupies approximately the 70% of the extraction basket. In this case, there is enough space for the spayed solvent during washing step without causing any cake disturbances. As regard to the solvent content, it is very challenging to keep it constant for similar cakes. Loss in mass during transportation of materials as well as errors during measurements, make it almost impossible to regulate the final amount of solvent in the formed cakes. Other parameters that are difficult to control and can influence the experimental results are; cake cracking and particle size distribution that affect the bed packing and therefore the solvent distribution in the cake as well as the extraction kinetics.

A way to obtain similar cakes and study the kinetics of the system by varying the operating conditions only, could be the replacement of paracetamol particles with glass beads of uniform sizes and the addition of a predefined amount of wash solvent. However, this work is focused on real life applications and is important to investigate all the potential parameters that affect the extraction kinetics.

5.2.3 Residual solvents in the final cakes

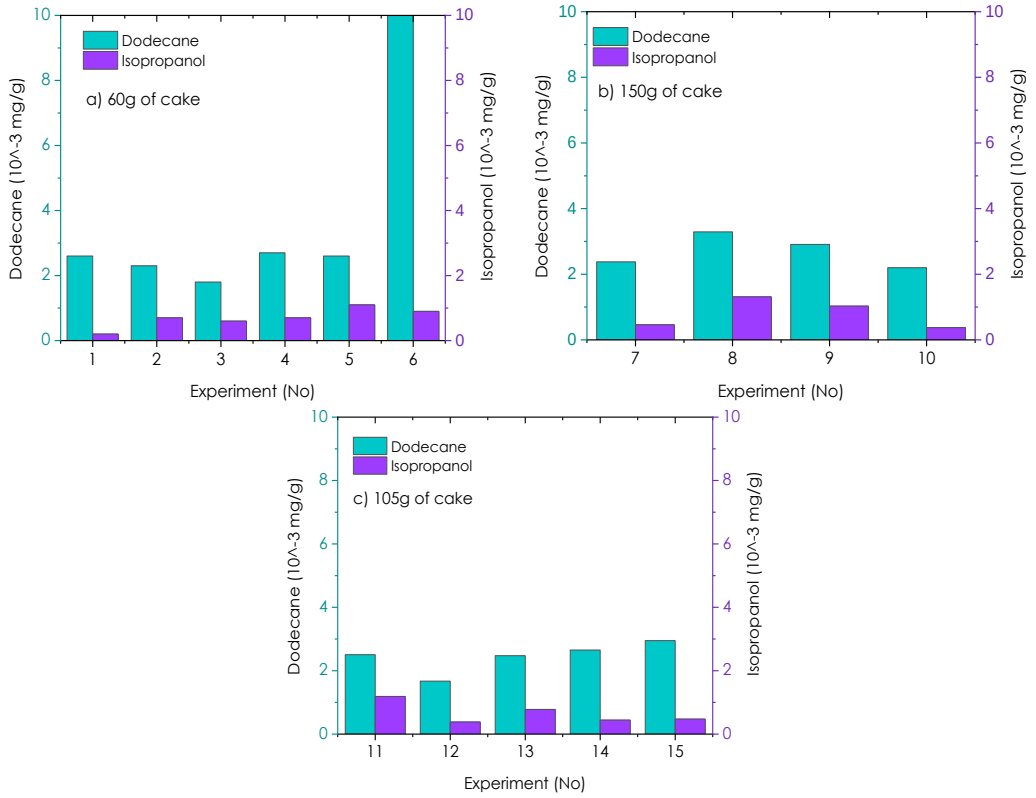

Figure 5.8. Dodecane and isopropanol concentrations measured in the headspace final samples using offline SIFT-MS analysis (number of repetitions, n=1).

Figure 5.8 shows the residual solvents in the headspace of the samples after extraction/drying. In all the experiments, the solvent levels are much lower than the targeted concentration of 12.5 mg per g of API (see section **3.4.2.2.2**). The dodecane residues varied between 0.002 and 0.003 mg/g with the exception of experiment 6, which reached 0.025 mg/g and the isopropanol concentrations ranged between 0.0002 and 0.001 mg/g. Since all the experiments met the criteria regarding dodecane and isopropanol, reaching similar concentration values, the

obtained data cannot be correlated with the operating variables using MODDE software.

5.2.4 Statistical evaluation of the experimental data using MODDE

By fitting MLR models in the obtained responses, it is possible to explore important operating variables in extraction/drying of dodecane from paracetamol. The fitted responses were the C_{fL}^*, extraction/drying time, particle size, agglomeration and ABI index. From the summary fit plot **Figure 5.13** (page **170**), the model showed good fit only for two responses involving the C_{fL}^* and the particle size. For those responses, the R^2, model validity and reproducibility bars are above 0.5 and the Q^2, which shows an estimate of the future prediction precision, is greater than 0.1 indicating a rather significant model.

5.2.4.1 Parameter C_{fL}^*

Table 5.8 gathers all the C_{fL}^* data estimated by BET based model. The greatest C_{fL}^* value (0.179 kg/kg) is obtained in experiment 7, where 150 g cake dried at 200 bar, 60 ^oC and 20 g/min flow rate. Following this, experiments with high C_{fL}^* (>0.09 kg/kg) are 1, 9, 10 and 11 which most of them involve large cakes and high operating pressures. **Figure 5.9,** shows the coefficient plot for the dodecane concentration in fluid phase. The cake size is indeed deemed significant

for the C_{fL}^*. As it is mentioned in previous sections, large cakes reduce the headspace in the vessel, increase the residence time of the CO_2 in the bed, and have higher solvent content. These factors eliminate the error in measurements and it is more likely for the CO_2 to be saturated at the exit of the vessel. Terms with less significant impact are pressure and flow rate. High pressures increase the density of fluid (657-787 kg/m^3), **Table 5.5,** and therefore the solvation power of CO_2. The flow rate is not anticipated to influence the C_{fL}^* value, unless there are limitations in mass transfer leading to measurement inaccuracies.

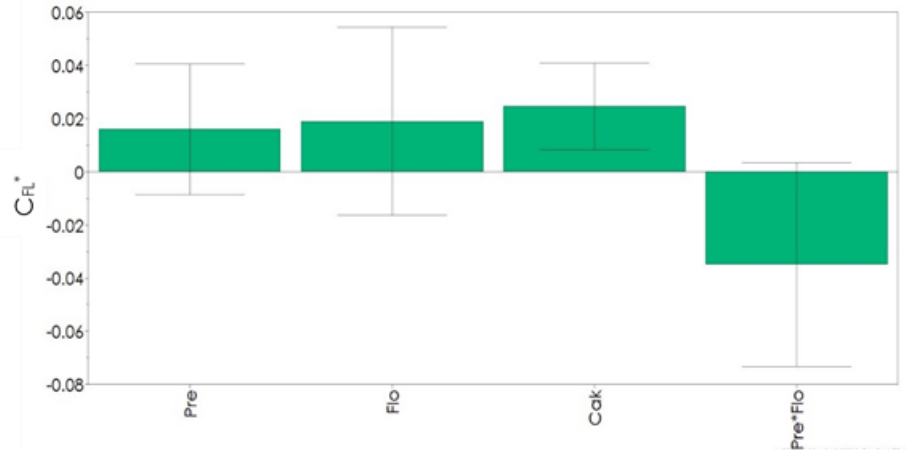

Figure 5.9. Regression coefficients of C_{fL}^* after removing no-significant terms from the model (Pre=Pressure, Temp=Temperature, Flo=Flow rate, Cak=Cake size).

5.2.4.2 Particle size D_{50}

The variations in particle size for all percentile values, D_{10}, D_{50} and D_{90} were determined by **Eq. (5.31)** and are presented in **Figure 5.10.** The dashed line represents the raw paracetamol, which is used as a reference point. It appears

that the particle size has increased or decreased in all samples. For D_{10}, D_{50} and D_{90} the absolute deviation ranges from raw paracetamol are 1-31%, 1.5-35% and 3.2-42.6% respectively. For the D_{90}, an extremely high value was obtained in the case of experiment 13, which is due to particle agglomeration.

$$D_x = \frac{D_x \text{ of the dried PCM}}{D_x \text{ of the raw PCM}} \quad \textbf{Eq. (5.31)}$$

In order to investigate the effect of the selected factors on particle size, the change of the volume median diameter, D_{50}, was used in the experimental design. The regression coefficient plot shows that temperature, flow rate and mass of cake impact the particle size. The increase in temperature facilitates the solubility of paracetamol in the organic solvent, resulting in particle size enlargement; a phenomenon that is also common in conventional drying. The large cakes also result in particle size increase. It is possible that after washing, the concentration of crystallisation solvent residues is likely higher than in smaller cakes, which therefore leads to particle bridging. The opposite effect is observed at high flow rates. Generally, the CO_2 flow is not expected to influence the particle size, therefore it is assumed that sieving prior to the PSD measurements could have led to particle attrition. However, in most of the cases

the deviation in PSD between the reference raw material and the processed samples is within acceptable limits.

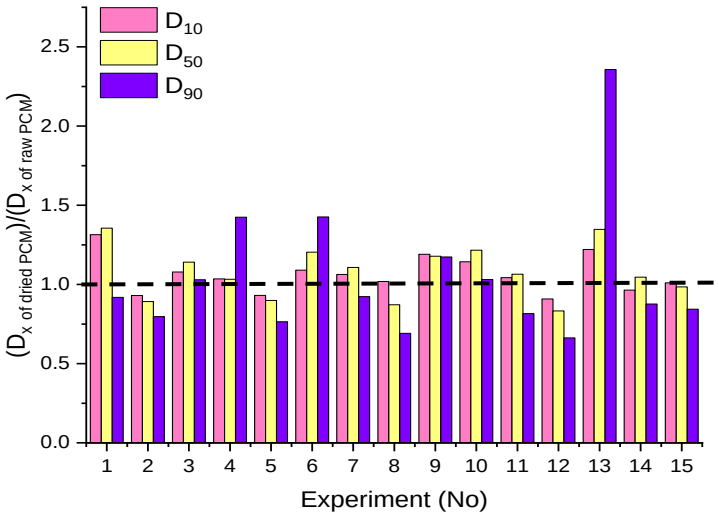

Figure 5.10. Changes in particle size after extraction/drying; the dashed line corresponds to raw paracetamol and is used as a reference point (number of repetitions, n=1).

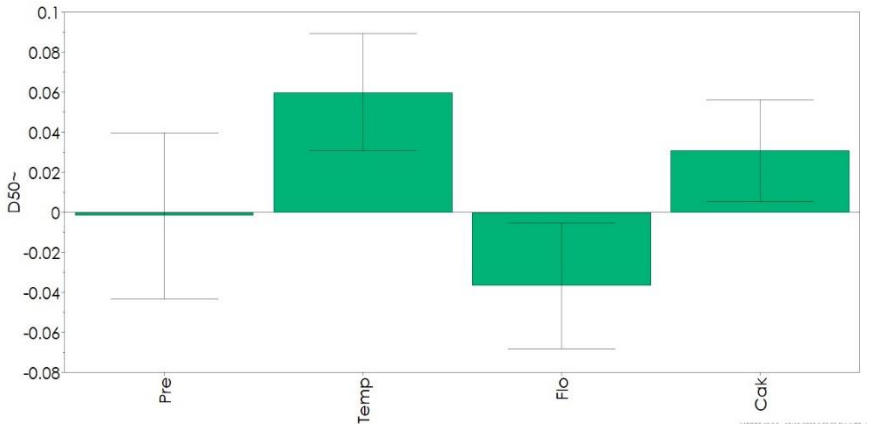

Figure 5.11. Regression coefficients of particle size after removing non-significant terms from the model (Pre=Pressure, Temp=Temperature, Flo=Flow rate, Cak=Cake).

5.2.4.3 Extent of agglomeration and agglomeration brittleness index

All the dried samples exhibited agglomerates in the range of 46-86%. Under more forcing conditions of high pressure and temperature, it is expected this phenomenon to be intensified since the solubility of paracetamol increases in the $scCO_2$ phase [143] and in organic solvents at elevated pressures and temperatures. Even though it is not so obvious from the experimental design which term had the most significant effect on particle agglomeration, the extent of agglomeration seems to be independent from the cake size. Moreover, the formed agglomerates were relatively friable. As it is seen in **Figure 5.12**, nine out of fourteen samples have ABI index greater than 0.43, which means that relatively soft agglomerated material was generated in most of the experiments (see section **3.4.2.2.6**). In the case of experiment 10, all the formed clusters in the sample were completely shattered before the completeness of the fourth cycle.

The MLR model performed poorly for agglomeration and ABI. However, it is well understood that responses related to many parameters such as particle size distribution, washing conditions and efficiency, drying factors etc. give inconsistent results that are challenging to predict by modelling.

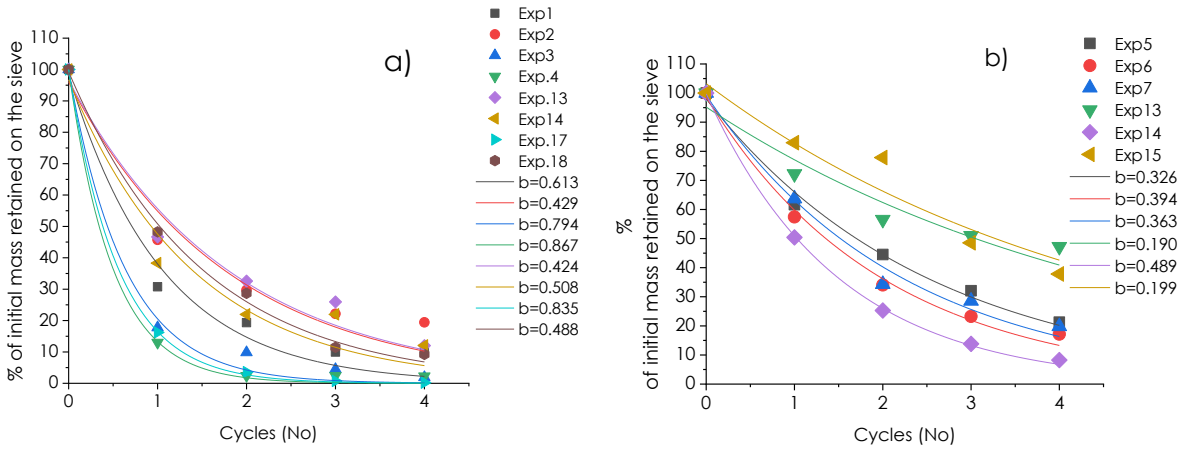

Figure 5.12. Exponential decay fit to the experimental data points obtained from sieving. The b parameter indicates the softness index of the agglomerated sample. The higher this value, the softer the agglomerates in the samples and vice versa.

5.2.4.4 Extraction/drying time

The shortest extraction/drying times are mainly observed at high CO_2 flow rates and vary between 45-130 min without including the preheating period. As described previously, high flow rates enhance the extraction/drying rates due to greater amounts of fresh CO_2 passing through the packed bed. Pressure also influences the extraction/drying time. A slow extraction/drying rate was observed when the pressure was set at 80 bar, while steeper initial slopes at high

pressures indicated the rapid removal of the solvent. Temperature and mass of cake are non-significant terms for this response.

Table 5.8. Overall experimental results fitted to the MLR regression model.

Exp.	Temperature	Pressure	CO_2 flow rate	Cake size	Time	C_{fL}^*	$\frac{D_{50\ sample}}{D_{50\ raw}}$	Agglomeration	ABI
No	(°C)	(bar)	(g/min)	(g)	(min)	(kg/kg)		(%)	
1	50	200	10	60	80	0.092	1.35	48.3	0.613
2	50	140	10	60	130	0.03	0.89	85.9	0.429
3	70	200	10	60	77	0.045	1.14	49.2	0.794
4	60	140	20	60	75	0.032	1.03	65.9	0.867
5	60	200	30	60	45	0.051	0.89	72.8	0.326
6	70	200	20	60	70	0.061	1.20	46.9	0.394
7	60	200	20	150	78	0.175	1.11	58.1	0.363
8	50	200	30	150	86	0.075	0.87	49.2	0.424
9	70	200	30	150	62	0.09	1.18	59.9	0.508
10	60	140	20	150	82	0.114	1.21	65.3	1.00
11	50	200	10	105	133	0.1	1.06	74.1	0.835
12	70	140	10	105	150	0.036	0.83	71.1	0.448
13	60	140	20	105	86	0.054	1.35	53.7	0.19
14	60	140	20	105	107	0.077	1.04	64.2	0.489
15	60	140	20	105	134	0.045	0.98	67.5	0.199

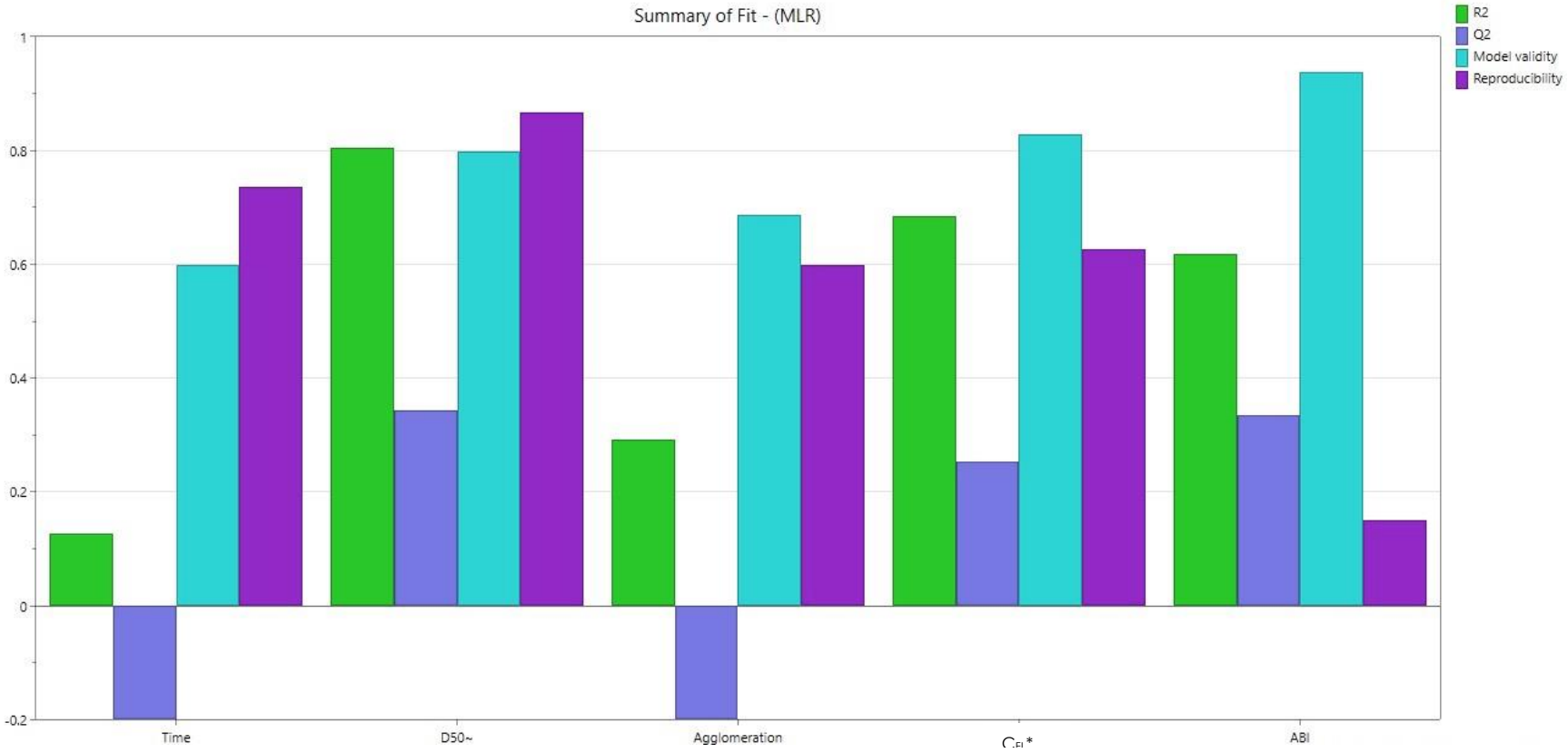

Figure 5.13. Summary fit plot for all the responses.

5.3 Conclusions

An experimental design approach combined with a simple mathematical BET based model used here for optimisation of the extraction/drying process. In comparisons of the model with the experimental data, the model performed reasonably well and gave an approximation of the solubility of dodecane in $scCO_2$ under various operated conditions. From overall data observations, pressure, CO_2 flow rate and solid load had major effects on the extraction/drying kinetics. Pressure and CO_2 flow rate enhance the mass transfer and reduce dramatically the extraction/drying time. Whilst high solids loading, reduce the headspace in the extraction basket and increase the residence time of the fluid in the bed. In this way, a smaller amount of CO_2 is spent during the process and the fluid may reach saturation at the exit of the vessel. In all the experiments, dodecane was removed successfully reaching concentrations of 0.002-0.003 mg/g, which is far below the target specification value (12.5 mg/g) set from the ICH guidelines. Particle agglomeration was prominent, varying between 46-86% and particle size changes where observed in all the CO_2 treated samples. On the other hand, the agglomerated material exhibited high ABI in the majority of the samples, highlighting the applicability of the process if the avoidance of hard agglomerates is desired to minimize the need for subsequent high-energy milling. From the

data obtained through MODDE, it was difficult to predict the optimal conditions due to the poor performance of the MLR model. Therefore, the results from the regression coefficient plots were used together with the information obtained from the BET model to define the best combination of factors based on the current DOE design. The selected optimised process conditions for the studied system are 150 g paracetamol cakes, 200 bar pressure, 60 °C temperature and 20 g/min CO_2 flow rate. Experiment 7 resulted in highest C_{fL^*}~ 0.175 kg/kg, and delivered solvent free powder within 2 hr. In conclusion, extraction/drying with $scCO_2$ is applicable to purification of APIs as a new, alternative method to conventional procedures.

6 Energy consumption analysis

Chapter 6 is focused on the energy consumption analysis, conducted for both drying technologies at the studied operating conditions. In the case of dodecane removal using conductive drying under vacuum, the energy consumption included the heat supplied to the dryer and nitrogen as well as the power demand for vacuum generation. Whereas, the energy consumption associated with the scCO_2 extraction/drying process, involved four key operation units; chiller, high-pressure pump, CO_2 heater and extraction vessel. Additionally, the power requirement for gas phase compression of CO_2 to create liquid was included to the total energy demand. Here, the optimum conditions were used as an example for the energy calculations and from the overall results, the effect of different parameters on the energy consumption was investigated for each drying technology.

It should be noted that this study evaluated the energy consumption of the two drying processes as operated in the lab.

6.1 Energy consumption for agitated filter dryer (AFD)

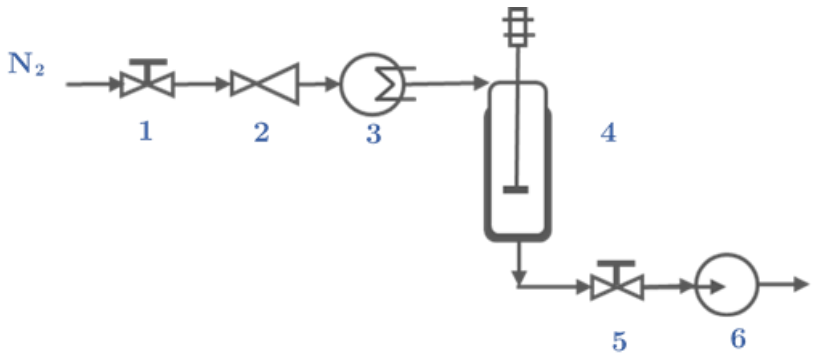

Figure 6.1. Flow sheet diagram of the agitated drying using AWL unit; 1) manual valve, 2) pressure reduction valve, 3) heat exchanger, 4) jacketed dryer, 5) manual valve and 6) vacuum pump.

The energy consumption associated with the dodecane removal was estimated for the agitated drying process (**Figure 6.1**). The best combination of factors using the AWL fabricated setup was 60 g cake, 70 °C temperature, 0.8 L/min N_2 flow rate and intermittent agitation. Pressure was the only fixed operated parameter for this study and it was set at 500 mbar. The time required to remove dodecane from 60 g paracetamol cake at the optimum conditions was t_b=3 hr.

6.1.1 Energy associated with the heat supplied to the product

The heat supplied to the wet paracetamol cake involves the sensible heat to raise its temperature from 20 °C to 70 °C and the latent heat of vaporization of dodecane.

Before estimating the energy supplied to the cake, the specific heat capacity of the bed was calculated. Based on the experimental data, the wet bed constituted of 87.5% paracetamol and 12.5% of dodecane. This excludes mechanical cake deliquoring and involves the removal of the critical amount of solvent (in this case 8.5 g of dodecane) during the falling rate period. Since tiny amounts of crystallisation solvent left in the cake after washing, isopropanol was neglected from these calculations. The specific heat capacity of the wet cake takes into account both paracetamol C_{ps} and dodecane C_{pl} as described in **Eq. (6.1).** The C_p values for paracetamol and dodecane at 70 °C are 1.77 and 2.35 $\mathbf{kJ \cdot kg^{-1} \cdot K^{-1}}$ respectively.

$$\mathbf{C_{pwet} = C_{p,s} \cdot x_s + C_{p,l} \cdot x_l \quad Eq.\,(6.1)}$$

where x is the mass fraction of each phase in the bed

$$\mathbf{C_{pwet} = 1.77 \cdot 0.875 + 2.35 \cdot 0.125 = 1.84\ kj \cdot kg^{-1} \cdot K^{-1}}$$

Hence, the heat consumed to increase the temperature of the bed from 20 °C to 70 °C was calculated as follows:

$$\mathbf{Q_1 = m_{bed} \cdot C_{pwet} \cdot \Delta T = 0.07 \cdot 1.84 \cdot 50 = 6.4\ kJ \quad Eq.\,(6.2)}$$

In order to evaporate dodecane, the latent heat of evaporation must be supplied to turn each kilogram of moisture into vapour. For dodecane, the latent heat of vaporisation at 70 °C was found to be 337.4 $\mathbf{kJ \cdot kg^{-1}}$. So, the energy supplied to the process for dodecane only, is calculated as follows:

$$Q_2 = \Delta H_{vap} \cdot m_{c,dodecane} = 337.4 \cdot 8.5 \cdot 10^{-3} = 2.9\ \text{kJ} \quad \textbf{Eq. (6.3)}$$

In addition, a small flow of heated nitrogen was used to enhance the heat transmission within the bed. The gas was heated from 20 °C to 70 °C. The mass of nitrogen used per hour was 0.055 kg, the C_p at 70 °C was 1.04 $\text{kJ} \cdot \text{kg}^{-1} \cdot \text{K}^{-1}$ and the ΔT was 50 °C. Therefore, the heat required is presented below.

$$Q_3 = m_{N2} \cdot C_{pN2} \cdot \Delta T \cdot t_b = 0.055 \cdot 1.04 \cdot 50 \cdot 3 = 8.6\ \text{kJ} \quad \textbf{Eq. (6.4)}$$

The total dryer energy supply is the sum of Q_1, Q_2 and Q_3. In practice the actual energy is normally greater than the calculated value. There are many additional energy penalties that should be considered such as heat losses from the dryer body, additional energy to break bonds and release bound moisture and thermal inefficiencies in the heat supply system. Based on the literature, for a contact dryer, the maximum practicable efficiency would fall to 70% [154]. An approximation of the required energy considering the heat losses is showed below.

$$\frac{Q_1 + Q_2 + Q_3}{0.7} = \frac{6.4 + 2.9 + 8.6}{0.7} = 25.6\ \text{kJ or } 0.007\ \text{kWh} \quad \textbf{Eq. (6.5)}$$

6.1.2 Other energy demands

After sufficient energy has been provided to vaporise the solvent, vacuum was pulled to carry the vapors away from the solids. The ideal power demand of a vacuum pump can be calculated on the basis of the pumps volume flow rate, inlet and outlet pressure. Isothermal or isentropic compression can be assumed,

depending on the vacuum pump type. Isothermal compression is typically used for cooled compression, and isentropic can be used with dry vacuum pumps [155]. In this case, a diaphragm free-oil pump was used and the isentropic P_s power is calculated by **Eq. (6.6)**.

$$P_s = \frac{k}{k-1} \cdot q_v \cdot p_{in} \cdot \left(\left(\frac{P_{out}}{P_{in}} \right)^{\frac{k-1}{K}} - 1 \right) * t_b = \frac{1.4}{1.4-1} \cdot 25 \cdot 10^{-3} \cdot 50 \left(\left(\frac{100}{50} \right)^{\frac{1.4-1}{1.4}} - 1 \right) \cdot 3 = 335.4\text{kJ or } 0.093\ \text{kWh} \quad \textbf{Eq. (6.6)}$$

$$P_1 = \frac{P_s}{n_s} = \frac{0.093}{0.7} = 0.133\ \text{kWh} \quad \textbf{Eq. (6.7)}$$

where p_{out} and p_{in} is the outlet and inlet pressure of the vacuum pump, qv is the volume flow rate assuming that the pump is working at its half maximum capacity to compensate for nitrogen flow and air bleeding in the system, k is the isentropic exponent which for ideal gases is equal to 1.4 and n_s is the isentropic efficiency of the pump

Therefore, the total energy consumption for drying 60 g cake using agitated dryer is:

$$P_{tAFD} = 0.007 + 0.133 = 0.14\ \text{kWh} \quad \textbf{Eq. (6.8)}$$

6.2 Energy consumption for supercritical CO_2 extraction/drying

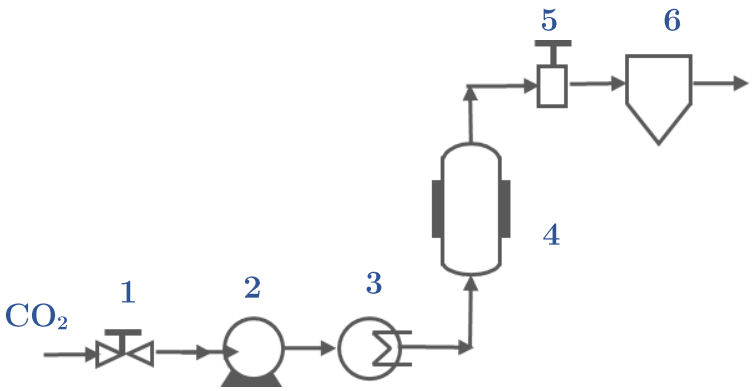

Figure 6.2. Flow sheet diagram of the supercritical CO_2 extraction/drying process; (1) manual valve, (2) piston pump, (3) heat exchanger, (4) extractor, (5) back pressure regulator and (6) cyclone.

Energy analysis was carried out for dodecane extraction/drying using $scCO_2$. The highest C_{fL}^* value, 0.175 kg/kg, was obtained at 150 g cake with 200 bar pressure, 60 °C temperature and 20 g/min CO_2 flow rate. The wet cake was preheated for a couple of hours before the extraction/drying began, while the process itself lasted for 2 hr at the optimal DOE point. **Figure 6.2** provides a flow diagram with the main operation units of the $scCO_2$ process.

6.2.1 Energy associated with heating up the product

The energy supplied to the product involves both the preheating and the extraction/drying periods. Preheating the wet cake prior $scCO_2$ treatment, it was proved to enhance the extraction/drying kinetics significantly and therefore reduce the energy and CO_2 consumption during the process. The energy supplied

to the extractor for heating up the product was calculated in a similar way as described in section **6.1.1**. The cake was saturated with solvent and its composition was 75 % of paracetamol and 25 % of dodecane. The equation **Eq. (6.9)** gives the total energy that is supplied to the product assuming 70% efficiency for the energy losses.

$$Q_4 = m_{bed} \cdot C_{pwet} \cdot \Delta T = 0.2 \cdot 1.93 \cdot 40 = 15.3\ \text{kJ} \quad \textbf{Eq. (6.8)}$$

$$\frac{Q_4}{0.7} = \frac{15.3}{0.7} = 21.9\ \text{kJ or } 0.006\ \text{kWh} \quad \textbf{Eq. (6.9)}$$

6.2.2 Energy associated with the chiller

For the compression of the fluid, a dual piston CO_2 pump was used from Waters. A recirculated coolant inside each pump head increased the compression efficiency by removing the generated heat and decreasing its temperature. Liquefied CO_2 was released from the bottle at approximately 55 bar and 15 °C, and it was assumed that entered the pump at around 7 °C. The specific heat capacity of CO_2 at 7 °C and 55 bar is 2.61 $\text{kJ} \cdot \text{kg}^{-1} \cdot \text{K}^{-1}$ [156] and the mass of carbon dioxide used per hour was 1.2 kg. Hence, the energy consumption from the chiller is calculated as follows (assuming 50% efficiency):

$$Q_5 = \frac{m_{CO2} \cdot C_{pCO2} \cdot \Delta T \cdot t_{extraction}}{0.5} = \frac{1.2 \cdot 2.61 \cdot 8 * 2}{0.5} = 101.1\ \text{kJ or } 0.028\ \text{kWh} \quad \textbf{Eq. (6.10)}$$

6.2.3 Energy associated with the CO_2 heater

The CO_2 has to be heated from 7 °C (temperature of the CO_2 inside the pump) to 60 °C. The C_{pCO2} at 60 °C and 200 bar was found to be 0.928 $kJ \cdot kg^{-1} \cdot K^{-1}$ and the ΔT was 53 °C. The heat required was estimated below (assuming 50 % efficiency) [157].

$$Q_6 = \frac{m_{CO2} \cdot C_{pCO2} \cdot \Delta T \cdot t_{extraction}}{0.5} = \frac{1.2 \cdot 0.928 \cdot 53 * 2}{0.5} = 236.1 \text{ kJ or } 0.065 \text{ kWh} \quad \textbf{Eq. (6.11)}$$

6.2.4 Energy consumption associated with the CO_2 pump

The pressure and temperature utilised in the extraction process give the specific enthalpy, from which the total energy used in the extraction process can be obtained by multiplying the variation of specific enthalpy by the extraction time and the CO_2 mass flow rate. In this case, the enthalpy change ΔH from H_1 at 55 bar and 7 °C to H_2 at 200 bar and 60 °C is approximately 108.7 $kJ \cdot kg^{-1}$. Therefore, the consumed energy associated with the CO_2 pump is calculated as follows:

$$P_3 = \frac{m_{CO2} \cdot \Delta H \cdot t_{extraction}}{0.9} = \frac{1.2 \cdot 108.7 \cdot 2}{0.9} = 292.7 \text{ kJ or } 0.08 \text{ kWh} \quad \textbf{Eq. (6.12)}$$

6.2.5 Energy associated with the CO_2 compressed in the cylinder

Liquid carbon dioxide is recovered from a variety of sources such as ammonia and hydrogen plants, purified and liquefied. To calculate the energy requirement for compressing the CO_2, a case study is considered where the gas is captured

during ammonia processes and is compressed to 55 bar [158] . In this case study, a nominal 17 bar capture system discharge is selected because this is the nominal range for this type of processes. Also, it is assumed that the initial ambient conditions are 35 °C and dry. Hence, in a single compression stage, the enthalpy change across the compressor is 70 $\mathbf{kJ \cdot kg^{-1}}$ of CO_2 [156]. Then the CO_2 is cooled from 130 °C to 15 °C and the heat discharge is recovered. The heat removal from the gas is not included in the energy calculations. To this end, the power demand for the CO_2 compression as well as the total energy required for the $scCO_2$ process are estimated as follows:

$$P_4 = \frac{m_{CO2} \cdot \Delta H \cdot t_{extraction}}{0.9} = \frac{1.2 \cdot 70 \cdot 2}{0.9} = 188 \text{ kJ or } 0.052 \text{ kWh} \quad \textbf{Eq. (6.13)}$$

$$P_{tscCO2} = 0.013 + 0.028 + 0.065 + 0.08 + 0.052 = 0.237 \text{ kWh} \quad \textbf{Eq. (6.14)}$$

6.3 Results and discussion

In a similar way as described above, the energy consumption for the two drying techniques was calculated at different operated conditions. **Table 6.1** and **Table 6.2** gather the overall energy results, which are discussed in the following subsections.

6.3.1 Energy consumption in agitated filter dryer

The energy analysis results showed that the minimum energy required for dodecane removal was 0.07 kWh, which occurred with 60 g cakes dried at 70 °C and 0.8 L/min N_2 flow rate, while the maximum energy requirement was 0.15 kWh observed in the largest cakes that did not meet the ICHI criteria. Furthermore, the most energy intensive process step in conventional drying is the pressure decrease in the dryer. In other words, the energy consumption related to the vacuum pump determines the total energy need.

According to **Figure 6.3**, temperature and solid load are the most important energy consumption factors. Increasing temperature results in decreased drying time and consequently in lower energy consumption, while the solid load impedes significantly the drying rates and has the opposite effect. Nitrogen flow rate and drying mode are non-significant parameters for the energy consumption; although the power demand related to the overhead stirrer was not included. In summary, the energy consumption is a function of the drying kinetics, which is an expected outcome since the vacuum parameter is fixed in this study.

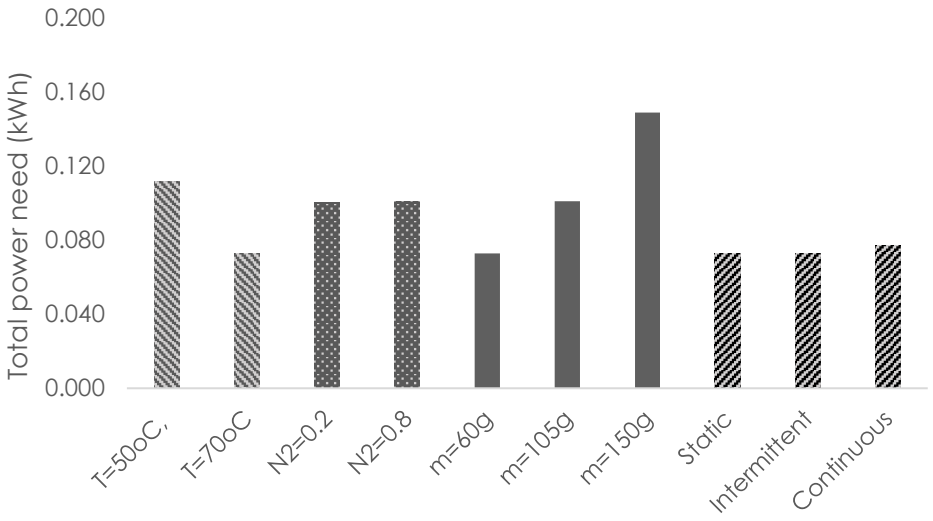

Figure 6.3. Effect of key factors on energy consumption for agitated drying of paracetamol wet in dodecane cakes; **Temperature effect** for 60 g cakes: N_2=0.8 L/min and static mode; **Nitrogen effect** for 105 g cakes: T=70 °C and static mode; **Mass of cake effect**: T=70 °C, N_2= 0.8L/min and static mode; **Drying mode effect:** m=60 g, T=70 °C and N_2=0.8 L/min.

Moreover, **Table 6.1** displays the energy consumption normalised by the solid load and critical moisture content (refer to the sections **3.4.2.2.4** and **6.2.1** for details). The highest energy values (1173-1615 kWh/kg $_{solids}$/kg $_{solvent}$) were associated with cakes that did not fully dry at 50 °C with intermittent agitation. On the other hand, the lowest energy values (56-133 kWh/kg $_{solids}$/kg $_{solvent}$) were observed during static drying at 70°C. Additionally, it appears that the nitrogen flow rate does not have a significant impact on energy consumption, as indicated by experiments 9 and 16. It is noteworthy to mention that based on the normalised energy data, the optimal conditions regarding drying efficiency

appear to involve static drying, 105 g cakes, a temperature of 70°C, and a flow rate of 0.2 L/min, as observed in experiment 9.

6.3.2 Energy consumption in supercritical CO_2 extraction/drying

As it is seen in **Figure 6.4**, pressure and CO_2 flow rate are important factors affecting the energy consumption in $scCO_2$ extraction/drying. Increasing pressure enhances the solubility of dodecane in supercritical CO_2 phase and the extraction/drying occurs in a shorter period. Besides, the difference in ΔH for increasing the pressure from 55 bar to 140 bar and 200 bar at 50 °C is 20 $\mathbf{kJ \cdot kg^{-1}}$, which is quite small. Increasing the CO_2 flow rate when 60 g cakes are dried, the energy consumption is higher. For example, the energy difference between 20 g/min and 10 g/min is almost double. Another factor with less significant impact on the energy consumption is the mass of cake. At 140 bar pressure, 60 °C temperature and 20 g/min, the energy consumption increases slightly with increased solid load. This is due to the better extraction/drying kinetics at larger cakes, explained thoroughly in previous sections. The mass of cake has an impact on energy supply to the extractor, which is ~5% of the total energy, while the ~95 % is affected by the extraction/drying time. Temperature has minor influence on the extraction/drying kinetics at 200 bar and therefore, on energy consumption. Finally, the overall results showed that the lowest value

of energy demand for dodecane extraction was 0.071 kWh and was obtained at 60 g cake dried under 200 bar pressure, 50 °C temperature and 10 g/min CO_2 flow rate. The highest energy value (0.289 kWh) was observed in experiment 15, where 105 g cake dried at 140 bar pressure, 20 g/min CO_2 flow rate and 60 °C.

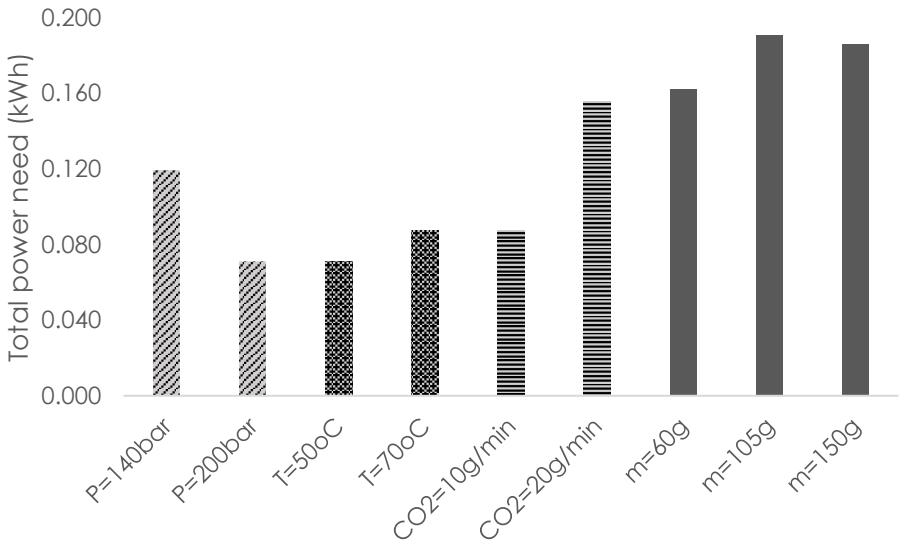

Figure 6.4. Effect of key factors on energy consumption for $scCO_2$ extraction/drying of wet in dodecane paracetamol cakes; **Pressure effect** for 60 g cakes: T=50 °C and CO_2=10 g/min; **Temperature effect** for 60 g cakes: P=200 °C and CO_2=10 g/min; **CO_2 flow rate effect**: P=200 bar, T=70 °C and m=60 g; **Mass of cake effect:** P=140 bar T=60 °C and CO_2=20 g/min.

Normalising the energy consumption by solid load and solvent quantity makes it difficult to identify the operational conditions with a significant impact on energy use. A large number of experiments exhibited energy values ranging from 21 to 59 kWh/kg $_{solids}$/kg $_{solvent}$. However, experiments 2 to 6 involving 60 g cakes,

demonstrated higher energy consumption (92-145 kWh/kg $_{solids}$/kg $_{solvent}$), indicating that the headspace in the vessel might affect the process performance, leading to longer extraction/drying times and consequently increased energy usage. Experiments 13, 14, and 15 are identical, and one would anticipate similar outcomes. However, experiment 15 exhibited a prolonged extraction/drying time, leading to higher energy consumption compared to the other two.

Table 6.1. Overall energy results for agitated dryer.

Exp.	Temperature	Nitrogen Flow rate	Mass of cake	Solvent removed (critical moisture)	Drying Mechanism	Energy need for the dryer	Energy need for the pump	Total energy need	Total energy need
No.	**(°C)**	**(L/min)**	**(kg)**	**(kg)**		**(kWh)**	**(kWh)**	**(kWh)**	**(kWh/kg solids/kg solvent)**
1	50	0.8	0.060	0.008	Static	0.006	0.106	0.111	245.6
2	70	0.8	0.060	0.009	Static	0.007	0.066	0.073	133.0
3	70	0.8	0.060	0.006	Continuous	0.007	0.070	0.077	200.5
4*	50	0.2	0.060	0.007	Continuous	0.006	0.133	0.140	332.7
5*	50	0.8	0.060	0.001	Intermittent	0.006	0.133	0.139	1615.4
6	70	0.2	0.060	0.007	Intermittent	0.008	0.096	0.104	261.8
7*	50	0.2	0.060	0.002	Intermittent	0.006	0.133	0.139	1173.4
8	**70**	**0.8**	0.060	0.009	**Intermittent**	**0.007**	**0.066**	**0.073**	**142.1**
9	70	0.2	0.105	0.017	Static	0.011	0.089	0.100	56.0
10	50	0.5	0.105	0.016	Static	0.008	0.089	0.096	57.1
11*	50	0.8	0.105	0.011	Continuous	0.008	0.133	0.141	119.5
12	70	0.2	0.105	0.007	Continuous	0.010	0.100	0.110	158.6
13*	60	0.5	0.105	0.013	Intermittent	0.010	0.114	0.124	88.7
14*	60	0.5	0.105	0.008	Intermittent	0.010	0.133	0.143	165.8
15	60	0.5	0.105	0.007	Intermittent	0.008	0.103	0.111	161.5
16	70	0.8	0.105	0.017	Static	0.012	0.089	0.101	56.2
17*	50	0.2	0.150	0.020	Static	0.011	0.133	0.144	47.6
18*	70	0.8	0.150	0.021	Static	0.016	0.133	0.149	46.7
19*	70	0.2	0.150	0.016	Continuous	0.015	0.133	0.148	62.0

**The sample did not meet the ICHI criteria and is considered still wet*

Table 6.2. Overall energy results for $scCO_2$ extraction/drying.

Exp.	Temperature	Pressure	CO_2 flow rate	Mass of cake	Solvent removed	Energy need for the vessel	Energy need for the chiller	Energy need for the heater	Energy need for the pump	Energy need for the compressor	Total energy need	Total energy need
No.	(°C)	(bar)	(g/min)	(kg)	(kg)	(kWh)	(kWh)	(kWh)	(kWh)	(kWh)	(kWh)	(kWh/kg $_{solids}$/kg $_{solvent}$)
1	50	200	10	0.060	0.028	0.006	0.009	0.018	0.021	0.017	0.071	42.2
2	50	140	10	0.060	0.019	0.005	0.015	0.030	0.042	0.028	0.119	103.4
3	70	200	10	0.060	0.015	0.005	0.009	0.025	0.032	0.017	0.087	99.7
4	60	140	20	0.060	0.016	0.004	0.017	0.043	0.065	0.032	0.162	171.5
5	60	200	30	0.060	0.022	0.006	0.015	0.034	0.042	0.027	0.124	92.7
6	70	200	20	0.060	0.018	0.005	0.016	0.046	0.058	0.030	0.155	145.4
7	**60**	**200**	**20**	**0.150**	0.050	**0.013**	**0.018**	**0.042**	**0.052**	**0.034**	**0.159**	**21.2**
8	50	200	30	0.150	0.051	0.012	0.030	0.057	0.067	0.056	0.222	28.7
9	70	200	30	0.150	0.044	0.013	0.022	0.061	0.077	0.040	0.213	32.3
10	60	140	20	0.150	0.053	0.013	0.019	0.047	0.071	0.035	0.186	23.4
11	50	200	10	0.105	0.033	0.008	0.015	0.029	0.035	0.029	0.116	33.3
12	70	140	10	0.105	0.041	0.011	0.017	0.050	0.082	0.040	0.193	45.1
13	60	140	20	0.105	0.041	0.010	0.020	0.050	0.074	0.037	0.191	44.9
14	60	140	20	0.105	0.038	0.009	0.025	0.062	0.092	0.032	0.193	59.2
15	60	140	20	0.105	0.025	0.007	0.031	0.077	0.115	0.058	0.289	109.3

6.4 Conclusion

In this part of the project, energy consumption for the two studied drying methods was determined. From the agitated drying results, the total power demand is driven by the applied vacuum. However, pressure was a fixed parameter here and therefore temperature and mass of cake were the most significant factors. The lowest energy consumption was observed in small cakes that dried at 70 °C and was around 0.073 kWh. When normalising energy consumption by solid load and critical moisture content, the samples that dried at 70 °C without agitation exhibited the lowest values. Furthermore, it was observed that the nitrogen flow rate had an insignificant impact on energy consumption.

For the supercritical CO_2 extraction/drying the lowest energies (~0.071 kWh) were observed in low CO_2 flow rates. While the higher electricity consumptions occurred at higher values of each variable in their operative region, with CO_2 flow increase causing the most significant increases. From the normalised data, it is challenging to identify the operational conditions that significantly impact the energy consumption. However, it is observed that lower solids loading exhibited higher energy consumption values compared to the other experiments,

suggesting that the dead volume within the vessel impacts negatively the process performance.

7 Comparison of conventional drying and supercritical CO_2 extraction/drying

In this part of the thesis, the two studied drying technologies were evaluated based on the drying efficiency, final product properties and energy consumption results obtained in the previous chapters.

7.1 Comparison of the two methods

7.1.1 Drying efficiency

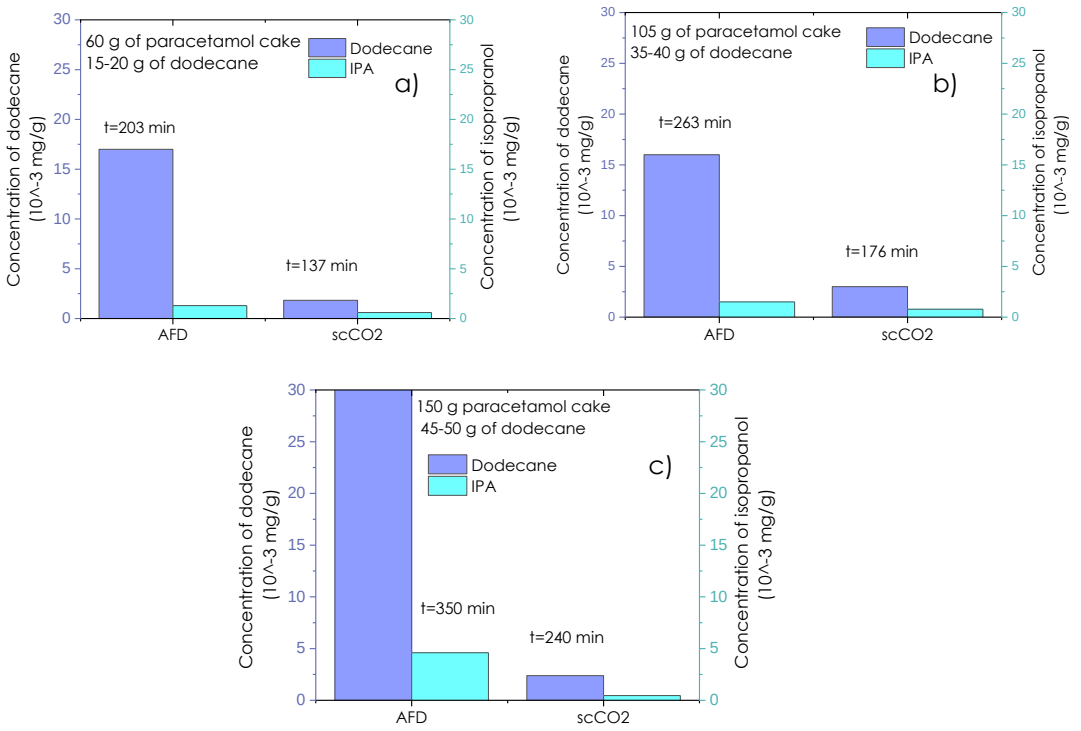

Figure 7.1. Comparison of the drying efficiency between AFD and $scCO_2$ treatment at different cake sizes expressed as residual concentration of dodecane and isopropanol.

For cakes dried with the agitated filter dryer, the solid load plays an important role in determining the drying performance. This is illustrated by the fact that lower dodecane residues with minimum drying time were achieved with 60 g of cake, as compared to 105 g or 150 g of cake. Nevertheless, this is not the case for extraction/drying with the $scCO_2$. The solvent concentrations were minimised in all the $scCO_2$ treated samples relatively quickly and showed

consistency at various cake sizes. **Figure 7.1**, compares the drying performance of the two techniques for selected experiments. As it seems, supercritical CO_2 extraction/drying is a faster method resulting in lower dodecane concentrations than conventional drying. The differences in solvent content might be small when comparing 60 and 105 g cakes, however the amount of residues should be as low as possible and it cannot be said how long it would have taken for the AFD to further reduce the dodecane residues in the cakes and if that was feasible. Moreover, as the cake quantity increases the drying time rises significantly for the conventional drying. Whilst for the $scCO_2$ treatment, the extraction/drying time differences for the samples (a), (b) and (c) are small if we consider the fact that the preheated period is also included in the total batch time. It should be noted that the preheated periods for 60, 105 and 150 g cakes are 60, 90 and 120 min respectively.

7.1.2 Product properties

Particle size changes were observed in all the dried samples regardless the drying method. For example at high operating conditions (200 bar pressure and 70 ^{o}C temperature) during the $scCO_2$ treatment, particle size enlargement was prominent possibly due to the increased solubility of the API in the solvents. As opposed to this, agitated drying produced smaller particles by attrition. These

type of changes are normally expected, and here they are noticeable but not to an extent that it would be problematic. One of the most notable product transformations was agglomeration. Agglomerates larger than 1mm size were present in both $scCO_2$ extraction and conventional drying in the ranges of 48-86 % and 30-70% respectively. These percentages might be very big; however, they represent samples, which constitute of both soft and hard agglomerates. Since similar cakes dried in two different ways, the impact on particle attributes of each drying method was evaluated by measuring the brittleness index of the dried material. For the samples dried conventionally, only three out of nineteen showed high ABI (> 0.4). Whereas $scCO_2$ extraction/drying generated softer agglomerated material with ABI index higher than 0.4 in the majority of the experiments. In the samples that exhibited ABI index above 0.4, at least the 80 % of the particle clusters were broken at the end of the analysis.

Apart from the drying efficiency, other factors that might reduce the formation of rigid solid bridges could be the up-flow extraction/drying mode in combination with the high solvent content in the bed at the beginning of the process. The up-flow mode seems to prevent bed compaction or even expand slightly the particle bed, which contributes to better solute-solvent contact. Whilst, by avoiding breakthrough filtration before extraction/drying there is less cake

compression and more particle motion, which might have a positive effect on the ABI index.

7.1.3 Normalised energy consumption

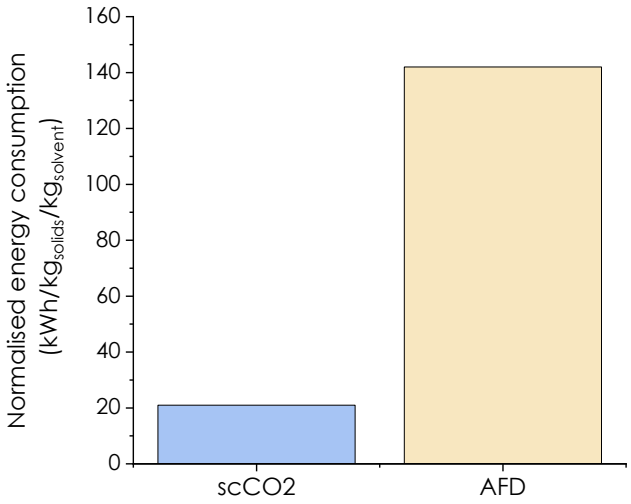

Figure 7.2. Normalised energy consumption for AFD and $scCO_2$ extraction/drying at the optimal conditions; AFD: m=60 g, T= 70 °C, N_2=0.8 L/min, static mode and $scCO_2$: m=150 g, T= 60°C, P=200 bar, CO_2=20 g/min.

From the overall results of the energy analysis, it was concluded that the normalised energy consumption for the agitated filter dryer was influenced by the temperature and the drying mode since applied vacuum, the most energy intensive step, was a fixed parameter in this study. The normalised energy values for fully dried samples ranged from 56 to 245 kWh/kg $_{solids}$/kg $_{solvent}$, representing the lowest and highest values, respectively. Regarding $scCO_2$ treatment, it was difficult to distinguish which operational parameter influences the power

consumption. Nevertheless, experiments conducted with cakes weighing 105 and 150 g displayed energy values within the range of 21 to 59 kWh/kg $_{solids}$/kg $_{solvent}$. In contrast, the majority of the 60 g cakes exhibited higher energy values ranging between 93-172 kWh/kg $_{solids}$/kg $_{solvent}$.

Figure 7.2 compares the normalised energy consumption of the two examined drying technologies under optimal conditions. The substantial difference observed highlights the process performance and energy efficiency of the $scCO_2$ technology.

8 Conclusions and future work

8.1 Conclusions

This thesis investigated $scCO_2$ processing technology towards highly efficient, fast and energy effective way of removing organic solvents from APIs. To achieve this, a systematic experimental study was carried out, where similar paracetamol cakes wet in dodecane dried under various conditions with the use of an agitated filter dryer and $scCO_2$ technology. The results of both drying systems were evaluated regarding the solvent residues in the dried cake, final product properties and energy consumption. Based on the main observations made during the study, the following conclusions have been drawn.

- $ScCO_2$ extraction/drying together with SIFT-MS online analysis minimised the dodecane residues to an extent that was not feasible with conventional drying. This was proved experimentally and the results showed consistency across the experiments.
- $ScCO_2$ treatment was much faster process than conductive vacuum drying. Particularly for large cakes, the differences in drying time were significant.
- A novel way for monitoring in real-time the solvent residues at the end of $scCO_2$ extraction/drying was demonstrated successfully using SIFT-MS

technology. This enabled to determine the endpoint of the process and optimise the extraction/drying.

- Moderate particle size changes and high particle agglomeration were observed in both drying techniques; however, $scCO_2$ extraction/drying generated softer agglomerates. This will minimise the need for subsequent milling which is energy-intensive step.
- The normalised energy consumption for supercritical CO_2 extraction/ drying process was significantly lower than the AFD at the optimal conditions.

To conclude, there are clearly many advantages of using $scCO_2$ technology as an alternative way of drying APIs. By adopting this method it is highly important to improve the overall process efficiency, especially nowadays, that there is an urgent need for developing processes with very low environmental impact. This could be achieved by further optimisation of the process and reduction of the electricity consumption, which is mainly related to the amount of CO_2 used during the process. Other potential improvements could be the energy recovery, heat insulation, CO_2 recycling and process integration that are not considered here.

8.2 Future work

This project addressed many challenges related to drying APIs and showed the potential of supercritical CO_2 technology compared to conventional methods. The obtained results are encouraging for further investigations so that benefits of using $scCO_2$ technology could be effectively utilised for solvent removal from APIs. For this purpose, it is important to explore more organic solvent-API systems, which are suitable for the $scCO_2$ process. For example, it would be interesting to investigate the removal of organic solvents from thermal labile compounds using $scCO_2$ technology at relatively low temperatures. Furthermore, it is worthwhile to investigate the potential application of supercritical CO_2 extraction/drying for pH-sensitive APIs, such as certain antibiotics or biopharmaceuticals like proteins, as pH changes may influence the stability or properties of these products. Regarding stability, it is also imperative to conduct research on the impact of supercritical CO_2 on crystal structure under various conditions. For example, if a suspension of crystals was held in supercritical CO_2 with a small quantity of an organic solvent for an extended period this might favour the nucleation of a new more stable polymorph due to the enhanced molecular mobility achieved in the supercritical phase surrounding the crystals. This would require X-ray diffraction (XRD) analysis on the isolated dried

material following exposure to this extended supercritical holding period since it would be very challenging to conduct XRD in-situ. This study is of high importance since polymorphic changes can lead to both desirable and undesirable alterations in the dissolution rate, activity, and stability of the drug product.

In terms of process efficiency, studies regarding the up-flow and down-flow mode of the process could help to understand their impact on drying and final product properties. The down-flow mode might reduce the extraction/drying time and consequently the energy consumption. Within this, investigations focusing in lower operating conditions, sub-critical or near critical, would also be beneficial from an economic perspective. Lastly, studies regarding VLE (Vapour-Liquid Equilibrium) data of solvent-CO_2 binary systems could help to fully understand the solvent's behaviour in $scCO_2$ to support the design of further experimentation.

Another field that could be of interest to expand its application, is the desolvation of solvates. The drying time can be significantly reduced and it would be ideal for compounds that are not stable at elevated temperatures. Additionally, the desolvation using $scCO_2$ technology at various conditions might result in solvent-free solids with desirable polymorph that cannot be accessed by other means. An anticipated benefit of significantly reducing the residual solvent

level would be to enhance the long-term stability of the isolated product, potentially extending shelf life. To the author's best of knowledge, there is no previously published work using $scCO_2$ technology in this area.

9 References

[1] M. Intelvi, Contact drying of particulate pharmaceuticals: Modelling and simulation, University of Padua, 2006.

[2] Len W. Haleen, Aggressive convective drying in a Nutsche type filter/dryer, 1996.

[3] A.P. and A.G. M. Guerrero,C. Albet, Ferrer, Drying in Pharmaceutical and Biotechnological Industries, Food Sci Tech Int. 9 (2003) 0237–7. https://doi.org/10.1177/108201303035567.

[4] R. B. Keey, Drying principles and practice, 1st ed., Pergamon Press, Oxford, New York, 1972.

[5] E.K. Sahni, B. Chaudhuri, Contact drying: A review of experimental and mechanistic modeling approaches, Int. J. Pharm. 434 (2012) 334–348. https://doi.org/10.1016/j.ijpharm.2012.06.010.

[6] Z.I.S.G. Adiya, A. Ismaila, Vacuum contact drying of pharmaceutical powders with and without agitation: a comparison, Niger. J. Chem. Res. 25 (2020).

[7] H. Lee, K.P. Hapgood, B. Haig, Understanding and preventing agglomeration in a fi lter drying process, Powder Technol. 300 (2016) 146–156. https://doi.org/10.1016/j.powtec.2016.03.003.

[8] L.X. Liu, I. Marziano, A.C. Bentham, J.D. Litster, E.T.White, T. Howes, Effect of particle properties on the flowability of ibuprofen powders, Int. J. Pharm. 362 (2008) 109–117. https://doi.org/10.1016/j.ijpharm.2008.06.023.

[9] E. Kougoulos, C.E. Chadwick, M.D. Ticehurst, Impact of agitated drying

on the powder properties of an active pharmaceutical ingredient, Powder Technol. 210 (2011) 308–314. https://doi.org/10.1016/j.powtec.2011.03.041.

[10] M. Kamihira, M. Taniguchi, T. Kobayashi, Removal of organic solvent from antibiotics with supercritical carbon dioxide, J. Ferment. Technol. 65 (1987) 71–75. https://doi.org/10.1016/0385-6380(87)90067-7.

[11] 2002. Bettini, R., Zampieri, M., Martini, M., Fumalli, P., Rossi, A., Zema, L., Gazzaniga, A., Giordano, F., Treatment of an anticancer drug with supercritical carbon dioxide: residual solvent removal and formation of a new crystal phase, in: AAPS Annu. Meet., 2002: p. no. T2327.

[12] I. Pasquali, R. Bettini, Are pharmaceutics really going supercritical?, Int. J. Pharm. 364 (2008) 176–187. https://doi.org/10.1016/j.ijpharm.2008.05.014.

[13] D. Am Ende, M. Birch, S.J. Brenek, M.T. Maloney, Development and application of laboratory tools to predict particle properties upon scale-up in agitated filter-dryers, Org. Process Res. Dev. 17 (2013) 1345–1358. https://doi.org/10.1021/op400080x.

[14] B.C. Ekneet Kaur Sahni, Robin H. Bogner, Systematic Investigation of Parameters Affecting The Performance of an Agitated Filter-Dryer, J. Pharm. Sci. 102 (2013) 2198–2213. https://doi.org/10.1002/jps.23572.

[15] Z.I.S.G. Adiya, F. Atiku, Drying Characteristic of Aspirin Powder and Agglomerates using Vacuum Contact Drying, Niger. J. Sci. 54 (2020) 13–19.

[16] P.K. Sharma, S. Murugesan, J.E. Tabora, Design of filtration and drying operations, John Wiley & Sons, Ltd, Hoboken, New Jersey, 2019.

https://doi.org/10.1002/9781119600800.ch35.

[17] M. Šimurda, Solvent selection for isolation of pharmaceutical products, University of Chemistry and Technology, Prague and the Department of Chemical & Process Engineering of the University of Strathclyde, Glasgow, 2017.

[18] M. Kohout, A.P. Collier, F. Stepanek, Vacuum contact drying kinetics: An experimental parametric study, Dry. Technol. 23 (2005) 1825–1839. https://doi.org/10.1080/07373930500209954.

[19] E. Tsotsas, E.U. Schlünder, Vacuum contact drying of free flowing mechanically agitated multigranular packings, Chem. Eng. Process. 20 (1986) 339–349. https://doi.org/10.1016/0255-2701(86)80012-5.

[20] M. Intelvi, A. Picado, J. Martínez, Contact Drying Simulation of Particulate Materials : A Comprehensive Approach, Int. Sch. Sci. Res. Innov. 5 (2011) 958–965. https://doi.org/10.13140/RG.2.1.2632.6008.

[21] A. Lekhal, K.P. Girard, M.A. Brown, S. Kiang, B.J. Glasser, J.G. Khinast, Impact of agitated drying on crystal morphology: KCl-water system, Powder Technol. 132 (2003) 119–130. https://doi.org/10.1016/S0032-5910(03)00056-1.

[22] E. Sahni, J. Hallisey, B. Morgan, J. Strong, B. Chaudhuri, Quantifying drying performance of a filter dryer: Experiments and simulations, Adv. Powder Technol. 23 (2012) 239–249. https://doi.org/10.1016/j.apt.2011.03.002.

[23] M. Birch, I. Marziano, Understanding and Avoidance of Agglomeration During Drying Processes: A Case Study, Org. Process Res. Dev. (2013). https://doi.org/doi.org/10.1021/op4000972.

[24] C.D. Papageorgiou, M. Langston, F. Hicks, J. Ende, E. Martin, S. Rothstein, J. Salan, R.H. Muir, Development of screening methodology for the assessment of the agglomeration potential of APIs, Org. Process Res. Dev. (2016). https://doi.org/10.1021/acs.oprd.6b00201.

[25] M. Perez, Gibbs – Thomson effects in phase transformations, Scr. Mater. 52 (2005) 709–712. https://doi.org/10.1016/j.scriptamat.2004.12.026.

[26] W. Li, Drying of Pharmaceutical Powders Using An Agitated Filter, The University of Leeds Institute, 2014.

[27] A.G. Dodda, K. Saranteas, M.A. Henson, Using Online Mass Spectrometry to Predict the End Point during Drying of Pharmaceutical Products, Org. Process Res. Dev. Remov. (2013). https://doi.org/doi.org/10.1021/op400272.

[28] E.W. Conder, A.S. Cosbie, J. Gaertner, W. Hicks, S. Huggins, C.S. MacLeod, B. Remy, B.S. Yang, J.D. Engstrom, D.J. Lamberto, C.D. Papageorgiou, The Pharmaceutical Drying Unit Operation: An Industry Perspective on Advancing the Science and Development Approach for Scale-Up and Technology Transfer, Org. Process Res. Dev. 21 (2017) 420–429. https://doi.org/10.1021/acs.oprd.6b00406.

[29] J. Burgbacher, J. Wiss, Industrial Applications of Online Monitoring of Drying Processes of Drug Substances Using NIR, Org. Process Res. Dev. 12 (2008) 235–242. https://doi.org/10.1021/op700293p.

[30] T.R.M. De Beer, M. Allesø, F. Goethals, A. Coppens, Y. Vander Heyden, H.L. De Diego, J. Rantanen, F. Verpoort, C. Vervaet, J.P. Remon, W.R.G. Baeyens, Implementation of a Process Analytical Technology System in a Freeze-Drying Process Using Raman Spectroscopy for In-Line

Process Monitoring, Anal. Chem. 79 (2007) 7992–8003. https://doi.org/10.1021/ac070549h.

[31] E. Tsotsas, M. Kwapinska, G. Saage, Modeling of contact dryers, Dry. Technol. 25 (2007) 1377–1391. https://doi.org/10.1080/07373930701439079.

[32] M. Intelvi, A. Picado, J. Martínez, Contact drying simulation of particulate materials: a comprehensive approach, Int. J. Mater. Metall. Eng. V. 5 (2011) 958–965.

[33] S.B. Pawar, R. Patil, A.S. Mujumdar, B.N. Thorat, Mathematical modeling of agitated thin-film dryer, Dry. Technol. 29 (2011) 719–728. https://doi.org/10.1080/07373937.2010.526732.

[34] D. Ramkrishna, M.R. Singh, Population balance modeling: Current status and future prospects, Annu. Rev. Chem. Biomol. Eng. 5 (2014) 123–146. https://doi.org/10.1146/annurev-chembioeng-060713-040241.

[35] M. Peglow, J. Kumar, S. Heinrich, G. Warnecke, E. Tsotsas, L. Mörl, B. Wolf, A generic population balance model for simultaneous agglomeration and drying in fluidized beds, Chem. Eng. Sci. 62 (2007) 513–532. https://doi.org/10.1016/j.ces.2006.09.042.

[36] M.A. McHugh, V.J. Krukonis, Supercritical fluid extraction : principles and practice, Butterworth-Heinemann, 1994.

[37] S.B. Hawthorne, D.J. Miller, M.S. Krieger, Rapid extraction and analysis of organic compounds from solid samples using coupled supercritical fluid extraction/gas chromatography, Fresenius' Zeitschrift Für Anal. Chemie. 330 (1988) 211–215. https://doi.org/10.1007/BF00515607.

[38] S. Bristow, T. Shekunov, B.Y. Shekunov, P. York, Analysis of the supersaturation and precipitation process with supercritical CO2, J. Supercrit. Fluids. 21 (2001) 257–271. https://doi.org/10.1016/S0896-8446(01)00100-0.

[39] Mark A. McHugh, Supercritical Fluid Extraction: Principles and Practice, 2nd ed., Elsevier, 2013, U.S.A, 1994. https://doi.org/https://doi.org/10.1016/C2009-0-26919-4.

[40] Knez, E. Markočič, M. Leitgeb, M. Primožič, M. Knez Hrnčič, M. Škerget, Industrial applications of supercritical fluids: A review, Energy. 77 (2014) 235–243. https://doi.org/10.1016/j.energy.2014.07.044.

[41] U.S.S. and P.K.B. Sapkale, G.N., S.M.Patil, Supercritical Fluid Extraction, Int. J. Chem. Sci. 8 (2010) 729–743. https://doi.org/10.1016/B978-0-12-384947-2.00675-9.

[42] E.J. Beckman, Supercritical and near-critical CO2 in green chemical synthesis and processing, J. Supercrit. Fluids. 28 (2004) 121–191. https://doi.org/10.1016/S0896-8446(03)00029-9.

[43] S. Ramdharee, E. Muzenda, M. Belaid, A Review of the Equations of State and their Applicability in Phase Equilibrium Modeling, Int. Conf. Chem. Environ. Eng. (2013) 84–87.

[44] M.M. Abbott, Cubic Equations of State: An Interpretive Review, Adv. Chem. (1979).

[45] E. RAMSEY, Q. SUN, Z. ZHANG, C. ZHANG, W. GOU, Mini-Review: Green sustainable processes using supercritical fluid carbon dioxide, J. Environ. Sci. 21 (2009) 720–726. https://doi.org/10.1016/S1001-0742(08)62330-X.

[46] D.M.T. and I.G. N. I. Diamantonis, G. C. Boulougouris, E. Mansoor, Economou, Evaluation of Cubic, SAFT, and PC-SAFT Equations of State for the Vapor–Liquid Equilibrium Modeling of CO2 Mixtures with Other Gases, Ind. Eng. Chem. Res. 52 (2013) 3933–3942.

[47] S. H. Huang and M. Radosz, Equation of State for Small, Large, Polydisperse and Associating Molecules, Ind. Eng. Chem. Res. 29 (1990) 2284–2294.

[48] G.J.J. and M.R. JW. G. Chapman, K. E. Gubbins, SAFT: Equation-of-State Solution Model for Associating Fluids, Fluid Phase Equilib. 52 (1989) 31–38.

[49] C. Latsky, High pressure phase equilibria of the system CO2 + n-dodecane + 3,7-dimethyl-1-octanol + 1-decanol, PhD Dissertation, 2019. https://scholar.sun.ac.za.

[50] D. Peng, D.B. Robinson, A New Two-Constant Equation of State, Ind. Eng. Chem.Fundam. 15 (1976) 59–64.

[51] S. Vitu, R. Privat, J.N. Jaubert, F. Mutelet, Predicting the phase equilibria of CO2 + hydrocarbon systems with the PPR78 model (PR EOS and kij calculated through a group contribution method), J. Supercrit. Fluids. 45 (2008) 1–26. https://doi.org/10.1016/j.supflu.2007.11.015.

[52] J.N. Jaubert, F. Mutelet, VLE predictions with the Peng-Robinson equation of state and temperature dependent kij calculated through a group contribution method, Fluid Phase Equilib. 224 (2004) 285–304. https://doi.org/10.1016/j.fluid.2004.06.059.

[53] R.B. Mukhopadhyay M, Modeling of supercritical drying of ethanol-soaked silica aerogels with carbon dioxide, J Chem Technol Biotechnol. 83 (2008)

1101-.

[54] Kistler SS, Coherent expanded aerogels and jellies, Nature. 127 (1931) 741.

[55] C.A. García-gonzález, M.C. Camino-rey, M. Alnaief, C. Zetzl, I. Smirnova, The Journal of Supercritical Fluids Supercritical drying of aerogels using CO2 : Effect of extraction time on the end material textural properties, J. Supercrit. Fluids. 66 (2012) 297–306. http://dx.doi.org/10.1016/j.supflu.2012.02.026.

[56] D. Karami, A Review of Aerogel Applications in Adsorption and Catalysis, J. Pet. Sci. Technol. 8 (2018) 3–15.

[57] E. Reverchon, I. De Marco, Supercritical fluid extraction and fractionation of natural matter, J. Supercrit. Fluids. 38 (2006) 146–166. https://doi.org/10.1016/j.supflu.2006.03.020.

[58] K.M. V. Louli, N. Ragoussis, Recovery of phenolic antioxi dants from wine industry by-products, Biores. Technol. 92 (2004) 201– 208.

[59] J. S. Lopez-Sebastian, E. Ramos, E. Ibanez, J.M. Bueno, L. Ballester, G.R. Tabera, Dearomatization of antioxidant rosemary extracts by treatment with supercritical carbon dioxide, J. Agric. Food Chem. 46 (1998) 13–19.

[60] G.R. E. Ibanez, A. Cifuentes, A.L. Crego, F.J. Senorans, S. Cavero, Combined use of supercritical fluid extraction, micellar electrokinetic chromatography, and reverse phase high performance liquid chromatogra_phy for the analysis of antioxidants from rosemary (Rosmarinus officinalis L.), J. Agric. Food Chem. 48 (2000)) 4060–4065.

[61] J.L.U. M.T. Tena, M. Valcarcel, P.J. Hidalgo, Supercritical fluid extraction of natural antioxidants from rosemary: comparison with liquid

solvent sonication, Anal. Chem. 69 (1997) 521–526.

[62] M.P. E. Reverchon, J. Daghero, C. Marrone, M. Mattea, Supercritical fractional extraction of fennel seed oil and essential oil: experiments and mathematical modelling, Ind. Eng. Chem. Res. 38 (1999) 3069–3075.

[63] T. J. Tabera, A. Guinda, A. Ruiz-Rodriguez, F.J. Senorans, E. Ibanez, G.R. Albi, Counter-current supercritical fluid extraction and frac_tionation of high-added-value compounds from a hexane extract of olive leaves, J. Agric. Food Chem. 52 (2004) 4774–4779.

[64] L.C. G. Vasapollo, L. Longo, L. Restio, Innovative supercritical CO2 extraction of Lycopene from tomato in the presence of vegetable oil as co-solvent, J. Supercrit. Fluids. 29 (2004) 87–96.

[65] A.P.P. E. Sabio, M. Lozano, V. Montero de Espinosa, R.L. Mendes, J.A.C. A.F. Palavra, Lycopene and carotene extraction from tomato processing waste using supercritical CO2, Ind. Eng. Chem. Res. (2003) 6641–6646.

[66] D.A.J.S. T. Baysal, S. Ersus, Supercritical CO2 extraction of carotene and Lycopene from tomato paste waste, J. Agric. Food Chem. 48 (2000) 5507–5511.

[67] B.W. Drennan, A.P. Wicker, B.K. Berger, K.A. Schug, Measurements of drugs and metabolites in biological matrices using SFC and SFE-SFC-MS, 1st ed., Elsevier Inc., 2022. https://doi.org/10.1016/B978-0-323-88487-7.00004-8.

[68] C. West, E. Lesellier, Selection of SFC stationary and mobile phases, 1st ed., Elsevier Inc., 2022. https://doi.org/10.1016/B978-0-323-88487-7.00008-5.

[69] S.K. Misra, K. Pathak, Supercritical fluid technology for solubilization of poorly water soluble drugs via micro- and naonosized particle generation, ADMET DMPK. 8 (2020) 355–374. https://doi.org/10.5599/admet.811.

[70] H.S.P. G. Sodeifian, N.S. Ardestani, S.A. Sajaadian, Experimental measurements and thermodynamic modeling of Coumarin-7 solid solubility in supercritical carbon dioxide: Production of nanoparticles via RESS method, Fluid Phase Equilib. 483 (2019) 122–143.

[71] H.H. H. Bagheri, G.A. Mansoori, A novel approach to predict drugs solubility in supercritical solvents for RESS process using various cubic EoS-mixing rule., J. Mol. Liq. 261 (2018) 174–188.

[72] C.S. B. Wang, Solid solubility measurement of ipriflavone in supercritical carbon dioxide and microparticle production through the rapid expansion of supercritical solutions process., J. CO_2 Util. 27 (2020).

[73] G. Liu, J. Li, S. Deng, Applications of supercritical anti-solvent process in preparation of solid multicomponent systems, Pharmaceutics. 13 (2021). https://doi.org/10.3390/pharmaceutics13040475.

[74] L. Lesoin, C. Crampon, O. Boutin, E. Badens, Preparation of liposomes using the supercritical anti-solvent (SAS) process and comparison with a conventional method, J. Supercrit. Fluids. 57 (2011) 162–174. https://doi.org/10.1016/j.supflu.2011.01.006.

[75] L. Yang, Z. Sun, Y. Zu, C. Zhao, X. Sun, Z. Zhang, L. Zhang, Physicochemical properties and oral bioavailability of ursolic acid nanoparticles using supercritical anti-solvent (SAS) process, Food Chem. 132 (2012) 319–325. https://doi.org/10.1016/j.foodchem.2011.10.083.

[76] A. Capuzzo, M.E. Maffei, A. Occhipinti, Supercritical fluid extraction of

plant flavors and fragrances, Molecules. 18 (2013) 7194–7238. https://doi.org/10.3390/molecules18067194.

[77] A. Pietsch, Decaffeination-Process and Quality, in: Cr. Sci. Coffee, 2017: pp. 225–143. https://doi.org/10.1016/B978-0-12-803520-7.00010-4.

[78] A.S. Smiline Girija, Caffeic and chlorogenic acids, in: A Centum Valuab. Plant Bioact., 2021: pp. 613–630. https://doi.org/10.1016/B978-0-12-822923-1.00001-7.

[79] F. Sahena, I.S.M. Zaidul, S. Jinap, A.A. Karim, K.A. Abbas, N.A.N. Norulaini, A.K.M. Omar, Application of supercritical CO2 in lipid extraction - A review, J. Food Eng. 95 (2009) 240–253. https://doi.org/10.1016/j.jfoodeng.2009.06.026.

[80] I. Djekic, N. Tomic, S. Bourdoux, S. Spilimbergo, N. Smigic, B. Udovicki, G. Ho, F. Devlieghere, A. Rajkovic, Comparison of three types of drying (supercritical CO 2 , air and freeze) on the quality of dried apple – Quality index approach, LWT - Food Sci. Technol. 94 (2018) 64–72. https://doi.org/10.1016/j.lwt.2018.04.029.

[81] A. Zambon, P. Facco, G. Morbiato, M. Toffoletto, G. Poloniato, S. Sut, P. Andrigo, S. Dall, M. De Bernard, S. Spilimbergo, Promoting the preservation of strawberry by supercritical CO 2 drying, Food Chem. 397 (2022). https://doi.org/10.1016/j.foodchem.2022.133789.

[82] Z.K. Brown, P.J. Fryer, I.T. Norton, S. Bakalis, R.H. Bridson, Drying of foods using supercritical carbon dioxide — Investigations with carrot, Innov. Food Sci. Emerg. Technol. 9 (2008) 280–289. https://doi.org/10.1016/j.ifset.2007.07.003.

[83] S. Bourdoux, A. Rajkovic, S. De Sutter, A. Vermeulen, S. Spilimbergo,

Inactivation of Salmonella , Listeria monocytogenes and Escherichia coli O157 : H7 inoculated on coriander by freeze-drying and supercritical CO 2 drying, S. Bourdoux Al. Innov. Food Sci. Emerg. Technol. 47 (2018) 180–186. https://doi.org/10.1016/j.ifset.2018.02.007.

[84] L. Chen, J. Hasanov, J. Chen, Y. Feng, Y. Kanda, A. Komiya, Supercritical fluid remediation for soil contaminants: Mechanisms, parameter optimization and pilot systems, J. Supercrit. Fluids. 189 (2022) 105718. https://doi.org/10.1016/j.supflu.2022.105718.

[85] A.H. Al-Marzouqi, A.Y. Zekri, A.A. Azzam, A.Y. Alraeesi, Optimization of supercritical fluid extraction of hydrocarbons from a contaminated soil: An experimental approach, Int. J. Environ. Sci. Dev. 10 (2019) 301–309. https://doi.org/10.18178/ijesd.2019.10.10.1191.

[86] R.K. Kankala, Y.S. Zhang, S. Bin Wang, C.H. Lee, A.Z. Chen, Supercritical Fluid Technology: An Emphasis on Drug Delivery and Related Biomedical Applications, Adv. Healthc. Mater. 6 (2017). https://doi.org/10.1002/adhm.201700433.

[87] K.A. Kravanja, M. Finšgar, Ž. Knez, M. Knez Marevci, Supercritical Fluid Technologies for the Incorporation of Synthetic and Natural Active Compounds into Materials for Drug Formulation and Delivery, Pharmaceutics. 14 (2022). https://doi.org/10.3390/pharmaceutics14081670.

[88] I.E. Santo, A.S. Pedro, R. Fialho, E. Cabral-Albuquerque, Characteristics of lipid micro- and nanoparticles based on supercritical formation for potential pharmaceutical application, Nanoscale Res. Lett. 8 (2013). https://doi.org/10.1186/1556-276X-8-386.

[89] A. White, D. Burns, T.W. Christensen, Effective terminal sterilization using supercritical carbon dioxide, J. Biotechnol. 123 (2006) 504–515. https://doi.org/10.1016/j.jbiotec.2005.12.033.

[90] V. Santos-Rosales, B. Magariños, R. Starbird, J. Suárez-González, J.B. Fariña, C. Alvarez-Lorenzo, C.A. García-González, Supercritical CO2 technology for one-pot foaming and sterilization of polymeric scaffolds for bone regeneration, Int. J. Pharm. 605 (2021). https://doi.org/10.1016/j.ijpharm.2021.120801.

[91] N. Ribeiro, G.C. Soares, V. Santos-Rosales, A. Concheiro, C. Alvarez-Lorenzo, C.A. García-González, A.L. Oliveira, A new era for sterilization based on supercritical CO2 technology, J. Biomed. Mater. Res. - Part B Appl. Biomater. 108 (2020) 399–428. https://doi.org/10.1002/jbm.b.34398.

[92] S.H. Soh, S. Agarwal, A. Jain, L.Y. Lee, S.K. Chin, S. Jayaraman, Mathematical modeling of mass transfer in supercritical fluid extraction of patchouli oil, Eng. Reports. 1 (2019) 1–11. https://doi.org/10.1002/eng2.12051.

[93] C. Pardo-castaño, M. Velásquez, G. Bolaños, Simple Models for Supercritical Extraction of Natural Matter School, J. Supercrit. Fluids. (2014) 1–34. https://doi.org/10.1016/j.supflu.2014.09.044.

[94] M. Taniguchi, T. Tsuji, M. Shibata, Extraction of Oils from Wheat Germwith Supercritical Carbon Dioxide point, Agric. Biol. Chem. 49 (1985) 2367–2367.

[95] P.O. Box, T.G. Hayes, J.C. Kiley, S.N. Deming, An Experimental Design Approach to the Optimization of Supercritical Fluid Extraction for the

Determination of Oil and Grease in Soil, J. Chromatogr. Sci. 31 (1993) 170–176.

[96] S.G. Özkal, M.E. Yener, Supercritical carbon dioxide extraction of flaxseed oil: Effect of extraction parameters and mass transfer modeling, J. Supercrit. Fluids. 112 (2016) 76–80. https://doi.org/10.1016/j.supflu.2016.02.013.

[97] J. Puiggené, M.A. Larrayoz, F. Recasens, Free liquid-to-supercritical fluid mass transfer in packed beds, Chem. Eng. Sci. 52 (1997) 195–212. https://doi.org/10.1016/S0009-2509(96)00379-X.

[98] M.S. and M.G. Bhupesh C. Roy, Effect of Temperature and Pressure on the Extraction Yield of Oil from Sunflower Seed with Supercritical Carbon Dioxide, J. Appl. Sci. 6 (2006) 71–75. https://doi.org/DOI: 10.3923/jas.2006.71.75.

[99] F.A. Espinosa-pardo, J. Martinez, H.A. Martinez-correa, Extraction of bioactive compounds from peach palm pulp (Bactris gasipaes) using supercritical CO_2, J. Supercrit. Fluids. (2014). https://doi.org/10.1016/j.supflu.2014.05.010.

[100] R.S. Tiejun Lua, Filipe Gaspar a, Ray Marriott b, Steve Mellor c, Colin Watkinson d, Bushra Al-Duri a, Jonathan Seville a, Extraction of borage seed oil by compressed CO_2 : Effect of extraction parameters and modelling, J. Supercrit. Fluids. 41 (2007) 68–73. https://doi.org/10.1016/j.supflu.2006.10.002.

[101] J. Yin, A. Wang, W. Wei, Y. Liu, W. Shi, Analysis of the operation conditions for supercritical fluid extraction of seed oil, Sep. Purif. Technol. 43 (2005) 163–167. https://doi.org/10.1016/j.seppur.2004.10.016.

[102] M.E.Y. S.G. Ozkal , U. Salgın, Supercritical carbon dioxide extraction of hazelnut oil, J. Food Eng. 69 (2005) 217–223. https://doi.org/10.1016/j.jfoodeng.2004.07.020.

[103] Z. Huang, X. han Shi, W. juan Jiang, Theoretical models for supercritical fluid extraction, J. Chromatogr. A. 1250 (2012) 2–26. https://doi.org/10.1016/j.chroma.2012.04.032.

[104] C.B. Mehr, R.N. Biswal, J.L. Collins, Supercritical Carbon Dioxide Extraction of Caffeine from Guaranh, J. Supercrit. Fluids. 9 (1996) 185–191.

[105] P. Subra, S. Castellani, P. Jestin, A. Aoufi, Extraction of b -carotene with supercritical fluids Experiments and modelling, J. Supercrit. Fluids. 12 (1998) 261–269.

[106] H. Sovová, Rate of the vegetable oil extraction with supercritical CO2-I. Modelling of extraction curves, Chem. Eng. Sci. 49 (1994) 409–414. https://doi.org/10.1016/0009-2509(94)87012-8.

[107] L. Fiori, D. Basso, P. Costa, The Journal of Supercritical Fluids Supercritical extraction kinetics of seed oil : A new model bridging the ' broken and intact cells ' and the ' shrinking-core ' models, J. Supercrit. Fluids. 48 (2009) 131–138. https://doi.org/10.1016/j.supflu.2008.09.019.

[108] H. Sovová, A.A. Galushko, R.P. Stateva, K. Rochová, M. Sajfrtová, M. Bártlová, Supercritical fluid extraction of minor components of vegetable oils : b -Sitosterol, J. Food Eng. 101 (2010) 201–209. https://doi.org/10.1016/j.jfoodeng.2010.07.002.

[109] S. Machmudah, A. Sulaswatty, M. Sasaki, M. Goto, T. Hirose, Supercritical CO 2 extraction of nutmeg oil : Experiments and modeling,

J. Supercrit. Fluids 39. 39 (2006) 30–39. https://doi.org/10.1016/j.supflu.2006.01.007.

[110] N. Ayas, O. Yilmaz, A shrinking core model and empirical kinetic approaches in supercritical CO_2 extraction of safflower seed oil, J. Supercrit. Fluids. 94 (2014) 81Gasp–90. https://doi.org/10.1016/j.supflu.2014.06.019.

[111] M. Lazrag, C. Lemaitre, C. Castel, A. Hannachi, D. Barth, Aerogel production by supercritical drying of organogels: Experimental study and modelling investigation of drying kinetics, J. Supercrit. Fluids. 140 (2018) 394–405. https://doi.org/10.1016/j.supflu.2018.07.016.

[112] İ. Şahin, Y. Özbakır, Z. İnönü, Z. Ulker, C. Erkey, Kinetics of supercritical drying of gels, Gels. 4 (2018). https://doi.org/10.3390/gels4010003.

[113] Paracetamol (Acetaminophen) Chemical and physical data, IARC Monogr. Eval. Carcinog. Risks to Humans. (1990).

[114] Joint Formulary Committee, BNF 81 (British National Formulary), 81st ed., Pharmaceutical Press, 2021.

[115] R.A. Granberg, C. Rasmuson, Solubility of Paracetamol in Pure Solvents, J. Chem. Eng. Data. 44 (1999) 1391–1395. https://doi.org/10.1021/je990124v.

[116] P. Diogo, M.E. Minas, Thermochemistry of paracetamol, J Therm Anal Calorim. 100 (2010) 391–401. https://doi.org/10.1007/s10973-009-0634-y.

[117] E.W. Lemmon, M.L. Huber, Thermodynamic Properties of n -Dodecane, Energy & Fuels. 24 (2004) 960–967. https://doi.org/10.1021/ef0341062.

[118] Fabian Triefenbach, Design of Experiments: The D-Optimal Approach

and Its Implementation As a Computer Algorithm, 2008.

[119] A.D. Vassileiou, M.N. Robertson, B.G. Warehamc, M. Soundaranathanc, S. Ottobonib, A.J. Florenceb, T. Hartwigd, A Unified ML Framework for Solubility Prediction Across Organic Solvents Digital Discovery, R. Soc. Chem. 00 (2023) 14. https://doi.org/10.1039/D2DD00024E.

[120] M. Shahid, C. Faure, S. Ottoboni, L. Lue, C. Price, Employing Constant Rate Filtration To Assess Active Pharmaceutical Ingredient Washing E ffi ciency, Org. Process Res. Dev. 26 (2022) 97–110. https://doi.org/10.1021/acs.oprd.1c00272.

[121] C.S. MacLeod, F.L. Muller, On the fracture of pharmaceutical needle-shaped crystals during pressure filtration: Case studies and mechanistic understanding, Org. Process Res. Dev. 16 (2012) 425–434. https://doi.org/10.1021/op200279m.

[122] D.J. Lamberto, B. Cohen, J. Marencic, C. Miranda, R. Petrova, L. Sierra, Laboratory methods for assessing API sensitivity to mechanical stress during agitated drying, Chem. Eng. Sci. 66 (2011) 3868–3875. https://doi.org/10.1016/j.ces.2011.05.016.

[123] M.B. Papageorgiou, C. D., Mitchell, C., Quon, J. L., Langston, M., Borg, S., Hicks, F., D. Ende, Development of a novel screening methodology for the assessment of the risk of particle size attrition during agitated drying, Org. Process Res. Dev. 2 (2020) 242–254. https://doi.org/DOI: 10.1021/acs.oprd.9b00502.

[124] I. EMA, ICH guideline Q3C (R8) on impurities : guideline for residual solvents, 2022. www.ema.europa.eu/contact.

[125] David Smitha and Patrik Spanel, Ambient analysis of trace compounds in

gaseous media by SIFT-MS, R. Soc. Chem. 136 (2011) 2009–2032. https://doi.org/10.1039/c1an15082k.

[126] C.J. Price, A. Barton, S.J. Coleman, Continuous Isolation of Active Pharmaceutical Ingredients, (2020).

[127] D. Skansi, S. Tomas, I. Pudić, A. Arapović, The influencf of pressure and temperature on the kinetics of vacuum drying of ketoprofen, Dry. Technol. 15 (1997) 1617–1631. https://doi.org/10.1080/07373939708917312.

[128] N.K. Nere, K.C. Allen, J.C. Marek, S. V. Bordawekar, Drying process optimization for an API solvate using heat transfer model of an agitated filter dryer, J. Pharm. Sci. 101 (2012) 3886–3895. https://doi.org/10.1002/jps.23237.

[129] I.C. Kemp, B.C. Fyhr, S. Laurent, M.A. Roques, C.E. Groenewold, E. Tsotsas, A.A. Sereno, C.B. Bonazzi, J.J. Bimbenet, M. Kind, Methods for processing experimental drying kinetics data, Dry. Technol. 19 (2001) 15–34. https://doi.org/10.1081/DRT-100001350.

[130] A. Lekhal, K.P. Girard, M.A. Brown, S. Kiang, J.G. Khinast, B.J. Glasser, The effect of agitated drying on the morphology of L-threonine (needle-like) crystals, Int. J. Pharm. 270 (2004) 263–277. https://doi.org/10.1016/j.ijpharm.2003.10.022.

[131] S.M. Abbott, J.B. Elder, P. Španěl, D. Smith, Quantification of acetonitrile in exhaled breath and urinary headspace using selected ion flow tube mass spectrometry, Int. J. Mass Spectrom. 228 (2003) 655–665. https://doi.org/10.1016/S1387-3806(03)00212-4.

[132] S.T. Senthilmohan, M.J. McEwan, P.F. Wilson, D.B. Milligan, C.G. Freeman, Real time analysis of breath volatiles using SIFT-MS in cigarette

smoking, Redox Rep. 6 (2004) 185–187. https://doi.org/10.1179/135100001101536166.

[133] N.K. Sharma, M. Choct, M.W. Dunlop, S. Wu, H.Z. Castada, R.A. Swick, Characterisation and quantification of changes in odorants from litter headspace of meat chickens fed diets varying in protein levels and additives, Poult. Sci. Assoc. Inc. 00 (2014) 1–10. https://doi.org/http://dx.doi.org/10.3382/ps/pew309.

[134] D. Volckaert, D.E.L. Ebude, H. Van Langenhove, SIFT-MS analysis of the removal of dimethyl sulphide, n-hexane and toluene from waste air by a two phase partitioning bioreactor, Chem. Eng. J. 290 (2016) 346–352. https://doi.org/10.1016/j.cej.2016.01.057.

[135] B.J. Prince, D.B. Milligan, M.J. Mcewan, Application of selected ion flow tube mass spectrometry to real-time atmospheric monitoring, Rapid Commun. Mass Spectrom. 24 (2010) 1763–1769. https://doi.org/10.1002/rcm.

[136] P. Španěl, D. Smith, Selected ion flow tube: a technique for quantitative trace gas analysis of air and breath, Med. Biol. Eng. Comput. 34 (1996) 409–419. https://doi.org/10.1007/BF02523843.

[137] S. Mendis, P.A. Sobotka, D.E. Euler, Expired Hydrocarbons in Patients with Acute Myocardial Infarction, Free Radic. Res. 23 (1995) 117–122. https://doi.org/10.3109/10715769509064026.

[138] O.A. Ajibola, D. Smith, P. Spaněl, G.A.A. Ferns, Effects of dietary nutrients on volatile breath metabolites., J. Nutr. Sci. 2 (2013) e34. https://doi.org/10.1017/jns.2013.26.

[139] P. Tonthubthimthong, S. Chuaprasert, P. Douglas, W. Luewisutthichat,

Supercritical CO2 extraction of nimbin from neem seeds – an experimental study, J. Food Eng. 47 (2001) 289–293. https://doi.org/10.1016/S0260-8774(00)00131-X.

[140] L.A. Follegatti-romero, C.R. Piantino, R. Grimaldi, F.A. Cabral, Supercritical CO2 extraction of omega-3 rich oil from Sacha inchi (Plukenetia volubilis L .) seeds, J. Supercrit. Fluids. 49 (2009) 323–329. https://doi.org/10.1016/j.supflu.2009.03.010.

[141] Y. Yang, A. Gharaibeh, S.B. Hawthome, D.J. Miller, Combined Temperature / Modif ier Effects on Supercritical COn Extraction Efficiencies of Polycyclic Aromatic Hydrocarbons from Environmental Samples, Anal. Chem. 67 (1995) 641–646.

[142] C. Hu, Y. Liu, Quality Control in Pharmaceuticals: Residual Solvents Testing and Analysis, Wide Spectra Qual. Control. 1990 (2012). https://doi.org/10.5772/23041.

[143] H. Bagheri, B. Notej, S. Shahsavari, H. Hashemipour, Supercritical carbon dioxide utilization in drug delivery: Experimental study and modeling of paracetamol solubility, Eur. J. Pharm. Sci. 177 (2022). https://doi.org/10.1016/j.ejps.2022.106273.

[144] A. Rai, K.D. Punase, B. Mohanty, R. Bhargava, Evaluation of models for supercritical fluid extraction, Int. J. Heat Mass Transf. 72 (2014) 274–287. https://doi.org/10.1016/j.ijheatmasstransfer.2014.01.011.

[145] S.A. Sajadian, N.S. Ardestani, Experimental optimization and mathematical modeling of the supercritical fluid extraction of essential oil from Eryngium billardieri: Application of simulated annealing (SA) algorithm, J. Supercrit. Fluids. 127 (2017) 146–157.

https://doi.org/10.1016/j.supflu.2017.04.007.

[146] E.L.G. Oliveira, A.J.D. Silvestre, C.M. Silva, Review of kinetic models for supercritical fluid extraction, Chem. Eng. Res. Des. 89 (2011) 1104–1117. https://doi.org/10.1016/j.cherd.2010.10.025.

[147] S.P. Cadogan, B. Mistry, Y. Wong, G.C. Maitland, J.P.M. Trusler, Diffusion Coefficients of Carbon Dioxide in Eight Hydrocarbon Liquids at Temperatures between (298.15 and 423.15) K at Pressures up to 69 MPa, J. Chem. Eng. Data. 61 (2016) 3922–3932. https://doi.org/10.1021/acs.jced.6b00691.

[148] A. Mouahid, H. Bouanga, C. Crampon, E. Badens, A. Mouahid, H. Bouanga, C. Crampon, E. Badens, S. Co, Supercritical CO2 extraction of oil from Jatropha curcas : An experimental and modelling study To cite this version : HAL Id : hal-02114700 and modelling study, J. Supercrit. Fluids. (2019) 2–11. https://doi.org/10.1016/j.supflu.2017.11.014.

[149] H. mu Lin, Peng-Robinson equation of state for vapor-liquid equilibrium calculations for carbon dioxide + hydrocarbon mixtures, Fluid Phase Equilib. 16 (1984) 151–169. https://doi.org/10.1016/0378-3812(84)85028-1.

[150] K. Kato, K. Nagahama, Generalized interaction parameters for the PREOS of carbon dioxide n paraffin binary systems, Fluid Phase Equilib. 7 (1981) 219–231. https://doi.org/DOI: 10.1016/0378-3812(81)80009-X.

[151] S.P. Cadogan, B. Mistry, Y. Wong, G.C. Maitland, J.P.M. Trusler, Diffusion Coefficients of Carbon Dioxide in Eight Hydrocarbon Liquids at Temperatures between (298 . 15 and 423 . 15) K at Pressures up to 69 MPa, J. Chem. Eng. Data. 61 (2016) 3922–3932. https://doi.org/DOI:

10.1021/acs.jced.6b00691.

[152] A. Fenghour, W.A. Wakeham, V. Vesovic, The viscosity of carbon dioxide, J. Phys. Chem. Ref. Data. 27 (1998) 31–39. https://doi.org/10.1063/1.556013.

[153] J.M. Philipe dos Santos, Ana C. de Aguiar, Juliane Viganó[1], Joana Schuelter Boeing, Jesuí V. Visentainer, Supercritical CO2 extraction of cumbaru oil (Dipteryx alata Vogel) assisted by ultrasound: Global yield, kinetics and fatty acid composition, J. Supercrit. Fluids. 107 (2015) 75–83. https://doi.org/10.1016/j.supflu.2015.08.018.

[154] I.C. Kemp, Fundamentals of Energy Analysis of Dryers, in: Mod. Dry. Technol., Wiley, 2014: pp. 1–45. https://doi.org/https://doi.org/10.1002/9783527631728.ch21.

[155] Manu Huttunen, Optimizing the specific energy consumption of vacuum filtration, 2019.

[156] NIST Chemistry WebBook, SRD 69, (2023). https://webbook.nist.gov/.

[157] T.M. Attard, C.R. McElroy, A.J. Hunt, Economic assessment of supercritical CO2 extraction of waxes as part of a maize stover biorefinery, Int. J. Mol. Sci. 16 (2015) 17546–17564. https://doi.org/10.3390/ijms160817546.

[158] P.B. Joseph Williams, Capturing CO_2: Gas Compression vs. Liquefaction, (2009). https://www.powermag.com/capturing-co2-gas-compression-vs-liquefaction/.

10 Appendix A

Fitted data using an exponential function

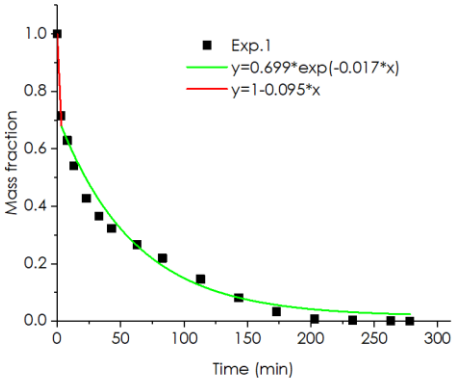

Figure A1. Drying curve procured at 50 °C temperature, 0.8 L/min nitrogen flow rate, 60 g solid. mass and static drying mode.

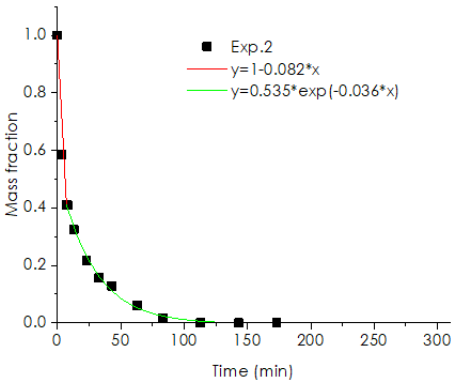

Figure A2. Drying curve procured at 70 °C temperature, 0.8 L/min nitrogen flow rate, 60 g solid mass and static drying mode.

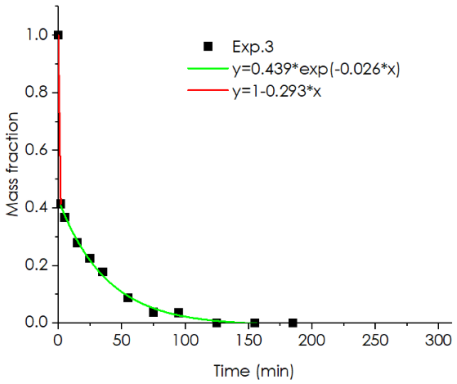

Figure A3. Drying curve procured at 70 °C temperature, 0.8 L/min nitrogen flow rate, 60 g solid mass and continuous agitated drying mode.

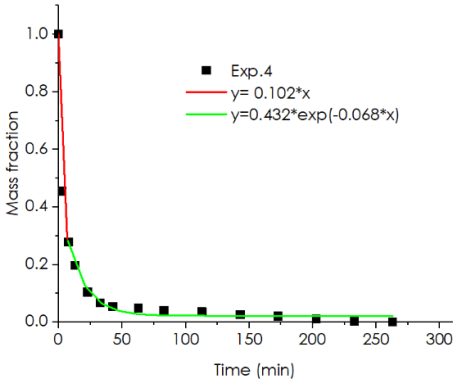

Figure A4. Drying curve procured at 50 °C temperature, 0.2 L/min nitrogen flow rate, 60 g solid mass and continuous agitated drying mode.

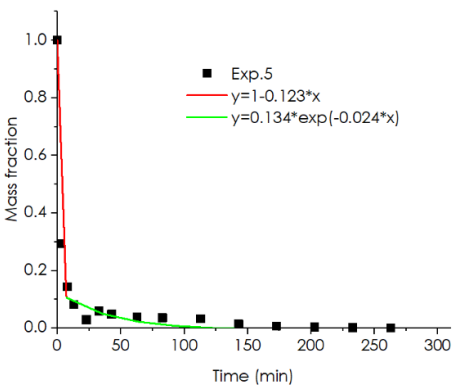

Figure A5. Drying curve procured at 50 °C temperature, 0.8 L/min nitrogen flow rate, 60 g solid mass and intermittent agitated drying mode.

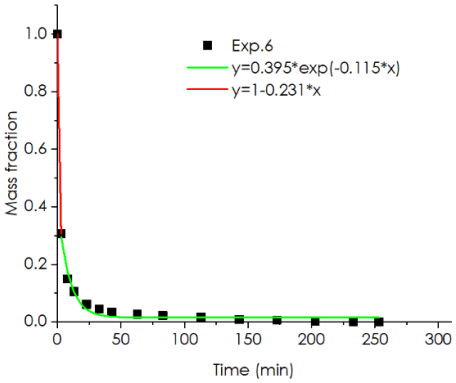

Figure A6. Drying curve procured at 70 °C temperature, 0.2 L/min nitrogen flow rate, 60 g solid mass and intermittent agitated drying mode.

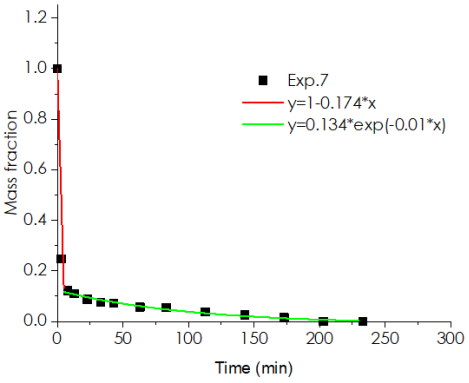

Figure A7. Drying curve procured at 50 °C temperature, 0.2 L/min nitrogen flow rate, 60 g solid mass and intermittent agitated drying mode.

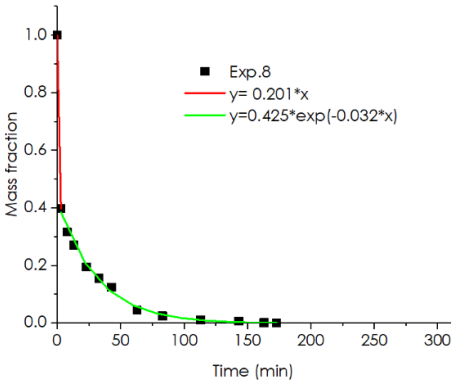

Figure A8. Drying curve procured at 70 °C temperature, 0.8 L/min nitrogen flow rate, 60 g solid mass and intermittent agitated drying mode.

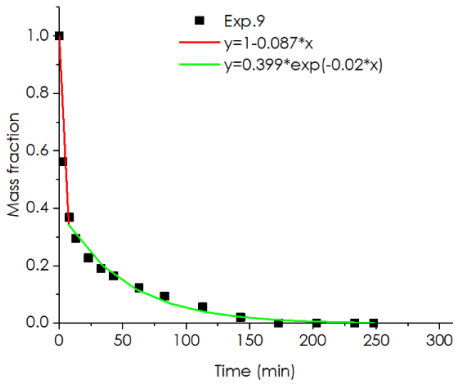

Figure A9. Drying curve procured at 70 °C temperature, 0.2 L/min nitrogen flow rate, 105 g solid mass and static drying mode.

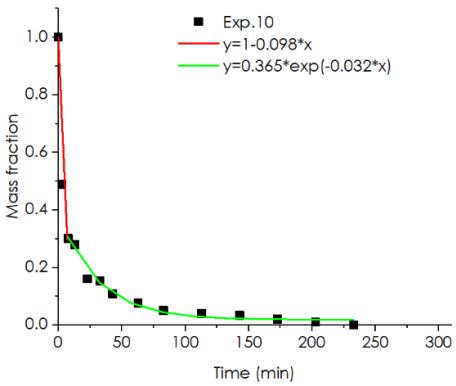

Figure A10. Drying curve procured at 50 °C temperature, 0.5 L/min nitrogen flow rate, 105 g solid mass and static drying mode.

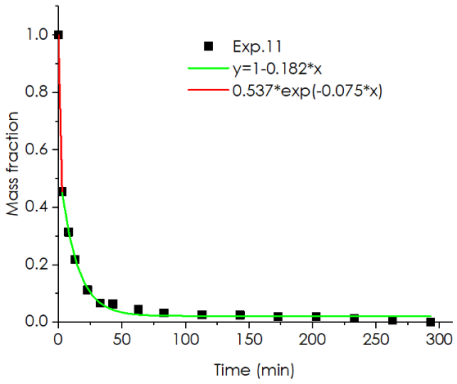

Figure A11. Drying curve procured at 50 °C temperature, 0.8 L/min nitrogen flow rate, 105 g solid mass and continuous agitated drying mode.

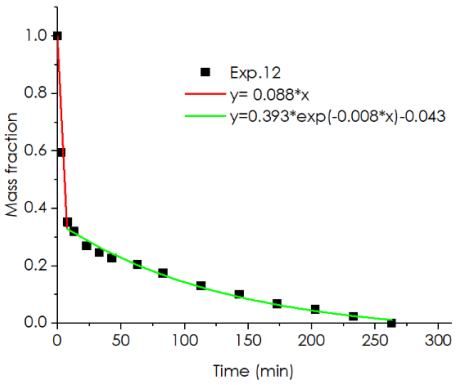

Figure A12. Drying curve procured at 70 °C temperature, 0.2 L/min nitrogen flow rate, 105 g solid mass and continuous agitated drying mode.

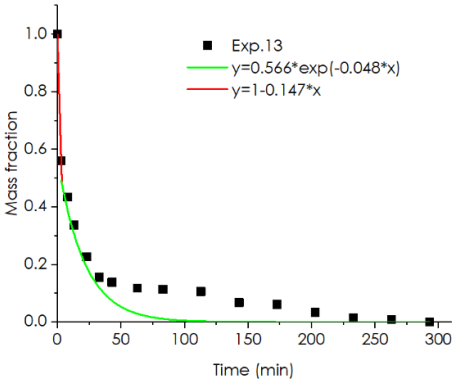

Figure A13. Drying curve procured at 60 °C temperature, 0.5 L/min nitrogen flow rate, 105 g solid mass and intermittent agitated drying mode.

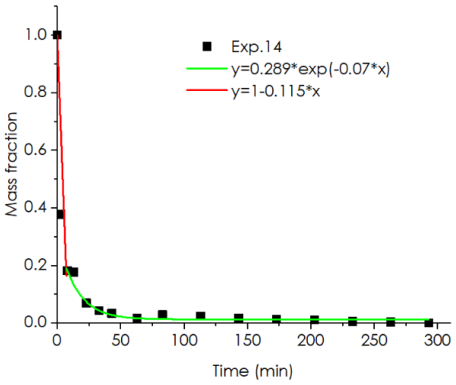

Figure A14. Drying curve procured at 60 °C temperature, 0.5 L/min nitrogen flow rate, 105 g solid mass and intermittent agitated drying mode.

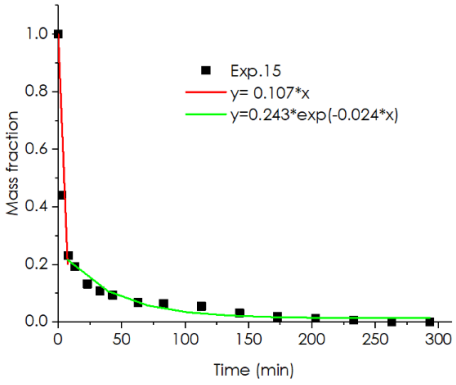

Figure A15. Drying curve procured at 60 °C temperature, 0.5 L/min nitrogen flow rate, 105 g solid mass and intermittent agitated drying mode.

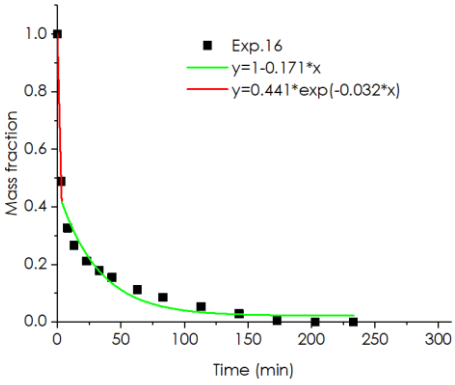

Figure A16. Drying curve procured at 70 °C temperature, 0.8 L/min nitrogen flow rate, 105 g solid mass and static drying mode.

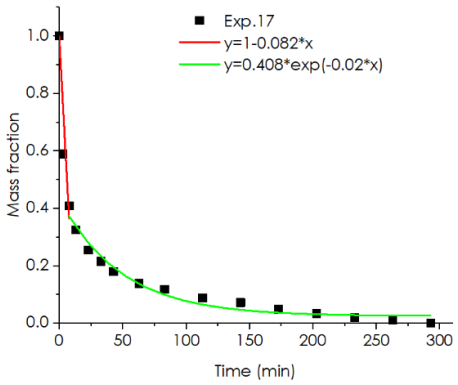

Figure A17. Drying curve procured at 50 °C temperature, 0.2 L/min nitrogen flow rate, 150 g solid mass and static drying mode.

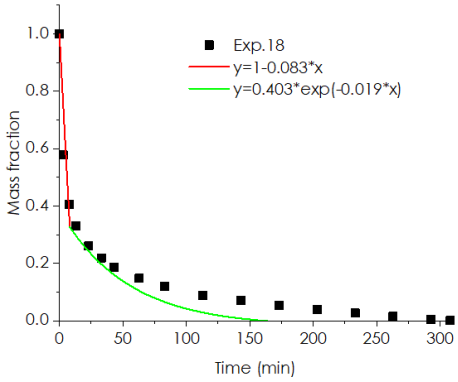

Figure A18. Drying curve procured at 70 °C temperature, 0.8 L/min nitrogen flow rate, 150 g solid mass and static drying mode.

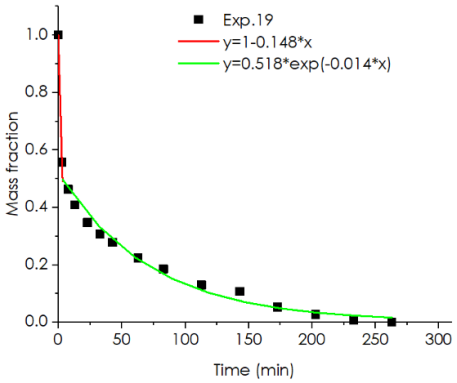

Figure A19. Drying curve procured at 70 °C temperature, 0.2 L/min nitrogen flow rate, 150 g solid mass and continuous agitated drying mode.

11 Appendix B

Binary diffusion coefficient D_{12}

The binary diffusion coefficient D_{12} is calculated from the equations below [147]:

$$D_{12} = D_0 \cdot \exp(-b \cdot (p - p_0)) \quad \textbf{Eq. (B1)}$$

Where D_0 is the diffusion coefficient at $p_0 = 0.1\ \text{Mpa}$ and coefficient b expresses the pressure-dependence of D_{12}.

Table B 1. D_0 and b coefficients for CO_2 diffusion coefficients D_{12} in dodecane at different temperatures.

T_{SCF} (k)	D_0	b
323	5.38	0.0078
333	6.12	0.0075
343	6.90	0.0075

Taking the values from **Table B 1** and solving the Eq. (B1) the D_{12} is estimated for different pressures. For example, at pressure 20 Mpa and temperature 323 K the D_{12} for the CO_2-dodecane is equal to $4.61 \cdot 10^{-9}\ m^2 \cdot s^{-1}$.

$$D_{12} = 5.38 \cdot \exp\big(-0.0078 \cdot (20 - 0.1)\big) = 4.607 \cdot 10 - 9\ m^2 \cdot s^{-1}$$

Table B 2. Diffusion coefficients D_{12} of CO_2 in dodecane at temperatures T and pressures P.

T (K)	**P(Mpa)**	**D_{12} ($10^{-9} \cdot m^2 \cdot s^{-1}$)**
323	20	4.607
	14	4.827
	8	5.058
333	20	5.270
	14	5.514
	8	5.769
343	20	5.948
	14	6.221
	8	6.507

Density of the CO_2

Python module was used for the calculation of the CO_2 properties at particular temperatures and pressures with the use of Peng-Robinson equation of state. (https://github.com/CorySimon/PREOS)

Table B 3. A comparison of carbon dioxide density and viscosity used in the calculations with the values retrieved from the NIST library.

Exp. No.	**Pressure (bar)**	**Temperature (°C)**	**ρ_{CO2} (kg/m^3)**		**$\mu_{CO2} \cdot 10^{-6}$ (Pa · s)**	
			Peng Robinson	**NIST**	**A.Fenghour, et al.** [152]	**NIST**
1	200	50	787	785	71.7	69.6
2	140	50	606	674	60.1	53.4
3	200	70	657	660	54.8	52.6
4	140	60	511	562	40.2	41.7
5	200	60	721	724	61.0	60.5
6	200	70	657	660	54.8	52.6
7	200	60	721	724	61.0	60.5
8	200	50	787	785	71.7	69.6
9	200	70	657	660	54.8	52.6
10	140	60	511	562	40.2	41.7
11	200	50	787	785	71.7	69.6
12	140	70	438	458	30.3	33.6
13	140	60	511	562	40.2	41.7
14	140	60	511	562	40.2	41.7
15	140	60	511	562	40.2	41.7

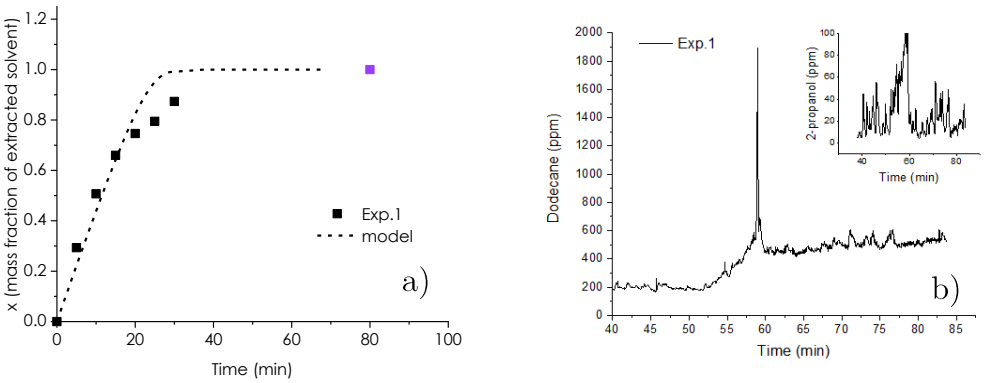

Figure B1. A) Mass fraction of extracted dodecane versus time; at T=50 °C, P=200 bar, CO_2 flow rate=10 g/min and mass of cake=60 g b) Dodecane and 2-propanol concentration changes over time obtained from SIFT-MS online analysis.

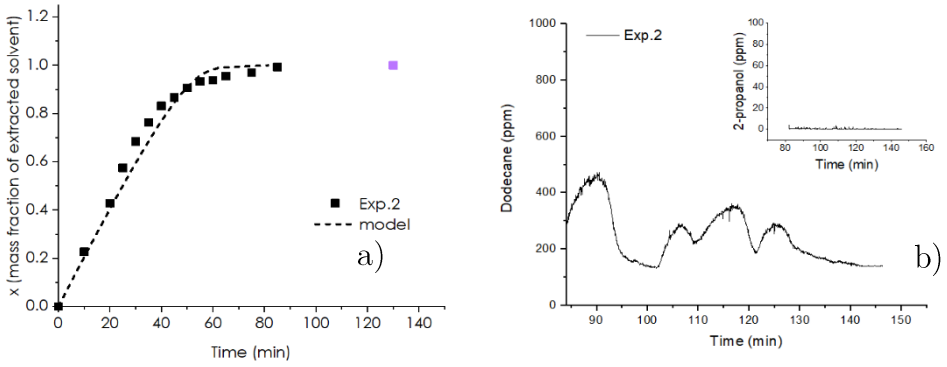

Figure B2. A) Mass fraction of extracted dodecane versus time; at T=50 °C, P=140 bar, CO_2 flow rate=10 g/min and mass of cake=60 g b) Dodecane and 2-propanol concentration changes over time obtained from SIFT-MS online analysis.

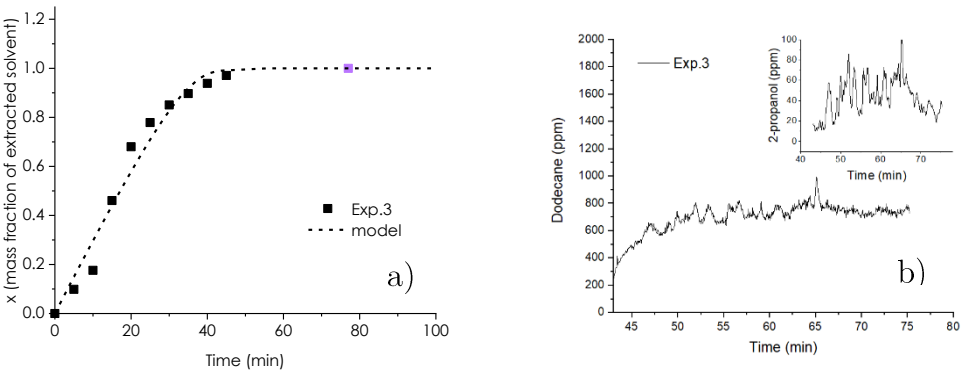

Figure B3. A) Mass fraction of extracted dodecane versus time; at T=70 °C, P=200 bar, CO_2 flow rate=10 g/min and mass of cake=60 g b) Dodecane and 2-propanol concentration changes over time obtained from SIFT-MS online analysis.

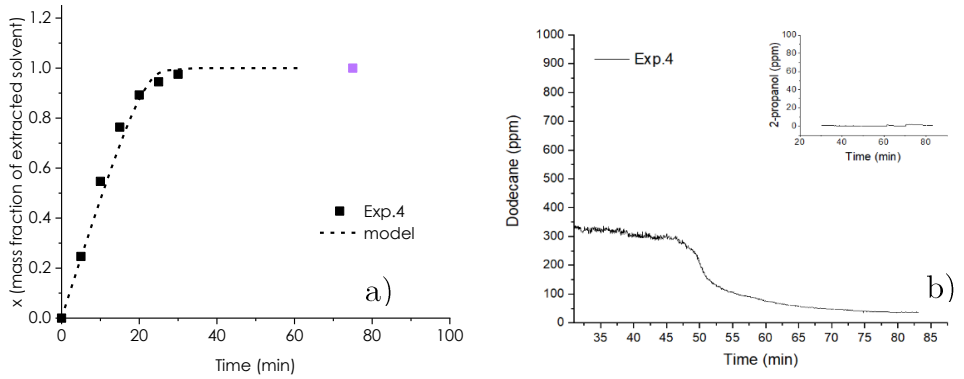

Figure B4. A) Mass fraction of extracted dodecane versus time; at T=60 °C, P=140 bar, CO_2 flow rate=20 g/min and mass of cake=60 g b) Dodecane and 2-propanol concentration changes over time obtained from SIFT-MS online analysis.

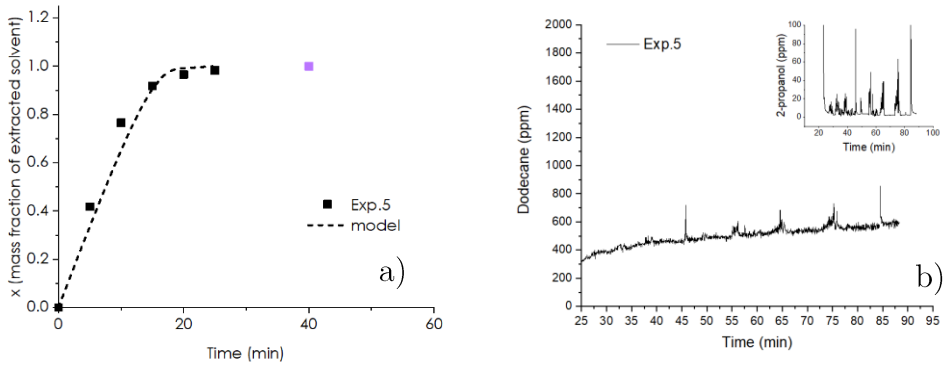

Figure B5. A) Mass fraction of extracted dodecane versus time; at T=60 °C, P=200 bar, CO_2 flow rate=30 g/min and mass of cake=60 g b) Dodecane and 2-propanol concentration changes over time obtained from SIFT-MS online analysis.

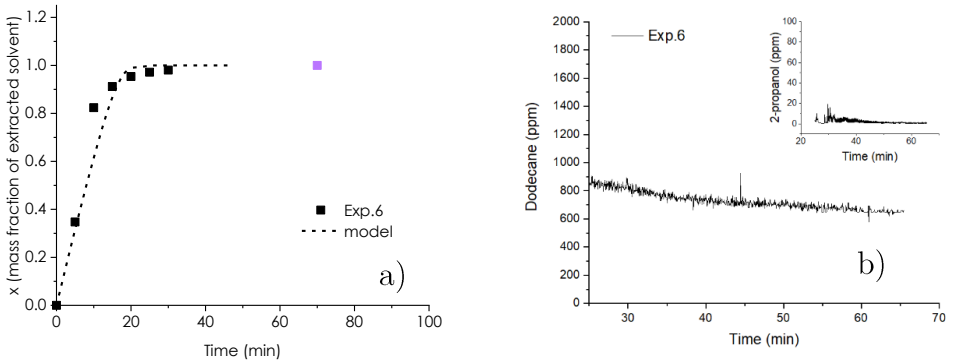

Figure B6. A) Mass fraction of extracted dodecane versus time; at T=70 °C, P=200 bar, CO_2 flow rate=20 g/min and mass of cake=60 g b) Dodecane and 2-propanol concentration changes over time obtained from SIFT-MS online analysis.

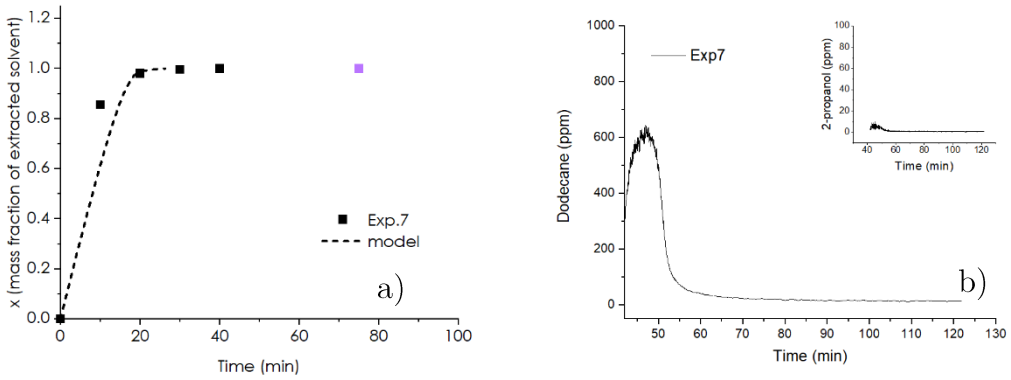

Figure B7. A) Mass fraction of extracted dodecane versus time; at T=60 °C, P=200 bar, CO_2 flow rate=30 g/min and mass of cake=150 g b) Dodecane and 2-propanol concentration changes over time obtained from SIFT-MS online analysis.

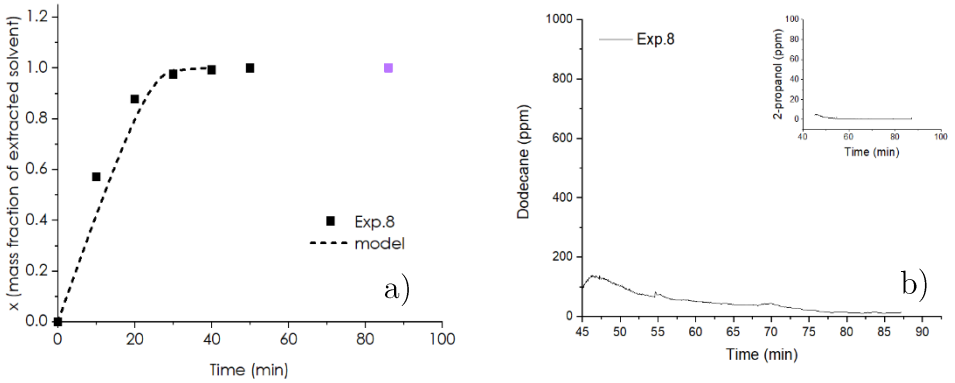

Figure B8. A) Mass fraction of extracted dodecane versus time; at T=50 °C, P=200 bar, CO_2 flow rate=30 g/min and mass of cake=150 g b) Dodecane and 2-propanol concentration changes over time obtained from SIFT-MS online analysis.

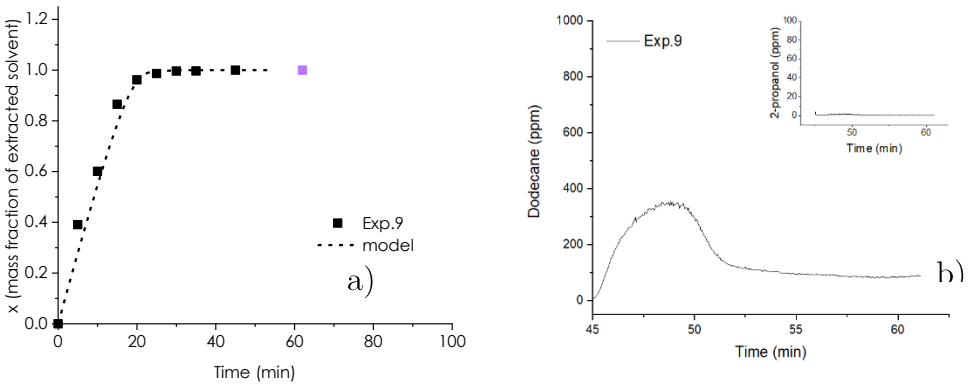

Figure B9. A) Mass fraction of extracted dodecane versus time; at T=70 °C, P=200 bar, CO_2 flow rate=30 g/min and mass of cake=150 g b) Dodecane and 2-propanol concentration changes over time obtained from SIFT-MS online analysis.

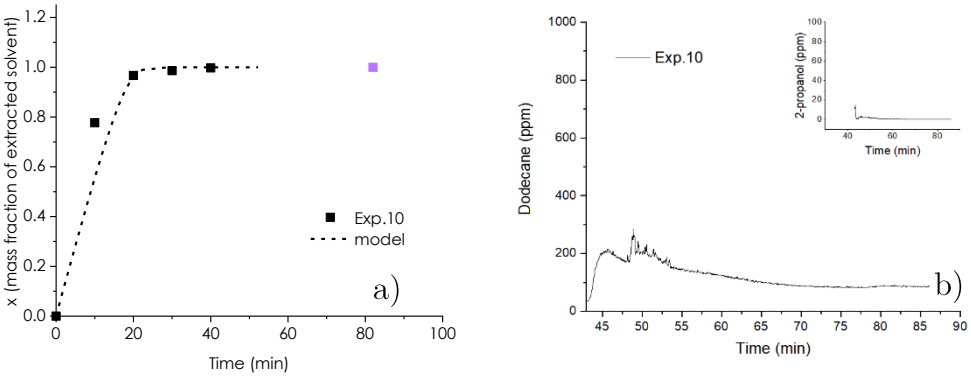

Figure B10. A) Mass fraction of extracted dodecane versus time; at T=60 °C, P=140 bar, CO_2 flow rate=20 g/min and mass of cake=150 g b) Dodecane and 2-propanol concentration changes over time obtained from SIFT-MS online analysis.

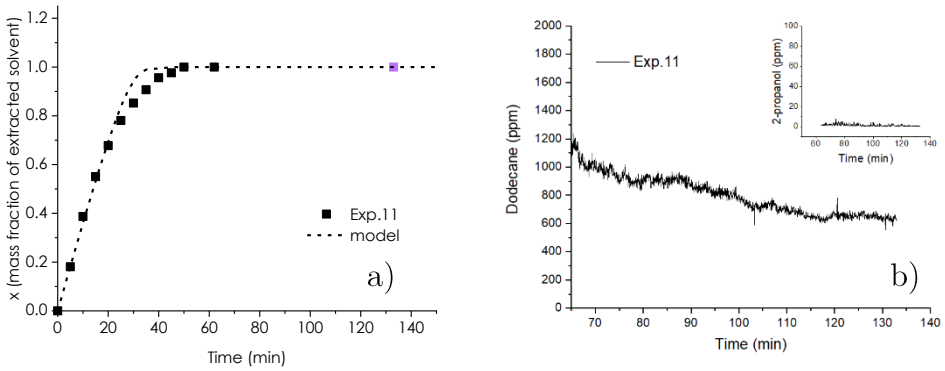

Figure B11. A) Mass fraction of extracted dodecane versus time; at T=50 °C, P=200 bar, CO_2 flow rate=10 g/min and mass of cake=105 g b) Dodecane and 2-propanol concentration changes over time obtained from SIFT-MS online analysis.

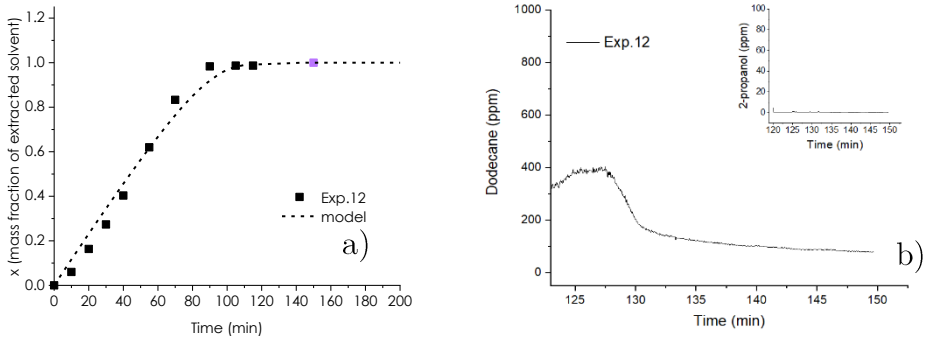

Figure B12. A) Mass fraction of extracted dodecane versus time; at T=70 °C, P=140 bar, CO_2 flow rate=10 g/min and mass of cake=105 g b) Dodecane and 2-propanol concentration changes over time obtained from SIFT-MS online analysis.

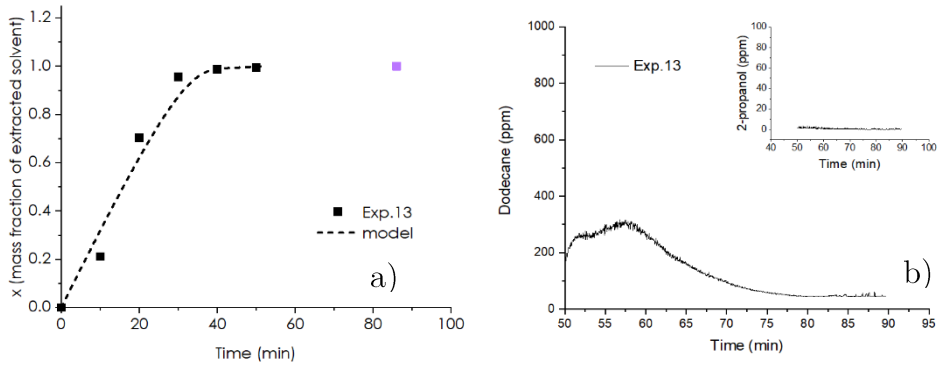

Figure B13. A) Mass fraction of extracted dodecane versus time; at T=60 °C, P=140 bar, CO_2 flow rate=20 g/min and mass of cake=105 g b) Dodecane and 2-propanol concentration changes over time obtained from SIFT-MS online analysis.

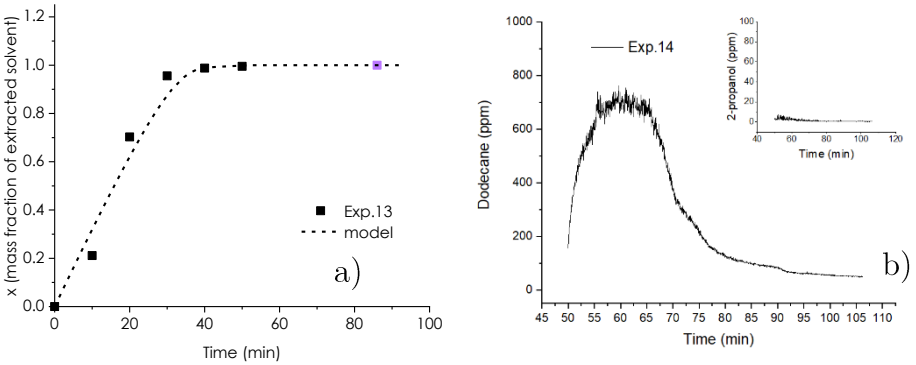

Figure B14. A) Mass fraction of extracted dodecane versus time; at T=60 °C, P=140 bar, CO_2 flow rate=20 g/min and mass of cake=105 g b) Dodecane and 2-propanol concentration changes over time obtained from SIFT-MS online analysis.

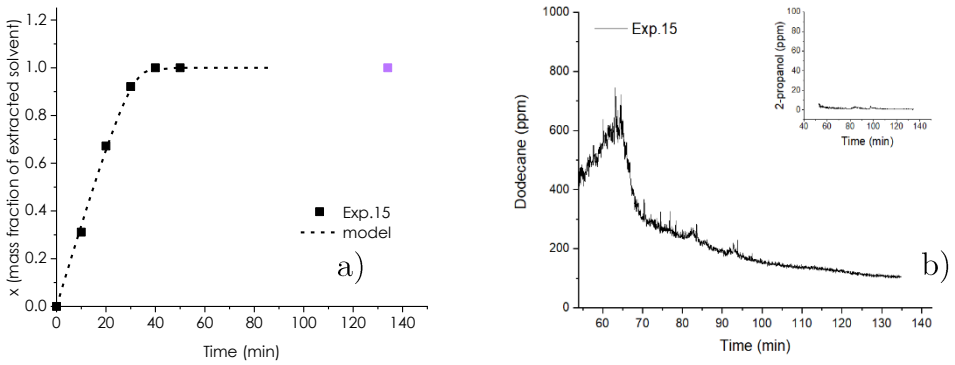

Figure B15. A) Mass fraction of extracted dodecane versus time; at T=60 °C, P=140 bar, CO_2 flow rate=20 g/min and mass of cake=105 g b) Dodecane and 2-propanol concentration changes over time obtained from SIFT-MS online analysis.